

ADA 136911



AN ANALYTICAL STUDY OF THE EFFECTS OF
 SURFACE ROUGHNESS ON A COMPRESSIBLE
 TURBULENT BOUNDARY LAYER

THESIS

Zakir H. Khan
 Squadron Leader, PAF

AFIT/GAE/AA/83D-9

This document has been approved
 for public release and sale; its
 distribution is unlimited.

DEPARTMENT OF THE AIR FORCE
 AIR UNIVERSITY

AIR FORCE INSTITUTE OF TECHNOLOGY

DTIC
 SELECTED
 JAN 18 1984

DTIC FILE COPY

Wright-Patterson Air Force Base, Ohio

84 01 17 133

AFIT/GAE/AA/83D-9

AN ANALYTICAL STUDY OF THE EFFECTS OF
SURFACE ROUGHNESS ON A COMPRESSIBLE
TURBULENT BOUNDARY LAYER

THESIS

Zakir H. Khan
Squadron Leader, PAF

AFIT/GAE/AA/83D-9

DTIC
COLLECTED
JAN 18 1984

A

Approved for public release; distribution unlimited

AN ANALYTICAL STUDY OF THE EFFECTS OF SURFACE ROUGHNESS
ON A COMPRESSIBLE TURBULENT BOUNDARY LAYER

THESIS

Presented to the Faculty of the School of Engineering
of the Air Force Institute of Technology
Air University

In Partial Fulfillment of the
Requirements for the Degree of
Master of Science in Aeronautical Engineering

Zakir H. Khan, B.S.
Squadron Leader, PAF

December 1983



Author	
Title	
Subject	
Availability Codes	
Dist	Special
AI	

Approved for public release; distribution unlimited

Preface

This thesis topic was proposed by Air Force Wright Aeronautical Laboratories, WPAFB, Ohio. It is an analytic study of the effects of surface roughness on compressible turbulent boundary layer. It interested me because of the mysterious nature of the turbulence, and I decided that I ought to undertake this investigation and attempt to learn as much as I could about this subject. The topic is also of current interest to USAF.

I take this opportunity to thank "Almighty Allah" who gave me the strength to accomplish this project. I wish to express my sincere gratitude to my thesis advisor, Dr. Urmilla Ghia, whose understanding of the subject was very impressive. Her continued guidance, contagious enthusiasm and above all unlimited patience throughout all phases of this study were invaluable. I also wish to thank Dr. William Hankey, Jr., for his sponsorship and continued assistance. I could not give this paper a proper preface without acknowledging Capt James K. Hodge for his constant interest. His support, be that in the form of enlightening criticism or compliments, often came as insight during times of frustrations. I will always remember with fondness his friendly and calm nature, and his devotion to duty. I also appreciate the diligence of Mrs. Cindy Boone who had immense patience to type this

manuscript flooded with mathematical equations and greek symbols.

Last but not the least, I express individual thanks to my sweet wife, for her loving support, assistance and understanding with which she took the late hours and the weekends not only during the thesis, but during my whole stay at AFIT. I also thank my children, Hannah, Ahad and Fahad for their patience with "Baba" as he reached for his goal of achieving higher learning.

Table of Contents

	<u>Page</u>
Preface.	ii
List of Figures.	v
List of Tables	vii
List of Symbols.	viii
Abstract	xii
I. Introduction.	1
II. Analysis of Problem	8
III. Method of Solution.	31
IV. Results and Discussions	39
V. Conclusions and Recommendations	81
Bibliography	84
Appendix A: Derivation of Sink Term	88
Appendix B: Derivation of Conservation Equations Including the Roughness Effect in Levy- Lees Variables.	90
Appendix C: Difference Relations.	107
Appendix D: Coefficient in Difference Equations	113
Appendix E: Program Listing	116
Appendix F: Four Key Subsystems Within Computer Code.	141
VITA	158

List of Figures

<u>Figure</u>		<u>Page</u>
1.	Dimension and Distribution of Roughness Elements with Circular Cross-Section.	28
2.	Coordinate System and Notations	29
3.	Matching the Inner and Outer Eddy Viscosity Models.	30
4.	Finite Difference Grid for Boundary Layer	30
5.	Flow Diagram of the Logical Steps to Solution with ITRACT.	38
6.	Dimensions and Distributions of Roughness Elements with Rectangular Cross-Section	52
7.	Comparison of Computed Velocity Profile for Smooth Plate with Data of AFWAL	53
8.	Comparison of Computed Temperature Profile for Smooth Surface with Experimental Data of AFWAL.	54
9.	Comparison of Computed Density Profiles for Smooth Surface with AFWAL Data.	55
10.	Comparison of Computed Mach Number Profile for Flow Over Smooth Surface with AFWAL Data.	56
11.	Comparison of Calculated Total Temperature Profile for Smooth Surface with AFWAL Data.	57
12.	Comparison of Computed Pressure Profile for Smooth Surface with AFWAL Data.	58
13.	Comparison of Computer Velocity Profiles for Flow Over Smooth Surface with Cole's Data.	59

<u>Figure</u>		<u>Page</u>
14.	Comparison of Computer Mach Number Profile With Cole's Data.	60
15.	Comparison of Computed Velocity Profile for Rough Surface with Experimental Data of AFWAL.	61
16.	Comparison of Temperature Profile for Rough Surface with Experimental Data of AFWAL.	62
17.	Comparison of Computed Density Profile for Rough Surface with Data of AFWAL.	63
18.	Comparison of Computed Mach Number Profile for Rough Surface with Data of AFWAL.	64
19.	Comparison of Calculated Total Temperature Profile for Rough Plate with Data of AFWAL.	65
20.	Comparison of Computed Pressure Profile for Rough Surface with Data of AFWAL.	66
21.	Comparison of Computed Velocity Profile for Flow Over Smooth and Rough Surfaces	67
22.	Comparison of Computed Temperature Profiles for Smooth and Rough Surfaces	68
23.	Comparison of Computed Density Profile for Smooth and Rough Surfaces	69
24.	Comparison of Calculated Mach Number Profiles for Smooth and Rough Surfaces	70
25.	Comparison of Computed Total Temperature Profiles for Smooth and Rough Flat Plate.	71
26.	Comparison of Computed Pressure Profiles for Smooth and Rough Surfaces	72
27.	Comparison of Velocity Profiles with Different Roughness Height.	73
28.	Comparison of Velocity Profiles with Different Roughness Density	74
29.	Comparison of Computed Skin Friction Coefficient for Smooth and Rough Surface.	75

List of Tables

<u>Table</u>		<u>Page</u>
I	Data for Smooth Flat Plate Probe Boundary Layer Profiles.	76
II	Data of Dr. Cole's Experiment for Turbulent Flow Over Smooth Surfaces	77
III	Data for Rough Flat Plate Probe Boundary Layer Profiles.	78
IV	Free Stream Conditions for Smooth and Rough Experimental Data	79
V	Comparison of Thickness for Smooth and Rough Cases	80

Nomenclature

A	Defined by Eq (44)
a	Speed of sound
B(y)	Defined in Eq (20)
c_f	Local coefficient of friction
c_p	Specific heat at constant pressure
F	Velocity ratio, $\frac{u}{u_e}$
f(y)	Defined in Eq (21)
H, h	Enthalpies, defined in the expression $H = h + \frac{u^2}{2}$
K_ℓ	Thermal conductivity
K_T	Eddy conductivity
L	Characteristic problem dimension, length of the model in question
ℓ	Defined in Eq (33)
M	Mach number
Pr	Prandtl number
p	Pressure
q	Heat flux or heat flow per unit area
R	Gas constant, 1716 ft ² /sec ² R for air
Re	Reynolds number
R_u	Sink term defined in Eq (15)
R_h	Source term defined in Eq (16)
$r(r_0)$	Radial coordinate (body radius) for the case of the axisymmetric cone, measured perpendicularly from the longitudinal centerline, Fig 2
S	Viscosity constant of Sutherland (198.6 R)
s	Nondimensional position, x/L

St	Stanton number, $\frac{q}{\rho_e u_e (H_e - h_w)}$
T	Temperature
t	Transverse curvature term equal to $\frac{r}{r_0}$
u(v)	Velocity component along (perpendicular to) the streamwise direction
u^+	Friction velocity, $(\tau_w/\rho_w)^{1/2}$
V	Transformed velocity expression defined in
X	Defined in Eq (24)
x,y	Body surface oriented coordinate system in which x runs parallel to the stream direction, point downstream, and y is perpendicular to x and its directed into the external flow
y^+	Dimensionless distance, $y\rho_w u^+/\mu_w$

Greek Symbols

α	Defined in Eq (32)
β	Defined in Eq (35)
ψ	Stream function
ϕ	Defined in Eq (37)
Γ	Streamwise intermittency distribution or probability factor
γ	The gas constant, ratio of specific heats
γ'	The intermittency factor of Klebanoff
Δ	Change in variable quantity
δ	Boundary layer thickness
δ^*	Displacement thickness
ϵ	Eddy viscosity
$\bar{\epsilon}$	Eddy viscosity function defined following Eq (38)

ϵ	Eddy viscosity function defined following (Eq 39)
η	Transformed perpendicular boundary layer coordinate and nondimensional distance along this coordinate
θ	Static temperature ratio, $\frac{T}{T_e}$
θ	Momentum thickness
μ	Molecular viscosity
ν	Kinematic viscosity, $\frac{\mu}{\rho}$
ξ	Transformed streamwise boundary layer coordinate and nondimensional length along this coordinate
ρ	Density
τ	Shear Stress
w	Exponent of the viscosity law of Sutherland

Subscripts and Superscripts

e	Condition at the edge of the boundary layer, also indicative of the input or environmental conditions for ITRACT in the cone study
∞	Free stream or unperturbed condition
j	Flow index, $j = 1$ for conical flow, $j = 0$ for flow over a flat surface
$\delta^*(\theta)$	When used with Re , denotes Reynolds number based on displacement thickness (momentum thickness)
o	Total or stagnation condition except for r_o
$'$	Primed quantities indicate instantaneous departures from a mean state or condition in the turbulence model. The accompanying bars over the primed symbols denote a time averaged quantity.
ref	Reference

ss Source sink
t Turbulent condition
w Condition at the surface of the plate or cone
x Denotes a particular real x station along the
 surface of the model

Abstract

This study followed the work of Dr. Anthony Fiore, of Air Force Wright Aeronautical Laboratories, Wright-Patterson Air Force Base, Ohio. Dr. Fiore had carried out an experimental study ^{of} the effect of surface roughness on the turbulent boundary layer, ^(using) ~~Given~~ a Fortran code, ITRACT, written primarily by Dr. Shang, that solved for the characteristics of a laminar, transitional and turbulent boundary layer on smooth surfaces. ~~The purpose of the present study was to investigate~~ the influence of surface roughness on a compressible turbulent boundary layer and then ~~to~~ extend ~~the~~ usefulness of the existing computer code, ITRACT, by including in it the optional capability of rough-surface boundary-layer calculations.

To achieve this objective, the ~~the~~ surface roughness was represented by distributed sources and sinks in the appropriate governing equations. The most important term is a sink term in the mean momentum equation, representing the form drag due to the roughness element. ~~The~~ governing boundary-layer equations for continuity, momentum, and energy were derived in a form to account for ~~the~~ blockage effects ~~due to the~~ roughness elements. The modified governing equations were then transformed using ~~the~~ transformation ^(transformations) of Probstein-Elliott and Levy-Lees. The resulting equations, with appropriate boundary conditions, were solved by finite-difference techniques to determine the non-

dimensional velocity components and temperature at a finite number of nodes in the boundary-layer ^{field} of the flow.

To establish the authenticity of the original code, ITRACT, some smooth-surface results were first computed and compared with the experimental data of Dr. Fiore and Dr. Cole for turbulent flows over smooth surfaces. After the accuracy of the code was established for smooth-surface calculations, the code was modified in order to render it capable of predicting the influence of surface roughness on compressible turbulent flow. The modified code was then used to obtain results for rough-surface boundary layers and the computed results were compared with the experimental data of Dr. Fiore for the case of supersonic flow over a rough flat plate. The agreement between the computed and the measured velocity profiles was quite satisfactory. The corresponding temperature profiles agreed well everywhere, except very near the wall; a possible reason for this discrepancy is offered in this study. Unlike previous studies of rough-surface boundary layers, the present study makes no modification to the turbulence model employed.

AN ANALYTIC STUDY OF THE EFFECT OF SURFACE ROUGHNESS
ON A COMPRESSIBLE TURBULENT BOUNDARY LAYER

I. Introduction

Preliminaries and Problem Analysis

Surface roughness can play an important role in turbulent boundary-layer skin friction and heat transfer for many high-speed flight applications. An understanding of the roughness effect is essential for accurate design prediction in a wide variety of applications, including ships, aircraft, compressor blades, turbine blades, missiles and re-entry vehicles. For example, the NASA Space Shuttle Program studied roughness as it augments heating. At low flight altitude, the thickness of boundary layer on the blunted nose region of hypersonic re-entry vehicle can easily be less than the inherent surface roughness of practical heat shield materials, and roughness dominates the heat transfer characteristics. Also recent experiments (Ref. 1) have shown that surface roughness alone can significantly influence the control effectiveness of maneuvering vehicle. Numerical analysis and computer programs have been developed over the last twenty years to solve turbulent boundary layers over smooth surfaces. A deficiency, however, exists with these programs as regards inclusion of roughness effects. Data has been accumulated

over the last few years in this area but a need for a computer code to accurately match this data still exists. The purpose of this study was to investigate the influence of surface roughness on a compressible turbulent boundary layer and then to modify an existing computer code for turbulent boundary layer over smooth surface to account for roughness effects.

Literature Survey

Most available models for analyzing the influence of surface roughness on boundary-layer behavior are essentially extension of Nikuradse's study (Ref. 2) of pipes roughened with sand and application of Nikuradse's results to flat plates by Prandtl and Schlichting (Ref. 3). Several correlations have been proposed to relate real surface-roughness heights, spacing and geometries to an equivalent sand-grain roughness height so that Nikuradse's data can be used. Examples of such correlations can be found in White and Grabow (Ref. 4:153-164). Dvorak (Ref. 5:1752-1759) used integral methods in which the skin-friction coefficient was specified as a function of boundary-layer thickness and roughness height. Using this specification, the moment equations were solved for the momentum and displacement thickness. Chen (Ref. 6:623-629) extended this approach to predict heat transfer, by using a Stanton number correlation derived from the subsonic data by Owean and Thomson (Ref. 7:321-334). In this approach, the stag-

nation enthalpy profile was assumed to have the same shape as the velocity profiles. A similar model has recently been developed for re-entry vehicles by Dahm et al. (Ref. 8). Here again a momentum integral approach is used, with the skin-friction and heat-transfer coefficients based on correlations of the low-speed data of Healzer et al. (Ref. 9) and flat plate measurements of Reda (Ref. 10) at a mach number of 2.9. The roughness augmentation of heat transfer was found to be about 60 percent of the skin-friction augmentation. More recently, effects of surface roughness have been evaluated by differential methods. Cebeci and Chang (Ref 11:730-735) numerically solved the incompressible boundary layer equations employing an algebraic eddy viscosity formulation modified for surface roughness. The modification was based on Rotta's (Ref. 12:1-219) model, which displaces the normal coordinate of the rough-wall velocity profile. An expression for this displacement and the resulting mixing length is given by Cebeci and Chang (Ref. 11) as a function of an equivalent sand-grain roughness height. Emphasizing compressible flows for a variety of edge and wall conditions, Hodge and Adams (Ref. 13) numerically solved the flow equations together with the equation of kinetic energy of turbulence. Roughness effects were accounted for by inclusion of a form drag term in the momentum equation and by modification, based on the results of Healzer, et al., of several of the nine empirical constants in the turbulence model. A

somewhat more involved approach was taken by Saffman and Wilcox (Ref. 14:541-546) utilizing a two-equation turbulence model. However, the effect of roughness was treated rather empirically by making the boundary conditions for the pseudo-vorticity at the wall a function of the roughness height. This dependence was derived so as to fit the observed variation of the "law of the wall" velocity deficit with roughness. Some encouraging profiles were also computed for the mean and fluctuating velocities. However, heat transfer was again determined by invoking a Reynolds analogy with the skin friction. Finson and Clark (Ref. 15:3-6) presented a technique which accounted for the surface roughness by calculating the form drag contribution by individual elements. Following the approach of Finson and Clark, Christoph and Pletcher (Ref. 16:509-510) used a two-layer algebraic mixing length model that explicitly accounts for mass addition and surface roughness, in addition to the modification of the boundary-layer equations as suggested by Finson and Clark.

Scope of Present Study

The Flight Dynamics Laboratory possessed a digital computer code called ITRACT, which computed the characteristics of laminar and turbulent boundary layers for either planar or axisymmetric flow over smooth surfaces. The

purpose of the present study was to modify this code for inclusion of the effects of surface roughness on compressible flow. Historically, roughness effects have been modelled by a law-of-the-wall velocity profile expression in terms of an equivalent sand-grain roughness height. Physically, the equivalent sand-grain roughness concept is not very satisfying since an equivalent sand-grain roughness height must be contrived for real roughness heights, spacing and geometries. A physically more meaningful method is that employed by Finson and Clark and followed by Christoph and Pletcher. In the present study, the same approach is followed but without invoking any modification of the turbulence model. Roughness is represented by distributed sources and sinks in the appropriate governing equations. The most important term is a sink term in the mean momentum equation representing the form drag on the roughness elements. The governing boundary-layer equations are cast in a form to account for the blockage effect due to the roughness elements. Accordingly, the fluxes along the streamwise direction are multiplied by $(1 - D(y)/\ell)$ where $D(y)$ is the element diameter at height y and ℓ the average centre to centre spacing of the element (Fig 1). Fluxes in a direction normal to the streamwise direction are multiplied by $(1 - \pi D^2/4\ell^2)$. Here, the shape of the elements has been restricted to circular cross-sections only, but the modified code would eventually have the provision to

predict the roughness effects due to rectangular elements as well. The computed results obtained by employing a Reynolds stress turbulence model in combination with a drag description for the effect of the roughness elements on the flow is compared against relevant data to establish the validity and accuracy of the theory and to offer explanations for the observed trends.

The model used in this study is aimed entirely at distributed roughness, i.e., three-dimensional roughness, appropriate to the vast majority of practical applications. Two-dimensional roughness such as machined grooves normal to the flow direction are not considered here. The two types of roughness may yield qualitatively similar trends in terms of roughness height, spacing, etc., but a substantial difference in the nature of the flow may be expected. This model makes the basic assumption that the forces on roughness elements can be viewed as form drag. This implicitly requires that the flow approaching an individual element be attached, whereas with 2-D roughness elements, cavity flow is likely to prevail immediately downstream of the roughness elements.

The next step in the study was to learn as much about the computer code, ITRACT, as possible. This step included a study of the equations of motion, continuity, and energy, together with the perfect gas law and Sutherland's viscosity law needed for a boundary-layer calculation. It also included the comparison of the computer code results for

turbulent flow over smooth surfaces to experimental data to establish the authenticity of the code.

After the accuracy of the present code was established, the next step was to modify the code in order to render it capable of predicting the effect of surface roughness on compressible turbulent flow. The modified code was verified by comparing the results predicted by modified computer code with the experimental data available at the Flight Dynamics Laboratory for the case of supersonic flow over rough flat plate. This comparison will also establish the extent to which the modification of the turbulence model is, or is not, needed for accurate prediction of rough-surface boundary layer flows.

The major accomplishment of this study is the extension of the usefulness of the existing computer code, ITRACT, by including in it the optional capability of rough-surface boundary-layer calculations.

II. Analysis of Problem

Governing Equations

This section presents the governing equations for the compressible turbulent boundary layer together with the required boundary conditions. In their final form, governing equations include the effect of surface roughness. The eddy viscosity and eddy conductivity models used to represent the apparent turbulent shear and heat flux terms appearing in the mean-flow boundary-layer equations are discussed in the latter part of this section.

Coordinate System

The coordinate system employed is shown in Figure 2. The boundary-layer coordinate system is denoted by x and y which are tangent and normal to the surface, respectively. The origin of the boundary-layer coordinate system x, y , as well as that of the body coordinate system z, r , for axisymmetric configurations is located at the stagnation point for blunt bodies, and at the leading edge for sharp-tipped bodies. The velocity components u and v are oriented along the x and y directions, respectively. Transverse curvature terms are retained because of their importance in the development of boundary-layer flow over slender bodies of revolution where the boundary-layer thickness may become of the order of the body radius r_0 . The angle ϕ is the angle between z axis and local tangent evaluated at $(x,0)$.

Differential Equations

The flow of a compressible, viscous, heat conducting fluid is mathematically described by the continuity equation, the Navier-Stokes equations and the energy equation, together with an equation of state, a heat conductivity law and a viscosity law. For flows at large Reynolds number, Prandtl (Ref. 17) has shown that the Navier-Stokes equations and the energy equation can be simplified to a form now recognized as the compressible boundary-layer equations. These equations may be written as follows:

Continuity:

$$\frac{\partial}{\partial x} (r^j \rho u) + \frac{\partial}{\partial y} (r^j \rho v) = 0 \quad (1)$$

Momentum:

$$\rho \left[u \frac{\partial u}{\partial x} + v \frac{\partial u}{\partial y} \right] = -\frac{dp}{dx} + \frac{1}{r^j} \frac{\partial}{\partial y} \left[r^j \left(\mu \frac{\partial u}{\partial y} \right) \right] \quad (2)$$

Energy:

$$\rho \left[u \frac{\partial}{\partial x} (C_p T) + v \frac{\partial}{\partial y} (C_p T) \right] = u \frac{dp}{dx} + \frac{1}{r^j} \frac{\partial}{\partial y} \left[r^j \frac{K \ell}{C_p} \frac{\partial}{\partial y} (C_p T) \right] + \mu \left(\frac{\partial u}{\partial y} \right)^2 \quad (3)$$

Osborne Reynolds, who was first to observe and study the phenomenon of transition from laminar to turbulent flow, assumed that the instantaneous fluid velocity satisfied the

Navier-Stokes equations and that the instantaneous velocity (u_i) could be considered to consist of a mean (time averaged) component \bar{u} and a fluctuating component u' , i.e.,

$$u_i(x_i, t) = \overline{u_i(x_i)} + u_i'(x_i, t) \quad \text{where } i = 1, 2, 3 \quad (4)$$

In order to obtain the conservation equations, the instantaneous quantities in the equations (1) to (3) were replaced by their mean and their fluctuating quantities. By taking the time average of the various terms appearing in these equations and making the boundary-layer assumptions, the following mean continuity, mean momentum and mean energy equations were derived (Ref. 18, 145, 216).

$$\frac{\partial}{\partial x} (r^j \rho u) + \frac{\partial}{\partial y} \left[r^j \rho \left(v + \frac{\overline{\rho' v'}}{\rho} \right) \right] = 0 \quad (5)$$

Momentum:

$$\rho \left[u \frac{\partial u}{\partial x} + \left(v + \frac{\overline{\rho' v'}}{\rho} \right) \frac{\partial u}{\partial y} \right] = -\frac{dp}{dx} + \frac{1}{r^j} \frac{\partial}{\partial y} \left[r^j \left(\mu \frac{\partial u}{\partial y} - \rho \overline{u' v'} \right) \right] \quad (6)$$

Energy:

$$\rho \left[u \frac{\partial (C_p T)}{\partial x} + \left(v + \frac{\overline{\rho' v'}}{\rho} \right) \frac{\partial (C_p T)}{\partial y} \right] = u \frac{dp}{dx} + \frac{1}{r^j} \frac{\partial}{\partial y} \left[r^j \frac{k \ell}{C_p} \frac{\partial (C_p T)}{\partial y} \right] + \left(\mu \left(\frac{\partial u}{\partial y} \right)^2 \right) + \frac{1}{r^j} \frac{\partial}{\partial y} \left[r^j (-C_{pp} \overline{v' T'}) \right] - \rho \overline{u' v'} \frac{\partial u}{\partial y} \quad (7)$$

These equations are identical to those for laminar flows, with the exception of the correlations of the turbulent fluctuating quantities which represent the apparent mass, shear, and heat-flux terms caused by turbulence. These fluctuating quantities were incorporated through mathematical modelling. The apparent mass flux term $\overline{\rho'v'}$, the apparent shear stress term $\overline{\rho u'v'}$ and the apparent heat flux term $C_p \overline{\rho v'T'}$ are represented by a new velocity component \tilde{v} , an eddy viscosity ϵ , and an eddy conductivity K_T , respectively.

These terms were defined by the following relationships:

$$\tilde{v} = v + \frac{\overline{\rho'v'}}{\rho} \quad (8)$$

$$\epsilon = -\rho \frac{\overline{u'v'}}{(\partial u / \partial y)} \quad (9)$$

$$K_T = -C_p \frac{\overline{v'T'}}{\partial T / \partial y} \quad (10)$$

The turbulent Prandtl number is expressed, in a manner analogous to the laminar Prandtl number expressed in terms of viscosity and eddy conductivity as:

$$P_{r,t} = \frac{C_p \epsilon}{K_T} \quad (11)$$

To this set of equations the following perfect gas law and the viscosity relation of Sutherland were also added.

Perfect-gas law:

$$p = C_p \left\{ \frac{\gamma-1}{\gamma} \right\} \rho T \quad (12)$$

Viscosity Law:

$$\frac{\mu}{\mu_e} = \left(\frac{T}{T_e} \right)^{1.5} \left\{ \frac{T_e + S}{T + S} \right\} \quad (\text{air only}) \quad (13)$$

where μ_e denotes the viscosity at the reference T_e and 'S' is a constant. This relation is approximated in theoretical calculation by the simpler power-law:

$$\frac{\mu}{\mu_e} = \left(\frac{T}{T_e} \right)^\omega \quad 0.5 < \omega < 1.0 \quad (14)$$

It has been found that Sutherland's formula can be approximated at high temperature by adopting values of ω between 0.5 and 0.75, whereas at lower temperature the value of $\omega=1.0$ appears to be adequate.

Rough-Wall Boundary Layer Model

The basic model for the rough-wall boundary-layer is the same as described thus far for smooth wall boundary-layer flow and free-shear flows. The roughness model makes the basic assumption that the additional forces due to the roughness elements can be viewed as form drag. This implicitly requires that the flow approaching an individual

element be attached. This model is more appropriate for distributed roughness, i.e., 3-D roughness elements, since cavity flow is likely to prevail with 2-D roughness.

The rough surface is idealized as being made up of identical elements. The bottom of the elements, or the underlying smooth wall, is at $y=0$ (Fig 1). The element height is K , and ℓ is the average element spacing measured from centre to centre of two adjacent elements. The total number of elements per unit area is given by $1/\ell^2$. The analysis presented here is for a case of roughness elements with circular cross-section at all heights, with $D(y)$ denoting the diameter of the element at height y for $0 < y < K$, but any general shape may be specified. Then, viewing flow around the element at height y as two dimensional, the form drag between $y - \frac{\delta y}{2}$ and $y + \frac{\delta y}{2}$ is:

$$\frac{1}{2} \rho u^2 C_D D(y) \delta y$$

where C_D is the form drag coefficient. To relate this to drag per unit volume, it is noted that there are ℓ^{-2} elements per unit area, so that the appropriate differential volume is $\ell^2 \delta y$ and, therefore, the sink term for mean momentum is:

$$R_u = -\frac{1}{2} \rho u^2 C_D \frac{D(y)}{\ell^2} \quad (15)$$

The drag coefficient could be specified to be equal to unity ($C_D = 1$), appropriate to infinite circular cylinders (two-

dimensional elements) at local Reynolds number above the Stokes-flow regime. However, lower values such as $C_D = 0.6$ are more appropriate for finite elements (3-D elements) such as cones, hemisphere, etc.

In addition, there should be source terms in the equation governing turbulent kinetic energy and its dissipation rate in order to describe the tendency of roughness to increase the velocity fluctuation. Specification of these terms is more speculative; their contributions are generally smaller than the natural production terms and, hence, less critical to the model. These terms are not very important compared to the indirect effect of roughness to increase the turbulent energy by increasing the mean shear. Except in the Stokes flow regime, heat transfer to an element should be small. Therefore, the only roughness term appearing in the thermal equations is a source term in the mean static enthalpy equation. This term is constructed such that, in combination with the sink term (Equation 15) for drag, the total enthalpy is not altered. Accordingly, the mean static-enthalpy differential equation must include a source term R_h , defined as:

$$R_h = +\frac{1}{2} \rho u^3 C_D D(y)/\ell^2 \quad (16)$$

The detailed derivation of this term is given in Appendix A.

If no further modification is made in the governing equations, it is implied that the roughness elements are

assumed to occupy no space (Ref. 25:2). This assumption becomes progressively worse as the roughness density increases, therefore, the model has been extended to account for the blockage effects due to the roughness elements. Accordingly, the boundary-layer equations are derived in a form to account for the blockage effect. This is done in the following manner:

(a) At a given height y , the fraction of flow area in the x -direction, that is open to the flow, is $\{1-D(y)/\ell\}$, hence, fluxes in the streamwise direction, represented via the convective operator $\rho u \partial/\partial x$, are multiplied by this factor.

(b) Fluxes across a surface area whose normal is in the y -direction, should be multiplied by $\{1- D^2(y)/4\ell^2\}$. However, the roughness terms discussed above are already based on the total volume, rather than the available flow volume, and need no such factor.

With the incorporation of these modifications, the conservation equations (5), (6), and (7) are recast as follows:

Continuity:

$$f(y) \frac{\partial}{\partial x} (r^j \rho u) + \frac{\partial}{\partial y} (r^j \rho \tilde{v}) = 0 \quad (17)$$

Momentum:

$$f(y) \rho u \frac{\partial u}{\partial x} + \rho \tilde{v} \frac{\partial u}{\partial y} = -f(y) \frac{dp}{dx}$$

$$\begin{aligned}
& + \frac{1}{r^j} \frac{1}{B(y)} \frac{\partial}{\partial y} \left[B(y) r^j \left[\mu \frac{\partial u}{\partial y} - \rho \overline{u'v'} \right] \right] \\
& - \frac{1}{2} \rho u^2 \frac{C_D D(y)}{B(y) \ell^2} \quad (18)
\end{aligned}$$

Energy:

$$\begin{aligned}
f(y) \rho u \frac{\partial (C_p T)}{\partial x} + v \frac{\partial (C_p T)}{\partial y} &= f(y) u \frac{dp}{dx} \\
& + \frac{1}{B(y) r^j} \frac{\partial}{\partial y} \left[B(y) r^j \left[\frac{K \ell}{C_p} \frac{\partial (C_p T)}{\partial y} \right] \right] + \mu \left[\frac{\partial u}{\partial y} \right]^2 \\
& + \frac{1}{B(y) r^j} \frac{\partial}{\partial y} \left[B(y) r^j (-C_p \rho \overline{v'T'}) \right] - \rho \overline{u'v'} \left[\frac{\partial u}{\partial y} \right] \\
& + \frac{1}{2} \rho u^3 \frac{C_D D(y)}{B(y) \ell^2} \quad (19)
\end{aligned}$$

In equations (17-19):

$$B(y) = \{1 - \pi D^2(y)/4\ell^2\} \quad (20)$$

$$f(y) = \{1 - D(y)/\ell\}/B(y) \quad (21)$$

Details of the derivation of equations (17) through (19) are given in Appendix B. The function $f(y)$ contains the main effect of blockage. If a stream function formulation were incorporated, $f(y)$ may be absorbed in the definition of

the stream function that is introduced to eliminate the normal velocity.

$$\frac{\partial \psi}{\partial y} = f(y)\rho u \quad (22)$$

$$\frac{\partial \psi}{\partial x} = -\rho \tilde{v} \quad (23)$$

However, it is not done in the present work. It should be noted that, if the elements are packed so tightly that they are touching over some range of y , then $D = \lambda$ and $f(y) = 0$ over that range. This formulation forces the velocity to remain zero up to the height where $D < \lambda$ and the flow is blocked. In such cases, $Y = 0$ is redefined as the lowest point where the flow is unblocked. (Fig 1)

A major advantage of this model is that solutions are obtained for both velocity and thermal variables. Heat transfer is obtained directly without invoking a Reynolds analogy. Finite-difference solutions are obtained using the boundary conditions that, (i) Fluctuating quantities are zero at the base of the wall, $Y = 0$ and (ii) At the outer edge, fluctuating quantities are zero and the flow variables approach the free-stream values.

Transformation of Boundary-Layer Equations

Equations (17-19), which are expressed in the surface-normal coordinates in the physical plane, require starting profiles, but these equations are singular at the stagna-

tion point. For this reason, the equations are transformed to a coordinate system that removes the singularity at the stagnation point, stretches the coordinate normal to the flow direction, thereby, resulting in a more gradual growth of the boundary-layer thickness and places the equations in an almost two-dimensional form (Ref. 15). A combination of the Probstein (Ref. 31) and Levy-Less was used in this analytic study. The transformed coordinates ξ and η are defined as:

$$\xi(x) = \int_0^x \rho_e u_e r_o^{2j} dx \quad (24)$$

and

$$\eta(x,y) = \frac{\rho_e u_e r_o^{2j}}{2\xi} \int_0^y t^j \frac{\rho}{\rho_e} dy \quad (25)$$

It may be pointed out here that turbulent boundary layers are characterized by two length scales, namely, the boundary-layer thickness and the wall-layer thickness, which are quite different in magnitude and vary in the streamwise direction depending upon the pressure gradient, wall boundary conditions, etc., thereby, making the analysis of turbulent layers more complicated than the laminar boundary layers where generally only one length scale is present. In compressible laminar flow, when the boundary-layer equations are expressed in terms of Levy-Lees variables, the streamwise growth of the boundary layer is significantly reduced thereby

simplifying the numerical solution of the boundary layer. But in turbulent flow since the Levy-Lees variables do not properly capture the boundary layer thickness, it is necessary to monitor the numerical solution and add computational points in the outer region to accommodate the boundary-layer growth. To overcome this problem, it would be better to use the new self-adaptive coordinate transformation for finite-difference solution of turbulent boundary-layer flows presented by J.E. Carter et al.

(ref. 32) as this permits a uniform mesh to be used in the computational coordinate which extends across the layer. This coordinate transformation uses the local value of the skin friction to scale the thickness of the wall-layer region, and the local maximum value of turbulent viscosity to scale the boundary-layer thickness.

To proceed with the derivation of the equations used in the present study, the dependent variables are non-dimensionalized according to:

$$F = \frac{u}{u_e}, \quad \theta = \frac{T}{T_e} \quad (26)$$

Next, the relations between derivative in the physical (x,y) plane and in the transformed plane (ξ,η) are obtained as follows:

$$\left[\frac{\partial}{\partial x} \right]_y = \rho_e u_e \mu_e r_o^{2j} \left[\frac{\partial}{\partial \xi} \right]_\eta + \left[\frac{\partial \eta}{\partial x} \right] \left[\frac{\partial}{\partial \eta} \right]_\xi \quad (27)$$

and

$$\left[\frac{\partial}{\partial y} \right]_x = \frac{\rho_e u_e r_o^{j_t j}}{2\xi} \frac{\rho}{\rho_l} \left[\frac{\partial}{\partial \eta} \right]_\xi \quad (28)$$

In Eqs (27) and (28), the subscript outside the square bracket indicates the coordinate that is held constant during the indicated differentiation process.

The transformed variable for the normal velocity V is obtained as:

$$V = \frac{2\xi}{\rho_e u_e \mu_e r_o^{2j}} f(y)F \frac{\partial \eta}{\partial x} + \frac{r_o^{j_t j} \rho \tilde{v}}{2\xi} \quad (29)$$

The detailed derivation of equation (29) is given in Appendix B.

With this, the final working form of the governing system, prior to linearization, was obtained as follows: (Ref. Appendix B)

Continuity:

$$V_\eta + f(y)F + 2\xi f(y)F_\xi = 0 \quad (30)$$

Momentum:

$$\begin{aligned} 2\xi f(y)FF_\xi + \beta f(y)(F^2 - \theta) + VF_\eta \\ = \frac{1}{B(y)} \{B(y)t^2 j \bar{\epsilon} l F_\eta\}_\eta - \phi_{ss} r^2 \end{aligned} \quad (31)$$

Energy:

$$2\xi f(y)F\theta_{\xi} + V\theta_{\xi} = \frac{1}{B(y)r^j} \left[t^{2j} r^j B(y) \bar{\epsilon} \frac{\ell}{Pr} \theta_{\eta} \right]_{\eta} + t^{2j} \ell \alpha \bar{\epsilon} \eta^2 + \phi_{ss} \alpha F^3 \quad (32)$$

Further, the additional symbols included in these equations are defined as follows:

$$\ell = \frac{\rho u}{\rho_e u_e} \quad (33)$$

$$\alpha = \frac{u_e^2}{C_p T_e} \quad (34)$$

$$\beta = \frac{2\xi}{U_e} \frac{dU_e}{d\xi} \quad (35)$$

$$t = \frac{r}{r_0} \quad (36)$$

$$\phi_{ss} = \frac{C_D D(y)}{B(y) \ell^2} \frac{\xi}{r_0^{2j} \rho_e u_e u_e} \quad (37)$$

$$\bar{\epsilon} = 1 + \frac{\epsilon}{\mu} \Gamma \quad (38)$$

and

$$\tilde{\epsilon} = 1 + \frac{\epsilon}{\mu} \frac{Pr}{Pr, t} \Gamma \quad (39)$$

The function Γ appearing in equations (38) and (39) represents the streamwise intermittency distribution in the transitional region of the boundary layer, and is a function of the x -coordinate only.

For the purpose of this study, the boundary conditions in the transformed plane were as follows:

Wall Boundary:

$$\begin{aligned} F(\xi, 0) &= 0 \\ V(\xi, 0) &= 0 \\ \theta(\xi, 0) &= \theta_w, \text{ a constant} \end{aligned} \quad (40)$$

Edge Conditions:

$$\begin{aligned} F(\xi, \eta_e) &= 1 \\ \theta(\xi, \eta_e) &= 1 \quad (\text{Ref 19, 20}) \end{aligned}$$

In the following section, the turbulent transport models (eddy viscosity and eddy conductivity) used in this work are discussed.

Turbulent Transport Models

The basic model used in this study was that of Cebeci, Smith, and Mosinkis (Ref. 27:1975-76). This model treats the turbulent boundary layer as a composite layer consisting of an inner region and outer region as shown schematically in Figure 3.

Inner-Region Model. The eddy viscosity model used for the inner region is based on the mixing-length hypothesis of Prandtl (Ref. 21). The eddy viscosity for this region, referenced to the molecular viscosity, may be expressed as:

$$\epsilon_i = \bar{\lambda}^2 \frac{\partial u}{\partial y} \quad (41)$$

where $\bar{\lambda}$, the mixing length, may be written as:

$$\bar{\lambda} = K_1 y \quad (42)$$

To account for the region close to the wall, Van Driest (Ref. 22) suggested a modification for the mixing length of Prandtl. The correct form for the mixing length in the viscous sub-layer was given as:

$$\bar{\lambda} = K_1 y \{1 - \exp(-y/A)\} \quad (43)$$

where the exponential term is due to the damping effect of the wall on the turbulent fluctuations. The parameter A is usually referred to as a damping constant. The exponential term approaches zero at the outer edge of the viscous sub-layer so that the law-of-the-wall, equation (42), is valid and it accounts for the effect of kinematic viscosity on the turbulence near the wall. The damping constant A is given as:

$$A = 26\nu \left[\frac{\tau_w}{\rho_w} \right]^{-\frac{1}{2}} \quad (44)$$

with the subscript w denoting values at the wall. Equation (43) was developed for a flat plate. To account for flows with non-zero pressure gradient, the constant A is modified as follows. From the momentum equation, it follows that the shear stress close to the wall may be written as:

$$\tau = \tau_w + \left(\frac{dp}{dx} \right) y \quad (45)$$

If A were redefined to be $26\nu(\tau/\rho)^{-\frac{1}{2}}$ then Eq (45) leads to:

$$A = \left[26\nu \left[\frac{\tau_w}{\rho} + \frac{dp}{dx} \frac{y}{\rho} \right]^{-\frac{1}{2}} \right]$$

Then, the corresponding expression for the inner-region eddy viscosity becomes:

$$\epsilon_{inner} = \left[K_1^2 y^2 \left[1 - \exp \left\{ -\frac{y}{26\nu} \left(\frac{\tau_w}{\rho} + \frac{dp}{dx} \frac{y}{\rho} \right)^{\frac{1}{2}} \right\} \right]^2 \left| \frac{\partial u}{\partial y} \right| \right] \quad (47)$$

Outer-Region Model. The eddy viscosity in the outer region is given by the expression:

$$\epsilon_{outer} = K_2 \int_0^{\infty} (u_e - u) dy$$

$$\text{or} \quad \left(\frac{\epsilon}{\mu} \right)_0 = K_2 \frac{\rho u_e}{\mu} \delta^* \quad (48)$$

$$\text{where} \quad \delta^* = \int_0^{y^e} \left[1 - \frac{u}{u_e} \right] dy \quad (49)$$

In order to account for the intermittent character of the outer-layer flow, equation (45) is modified by an intermittency factor obtained by Klebanoff (Ref. 28).

$$\frac{\epsilon}{\mu} = K_2 \frac{\rho u_e}{\mu} \delta^* \gamma \quad (50)$$

where the transverse intermittency factor $\gamma(y)$ is defined as:

$$\gamma = \frac{1}{2} [1 - \text{erf}\{5(y/\delta - 0.78)\}]$$

and approximated by

$$\gamma = \{1 + 5.5 (y/\delta)^6\}^{-1} \quad (51)$$

which is a convenient and sufficiently accurate approximation to the error function.

The choice of K_1 and K_2 in the eddy-viscosity formulae depends slightly on the definition of the boundary-layer thickness δ . In several previous studies, (for example Ref. 29:174-191), the values of the constants K_1 and K_2 are taken to be 0.4 and 0.0168 respectively, and δ is defined as the normal distance from the surface to a point in the field at which F was equal to 0.995.

The constraint used to define the inner and outer region is the continuity of the eddy viscosity. Starting from the wall, the expression for the inner-eddy viscosity applies until $\epsilon_i = \epsilon_o$, provided that $Y^+ \geq 50$. If $Y^+ < 50$ when $\epsilon_i = \epsilon_o$, then the switch point is delayed until Y^+ becomes 50 and ϵ_i becomes equal to ϵ_o at $Y^+ = 50$. This prevents the

suppression of the fully turbulent portion of the velocity profile that can occur at lower values of R_{e_θ} . This effect persists to higher and higher values of R_{e_θ} as the mach number increases. Figure 3 shows a typical eddy-viscosity variation across the boundary layer for flow over a flat plate.

Eddy Conductivity

The eddy conductivity is formulated in terms of a static turbulent Prandtl number $P_{r,t}$ and the eddy viscosity ϵ {see equations (9) to (11)}. The two-layer concept for the eddy viscosity model suggests that there should also be a two-layer model for static turbulent Prandtl number. Numerous assumptions have been made concerning the eddy conductivity, and one of the earliest assumptions, which has been used extensively, employed a constant value of unity for the static turbulent Prandtl number. However, experimental data definitely shows that $P_{r,t}$ is a function of (y/δ) ; hence, this assumption is expected to lead to error.

The incompressible data indicates that $P_{r,t}$ ranges between 0.7 and 0.9. Simpson, Whitten and Moffat (Ref. 30) found that $P_{r,t}$ ranges from approximately 0.95 at $(y/\delta) = 0.1$ to 0.45 at $(y/\delta) = 1.0$. The data in this region were predicted well by the expression

$$P_{r,t} = 0.95\{1 - 0.5(y/\delta)^2\}$$

as proposed by Rotta (Ref. 23).

For compressible flow, where very limited experimental data are available, $P_{r,t}$ has a value very near unity in the outer region of the boundary layer and a value between 0.7 and 0.9 at the wall boundary (Ref. 24). Meir and Rotta (Ref. 25) found that for $1.75 \leq M_\infty \leq 4.5$, $P_{r,t}$ increased above unity for $Y^+ < 50$ and ranged between 0.8 and 0.85 as the outer edge of the boundary layer was approached.

The assessment of the current value for $P_{r,t}$ must be based upon the agreement between experimental and calculated temperature profile over a wide range of flow variables. Due to inconclusiveness of much of the experimental data which exists to date, a constant value of $P_{r,t}$ equal to 0.9 is utilized in the present analysis.

The following chapter, discusses the linearization and discretization of the governing equation, followed by the computational technique to solve the system of non-linear parabolic finite-difference equations.

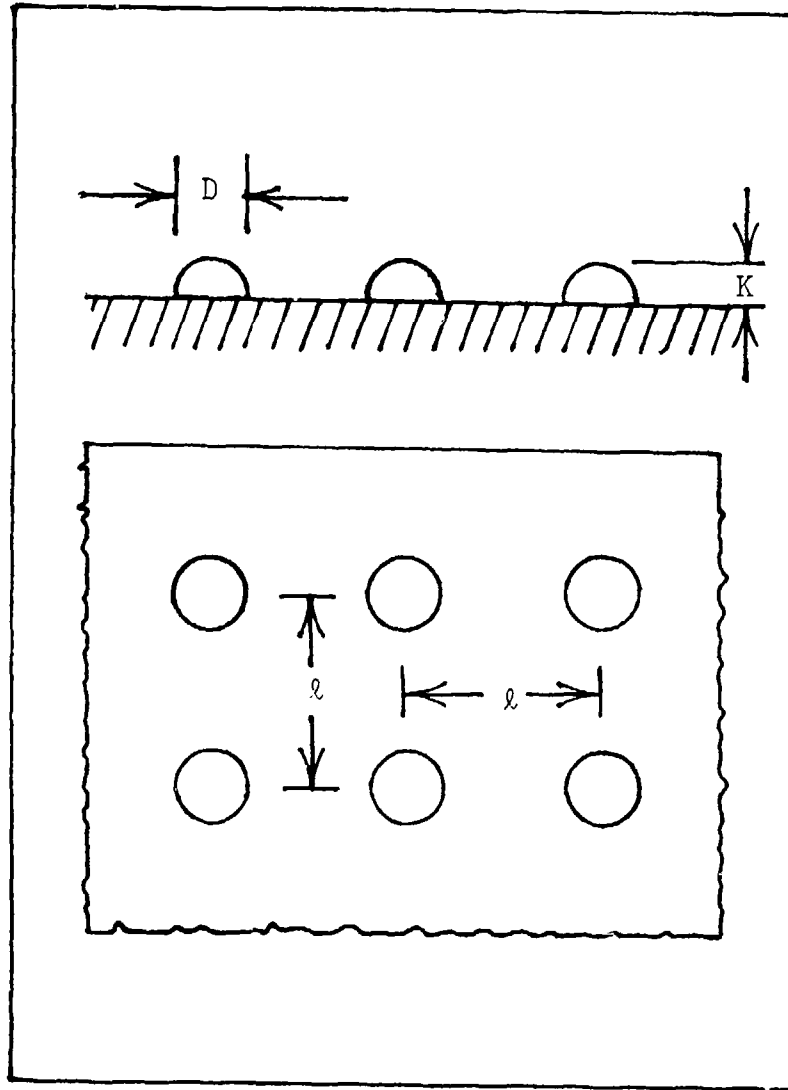


Fig. 1. Dimensions and Distribution of Roughness Elements with Circular Cross-section (From Ref 15:8)

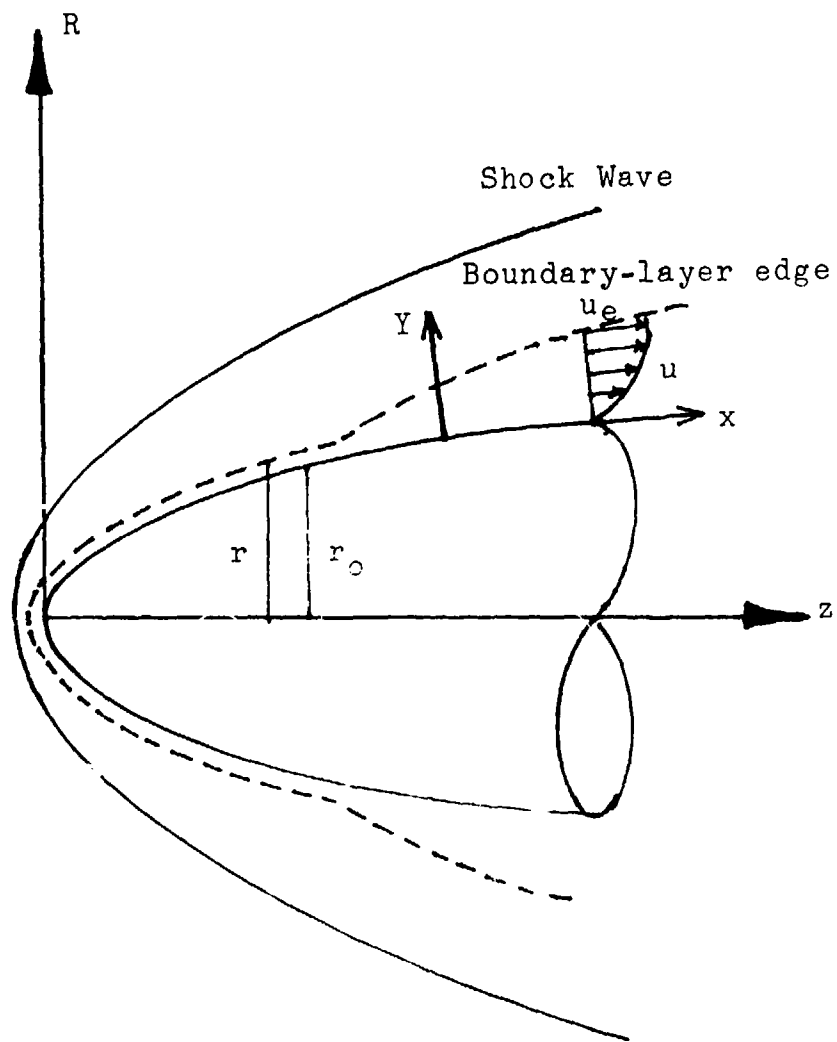


Fig. 2. Coordinate System and Notation
(From Ref 19:11)

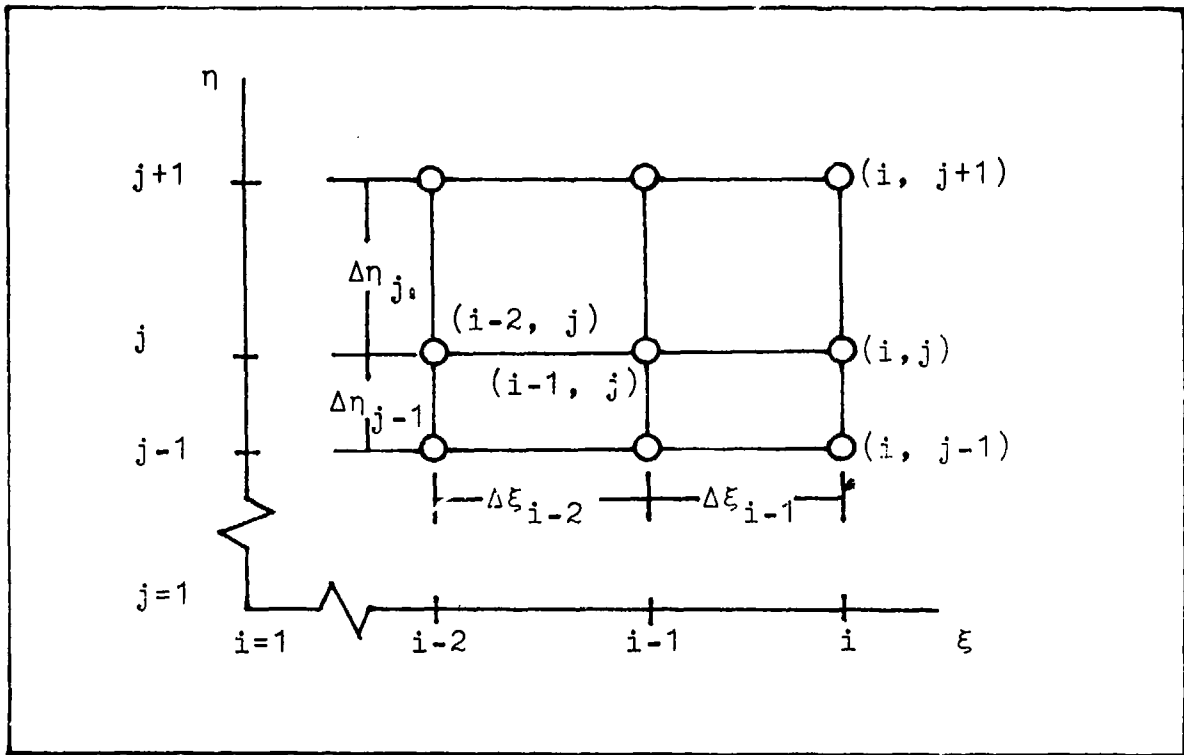


Fig. 4. Finite Difference Grid for Boundary Layer
(From Ref 19:33)

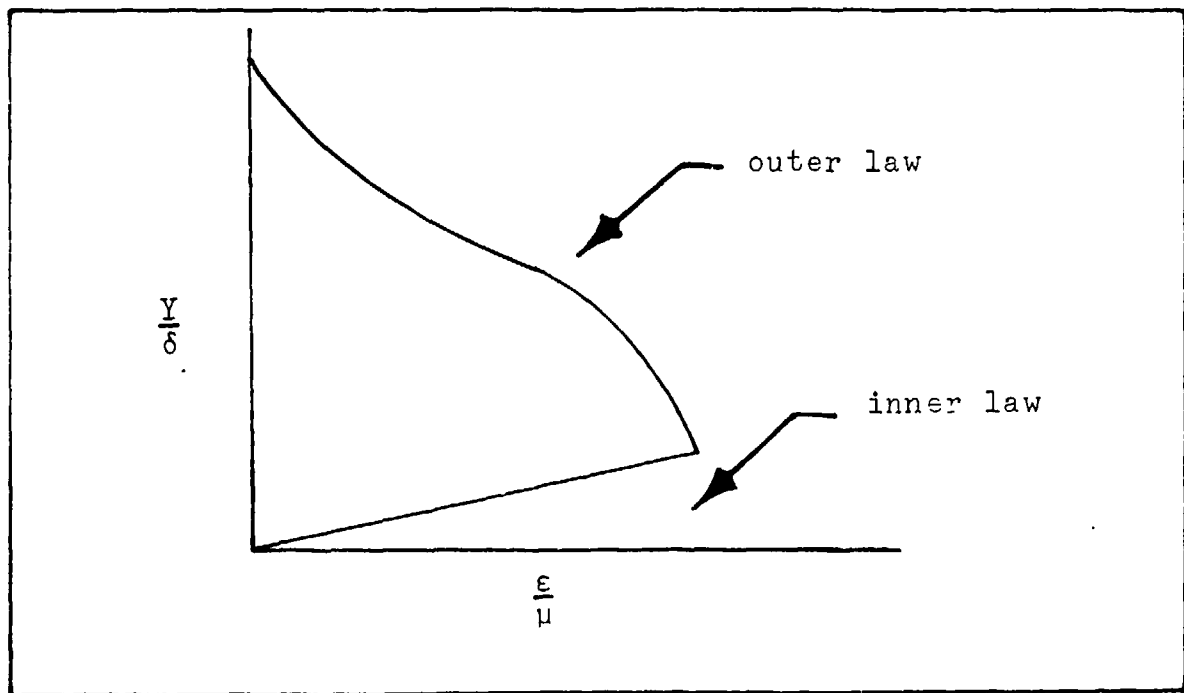


Fig. 3. Matching the Inner and Outer Eddy Viscosity
Models (From Ref 19:21)

III. Method of Solution

The system of governing equations for compressible laminar, transitional and turbulent boundary layers consists of three coupled non-linear partial differential equations (Equations (30) to (32)) and two algebraic relations (Equations (13) and (14)). The most important feature of this system is that it is parabolic and, therefore, can be numerically integrated in a step-by-step procedure in the streamwise direction. In order to cast the equations into a form in which the marching procedure can be efficiently utilized, the derivatives with respect to ξ and η are replaced by linear finite-difference quotients. In constructing the difference quotients, the sketch of the grid-point distribution presented in Figure 4 is useful for reference.

The solution is obtained in the transformed plane for arbitrary grid-point spacing in the ξ -direction and for a spacing in η -direction such that the ratio of the spacing between any two successive pairs of grid points is a constant.

The advantage of having variable grid-point spacing in the ξ -coordinate becomes clearly apparent for problems in which either the rate of change of the boundary conditions is large or discontinuous or the mean flow profiles are changing rapidly. Variable grid-point spacing in the

ξ -direction is implemented by having very small steps in the initial region where the flow gradient is very severe and again in some downstream region where transitional flow exists. In the present analysis, certain stations in the ξ -direction were designated where the streamwise step was doubled from its value at the preceding station. Hence, larger $\Delta\xi$ step sizes are utilized as the flow progresses downstream. Variable spacing in η -direction is even more critical since the flow gradients near the wall are extremely large, whereas these gradients vanish near the edge of the boundary layer. The relationship between $\Delta\eta_i$ for the chosen grid-point spacing is given by the following equation (Ref. 19:32-33)

$$\Delta\eta_i = (k)^{i-1} \Delta\eta_1 \quad (i = 1, 2, 3 \dots N) \quad (52)$$

where k is the ratio of any two successive steps.

Difference Equations

Three-point central-difference relations in η -direction and two-point backward or three-point backward difference relations in the ξ -direction are used to reduce the transformed continuity, momentum, and energy equations (Equations (30) to (32)) to a system of coupled difference equations. Following the quasilinearization (see Appendix C) of the non-linear terms, the difference quotients produce linear difference equations when substituted into the continuity, momentum, and energy equations. The resulting difference

difference equations are written symbolically as follows:

Momentum:

$$\begin{aligned} & A1(n,1)F_{n-1} + A1(n,2)F_n + A1(n,3)F_{n+1} \\ & + B1(n,1)\theta_{n-1} + B1(n,2)\theta_n + B1(n,3)\theta_{n+1} \\ & + C1(n,1)V_{n-1} + C1(n,2)V_n + C1(n,3)V_{n+1} = D1(n) \quad (53) \end{aligned}$$

Energy:

$$\begin{aligned} & A2(n,1)F_{n-1} + A2(n,2)F_n + A2(n,3)F_{n+1} \\ & + B2(n,1)\theta_{n-1} + B2(n,2)\theta_n + B2(n,3)\theta_{n+1} \\ & + C2(n,1)V_{n-1} + C2(n,2)V_n + C2(n,3)V_{n+1} = D2(n) \quad (54) \end{aligned}$$

Continuity:

$$\begin{aligned} & A3(n,1)F_{n-1} + A3(n,2)F_n + A3(n,3)F_{n+1} \\ & + B3(n,1)\theta_{n-1} + B3(n,2)\theta_n + B3(n,3)\theta_{n+1} \\ & + C3(n,1)V_{n-1} + C3(n,2)V_n + C3(n,3)V_{n+1} = D3(n) \quad (55) \end{aligned}$$

The coefficients $A1(n,1)$, $B1(n,1)$, $C1(n,1)$, and $D1(n)$, etc., are functions of known quantities at stations $i-1$ and $i-2$ and are detailed in Appendix D. The dependent variables F , θ , and V appear in a linear form as unknown at station i but are assumed to be known at stations $(i-1)$ and $(i-2)$. Since, the equations comprise

a system of parabolic partial differential equations, they can be solved by marching along ξ and a Gaussian elimination technique along η .

Computer Code

The computer code, ITRACT, available in the Flight Dynamics Laboratory computed the characteristics of laminar, transitional and turbulent flow for either planar or axisymmetric flow over smooth surfaces. This code was modified to include the present analysis for rough surfaces. To initiate this code, the following quantities were specified as inputs:

- γ - the ratio of specific heat
- P_r - laminar Prandtl number
- $P_{r,t}$ - turbulent Prandtl number
- ω - the exponent in Sutherland's viscosity law
- BO - ratio of wall temperature (T_w) to free stream stagnation temperature^w(T_o)
- X_{tr} - the streamwise location of transition from laminar to turbulent flow
- IDIFF - a flagged quantity, to specify the three-point or two-point differencing scheme for the streamwise derivative
- J2DA - a flagged quantity, to specify a 2-D or axisymmetric flow

The data regarding the size, shape and density of the roughness elements was provided to the program in subroutine RUFVAR (Appendix E). The computer code provided description of the boundary layer characteristics. Some of the output of interest in the computer code consists

of the boundary-layer profiles for Mach number, static temperature, velocity, density, eddy-viscosity, enthalpy and pressure. It also provides values of boundary-layer thickness, boundary layer momentum thickness, the coefficient of friction, eddy viscosity, and Stanton number which is a description of heat-transfer at the surface.

The transformation from the (x,y) plane to the (ξ,η) plane casts the boundary layer into a rectangular grid of nodes with the surface of the model located at the level $j=1$, as shown in Figure 4 where subscript (i,j) refers to ξ,η indices. The mesh spacing in the i,j direction are $\Delta\xi_i$ and $\Delta\eta_j$, respectively, which are not constant, for reasons explained earlier.

The computer code solves the linear difference equations (53) to (55). The solution of this system of equations was determined by computing values of F , θ , and V at each of the nodes within the grid. With all the values of these variables known at station $i-2$ and $i-1$, the values of F , θ , and V were solved at all points j at station i using a three-point differencing scheme and a Gaussian elimination technique. With the boundary-layer solution completed at the station i , the computer code marched to station $i+1$ in the streamwise direction and the dependent variables F , θ , and V were determined in a similar manner at the preceding station. The entire program was therefore a sequential solution at a series of ξ -stations from the leading edge to the trailing edge of

the model. Hence, the computer code followed the step-by-step procedure depicted in Figure 4. With a program listing included in Appendix E, the main portion of the logic presented in Figure 5 required further explanation; hence, Appendix F was included to discuss four important portions of the code. These included the non-dimensionalization of the working variables, the computation of eddy viscosity, Stanton-number, skin-friction coefficient and the roughness variables $f(y)$, $B(y)$, and ϕ_{ss} . A Fortran computer code key is also included as Appendix G.

Inputs including γ , Pr , P , r , t , M_∞ , T_∞ , stepping data is transformed plane, T_w/T_o , turbulent transition and intermittency consideration, L , ρ_o , dimensions and density of roughness elements.

Compute Re

Nondimensionalize the key working variables

Initialize the grid profile

Enter the Main Loop

Do to label 115 for each nodal point in a vertical direction at station s_i

Compute nondimensional properties at edge of boundary layer

Return from label 115 to recompute at station s_{i+1}

Compute ξ , $\Delta\xi$, Re_ξ , step length functions, α , and β

Label 6998
Set the total number of modal points in one column of the grid

Return from label 7005

Compute coefficients A, B, C, and D for finite difference equations

Compute current station s_i values of F , θ , and V

Continued on following page

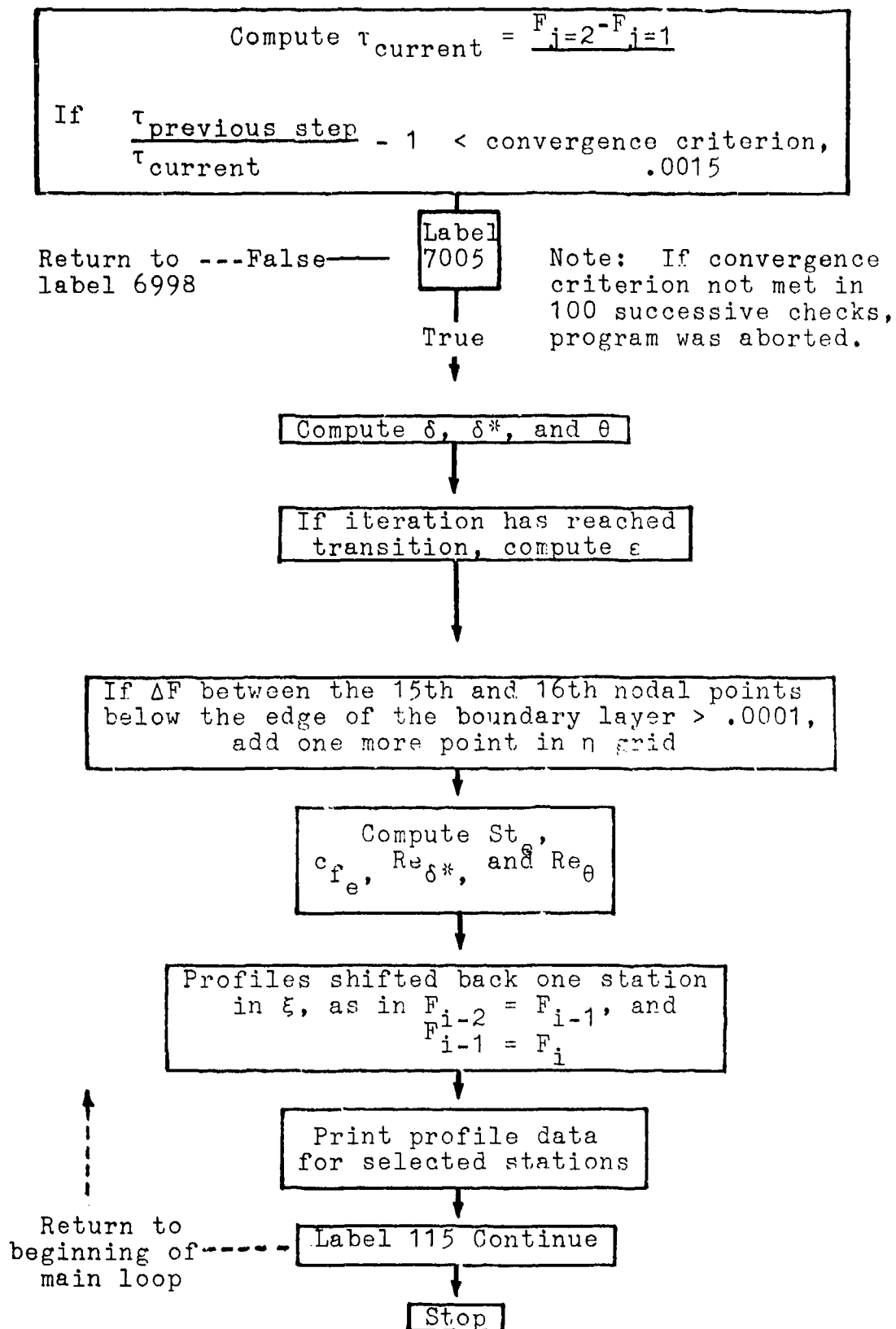


Fig 5. Flow Diagram of the Logical Steps to Solution With ITRACT

IV. Results and Discussions

The modified analysis and computer program are capable of predicting the effect of surface roughness on turbulent boundary layers. Prior to using it as a valid predictive method, it was necessary to establish the authenticity of the original code. For this purpose, results were first obtained using the original code, for turbulent flow over a smooth flat plate and compared with the experimental data of Dr. Fiore at the Air Force Wright Aeronautical Laboratories and Dr. Donald Coles, at the Jet-Propulsion Laboratory, California. Thereafter, calculations were made for the case of turbulent flow over rough surface and the computed boundary-layer profiles for velocity, static temperature, pitot pressure, Mach number, density and stagnation temperature were compared with the corresponding experimentally obtained boundary-layer profiles. Further, the computed profile for the rough surface were compared with the computed profiles for the smooth surface, so as to appreciate the effect of surface roughness on the flow.

In these studies, a number of important assumptions were made. First, the boundary-layer computation and the comparison were performed for flow over a flat plate; hence, the effect due to the stagnation region at the leading edge and the shocking phenomena were neglected.

Shapiro has alluded to the validity of the assumption of free-stream conditions existing at some distance downstream of the leading edge of a plate (Fig 2 -21(c) and the subsequent text (Ref. 35:1149-1150). Hence, free-stream conditions were assumed to exist downstream the shock wave. Further, the angle of incidence of the model was assumed to be zero with respect to the flow in the free stream. Second, the boundary-layer thickness, δ , was minutely small compared to the characteristic length L . Further, the pressure change across this boundary layer thickness was negligible. Third, the problem was limited to experimental cases where pressure change along the streamwise direction was also negligible. Numerically, $\frac{dp}{dx}$ was considered zero. Also, the flow was considered fully turbulent at the station where the comparison of the results were made. Fourth, the flow was considered inviscid and potential beyond the edge of the boundary layer. Finally, the Navier-Stokes equations were simplified to the boundary-layer equations to describe the flow characteristics for $y < \delta$ (Ref. 3:117-121).

In all cases presented herein, the gas is taken to be air and is assumed to behave as a perfect gas with a constant ratio of specific heats ($\gamma = 1.4$), a constant Prandtl number ($P_r = 0.72$), and a constant static turbulent Prandtl number ($P_{r,t} = 0.9$). The molecular viscosity μ is evaluated from Sutherland's viscosity law. The external pressure distribution used is either experimental

or obtained from an exact solution of the full inviscid
Euler equations.

Turbulent Flow Over Smooth Flat-Plate

Comparison With Dr. Fiore's Data (Ref 37). For the purpose of this study, the results obtained from the original computer were compared with Dr. Fiore's data for turbulent flow over a smooth flat plate. The experiment was conducted at a Mach number of 5.92 and a Reynolds number Re_x of $3.6(10)^7$. The free-stream stagnation temperature and stagnation pressure were $1098^\circ R$ or 1995.38 psia, respectively. The free-stream conditions and the data of this experimental study are tabulated in Table I. The computer code results were obtained for the same free-stream conditions. The point at which the transition from laminar flow to turbulent was initiated, was obtained from the transition Reynolds number of $1.5(10)^6$. The wall temperature was $602^\circ R$. The length of the model was 17.15 inches, and the boundary layer profiles computed at the end of the flat plate (i.e., $X/L = 1.0$) were compared with the experimental profiles.

There is excellent agreement between the computed and the experimental boundary-layer profiles as shown in Figures 7 through 12, except in the region close to the wall. The velocity profiles as shown in Fig. 7 compared very well, except in the sub-layer region where the computer code overpredicts the velocity slightly. On

the other hand, the temperature profile (Fig. 8) is slightly underpredicted in the same region, which is quite understandable due to the fact that the stagnation temperature remains constant. The same trend is observed in the boundary-layer profiles for density, Mach number, total temperature and pressure is depicted in Figures 9, 10, 11, and 12, respectively. The discrepancy in the sub-layer region could be associated with either of the following two sources of error:

(a) The Cebeci-Smith-Mosinski's model used in this study to describe the sub-layer region of the boundary layer was not adequately taking into account the intermittent nature of the turbulence in this region.

(b) The boundary-layer probe installed at the base of the model could influence the force-balance measurements. This could result in a lower experimental pressure ratio near the wall, thereby causing some error in the temperature profiles (Ref 39).

The two possibilities mentioned above were examined further. It was observed that the Cebeci-Smith-Mosinski's model has been used extensively in many previous studies (Ref. 19) and has been found to predict sub-layer region very accurately. While investigating the classical eddy viscosity models in an attempt to establish a benchmark for future development of turbulent boundary layer research, Shang, Hankey, and Dwoyer (Ref. 19) found that the Cebeci-Smith-Mosinski's model was adequate to predict

the boundary layer in the sub-layer region. Hence, the first possible source of error was discarded. The size of the probe used in the experimental study was of the order of the sub-layer thickness which could influence the flow, thereby leading to a lower experimental pitot pressure ratio near the wall (Ref. 39).

To correctly establish the cause of the error in the sub-layer region, it was decided to carry out another comparison of the computed velocity and Mach number profiles with the experimental data of Dr. Cole (Ref. 38) for turbulent flow over a smooth flat plate.

Comparison With Cole's Data (Ref. 38). The comparison with Cole's data was carried out to check the accuracy of the original code, since the comparison with Dr. Fiore's data showed some discrepancy between the computed and the measured results in the sub-layer region. The data of Dr. Cole, as tabulated in Table II, was obtained from experimental investigation of turbulent flow over a smooth flat-plate for the test conditions as follows:

$$\begin{aligned}M_{\infty} &= 4.554 \\P_o &= 8132.788 \text{ lbf/ft}^2 \\T_o &= 522.64^{\circ}\text{R} \\T_w/T_o &= .6764\end{aligned}$$

The length of the flat-plate was 21.48 inches and the boundary-layer profiles were compared at $X/L = 1.0$. In Figs 13 and 14, the comparison between the computed

and experimental velocity and Mach number profiles is presented. It is observed that excellent agreement exists between the computed and experimental profiles everywhere, including the sub-layer region near the wall.

Via this comparison, the authenticity of the original computer code was established. The next step was to verify the roughness model and the modified computer code by conducting a comparison of the boundary-layer profiles predicted by the modified computer code with the experimental data of Dr. Fiore (Ref. 20) for flow over a rough flat plate.

Turbulent Flow Over Rough Flat-Plate

Comparison With Dr. Fiore's Data (Ref. 40) After the authenticity of the original code was established, the next step was to modify the computer code and then verify its results. Prior to comparing the results of the modified computer code with the experimental data for turbulent flow over a rough flat-plate, results for turbulent flow over a smooth flat-plate were obtained from the modified code, by specifying roughness elements in the code to be of zero dimension. The results obtained were in complete agreement with those from the original code discussed in the previous section and plotted in Figs 7 through 12. This showed that the inclusion of the roughness model to the code has not affected the computer code for turbulent flow over smooth surfaces.

Next, to verify the roughness model used in this study, the results computed by the modified code were compared with the experimental data of Dr. Fiore (Ref 40) of AFWAL, for turbulent flow over a rough flat plate.

The experiment was conducted at the following test conditions:

$$\begin{aligned}M_o &= 5.534 \\P_o &= 2003.53 \text{ psia} \\T_o &= 1122.94^\circ\text{R} \\T_o/T_w &= .5829 \\Re_x &= 3.665(10)^7\end{aligned}$$

The roughness element distributed over the flat plate had the following dimensions (Fig. 6)

- (i) Height of the element = $k = 0.02$ inches
- (ii) Breadth of the element = $b = 0.04$ inches
- (iii) Depth of the element in the flow direction = $C = 0.04$ inches

The density of the roughness elements was specified as follows (Fig. 6):

- (i) Spacing between two adjacent elements located along a line perpendicular to the flow direction = $B = .08$ inches.
- (ii) Spacing between two adjacent elements located along a line parallel to the flow direction = $C = .08$ inches.

The length of the flat plate was 17.15 inches, and the boundary-layer profiles computed at $X/L = 1.0$ were compared with the experimentally obtained boundary-layer profiles. The free-stream conditions and the experimental data are tabulated in Table III.

The results presented here are quite encouraging, in that a rather basic model yields results that are in good agreement with many of the observed trends regarding the influence of surface roughness. Figure 15 shows the excellent agreement obtained for the velocity profiles. The computed profile shows the expected increase in thickness and change of shape due to the presence of the roughness elements. The maximum error in the computed and the experimental velocity is about 1.88 percent and occurs near the wall, and is attributed to the same cause as for the smooth-wall case as discussed earlier in this chapter.

The predicted and the measured temperature profiles shown in Fig. 16 show the same trend, except that the computer code has overpredicted the static temperature. The distributed roughness elements over the surface cause the flow to slow down due to form drag in the wall region of the elements. This results in a higher static temperature in order to keep the total temperature the same.

The initial rise in the static temperature to about 827°R occurs in the region corresponding to the height of

the roughness element, i.e., for $y \leq .02$ inches. At $y > h$ (height of the element), the flow is no longer obstructed by the roughness elements and the temperature profile follows the same decreasing trend as that for the smooth surface profile. In the experimental results, the static temperature is approximately 670°R at $y = .02$ inches and the error is about 20% at this point. This discrepancy occurs in the sub-layer region and could be traced back to the influence of the probe on the flow (Ref 39). The thin wall region plays a very dominant role in determining the entire structure of the boundary-layer.

The density profiles shown in Fig. 17 depicts a trend consistent with that of the static temperature profiles since the density at a point in the boundary-layer is simply the reciprocal of the corresponding static temperature. The profiles are in reasonably good agreement, except in the region close to the edge of the boundary layer.

The experimental boundary-layer thickness (δ) is .383 inches and the measured data exhibits a monotonic increase in the density from the wall to the edge of the boundary layer. The same trend is observed in the computed profile also. Hence, if the density were plotted against y/δ , for $0 \leq y/\delta \leq 1$, then the profiles would appear to be in reasonable agreement. As y increases slightly beyond 0.4 inches, there is a sudden decrease in the experimental density values, with the free-stream

density value being attained shortly beyond $y = 0.4$. Actually this trend is not consistent with the static temperature profile given in the experimental data (Fig. 16).

Comparison of Computed Rough and Smooth Boundary Layer

Results

The velocity profiles with and without roughness are compared in Fig 21. Both the profiles are for turbulent flow over a flat plate. The two cases have slightly different free-stream conditions, as tabulated in Table IV. The smooth-wall profile exhibits fully developed turbulent flow characteristics and a smooth monotonic increase in velocity from zero at the wall to the free-stream value at the edge of the boundary layer.

The effect of distributed surface roughness on the boundary layer development can be observed as a reduction in the values of the velocity in the wake of the roughness elements. In the roughness model, the rough surface is idealized as being made up of identical elements. The form-drag description of the roughness element causes the flow to slow down in their wake region; hence, the rough-wall profile is not as full as that corresponding to the smooth wall. Table V shows a corresponding increase in all the boundary-layer integral thicknesses when roughness is included.

Semi-empirical analysts of turbulent boundary layers

are often based on some form of law-of-the-wall correlation. The law-of-the-wall is defined most simply in terms of the dimensionless parameters

$$U^+ = \frac{U}{U_\tau} \text{ and } Y^+ = \frac{YU_\tau}{\nu_w} \quad (56)$$

where
$$U_\tau = (\tau_w/\rho_w)^{\frac{1}{2}} \quad (57)$$

Within the boundary layer, three distinct regions are found to exist; the sub-layer, the logarithmic region and the velocity-defect region. The general form of the relationships governing smooth-wall boundary layer is given by:

$$U^+ = Y^+ \quad \text{for } Y^+ < 11 \quad (58)$$

$$U^+ = \frac{1}{K} \ln Y^+ + C \quad \text{for } Y^+ > 11 \quad (59)$$

The effect of roughness on the law-of-the-wall equation has been shown to result solely in a shift in the intercept, C, in equation (59). The same trend has been predicted in the computed smooth and rough velocity profiles. The rough-wall profile looks similar to the corresponding smooth-wall profile, except that it is shifted towards lower values of velocities. This trend is consistent with the rough-wall results where the shift in the profile is directly related to the size and density of the roughness elements. The computed boundary-layer profiles show the expected increase in thickness and

change of shape due to roughness.

Skin Friction and Heat-Transfer

The addition of roughness elements to the smooth surface can significantly affect turbulent skin friction and heat transfer. The roughness model used in this study was tested for prediction of skin friction augmentation due to addition of roughness element to a smooth surface. A comparison between the computed skin friction values for a smooth surface and a rough surface was accomplished. The predicted skin friction coefficient for the two cases was plotted versus dimensional distance along the flat plate in Fig 29. In this study, square roughness elements with $K = .02$ " $b = d = .04$ " and $B = C = .08$ " were used. Fig 29 shows the expected increase in the skin friction. For rough surface the skin-friction was 40-60% higher as compared to smooth surface. The validity of the skin friction augmentation by the model could not be confirmed due to non-availability of any experimental data.

As regards heat transfer, the original model for calculation of Stanton number was not modified in this study, hence, the expected increase in the heat transfer due to roughness elements was not predicted by the code. On the other hand, a decrease in Stanton number was noted since smooth surface had a higher pressure gradient compared to the rough surface near the wall. Hence, a

need for incorporation of a suitable model for accurate prediction of heat transfer augmentation was felt. It may be noted, that, one particular useful aspect of this rough wall turbulence model is that the results can be examined to determine the nature of the roughness influence on turbulent boundary-layers. One rather conspicuous conclusion is that the Reynolds analogy between friction and heat transfer is not preserved with significant roughness. This result is well known and derives from the absence of a heat transfer analogy to form drag on elements. The computation shows that the velocity fluctuations increase in proportion to friction velocity $U^+ = (\tau_w/\rho_w)^{1/2}$, but the temperature fluctuations are hardly changed by roughness. Since $T_w \sim \overline{u'v'}$ and $q \sim \overline{v'T'}$, the heat transfer augmentation is the square root of the skin friction augmentation:

$$\frac{St}{St_o} - 1 = \frac{Cf}{Cf_o} - 1 \quad (60)$$

where subscript 'o' denotes smooth wall.

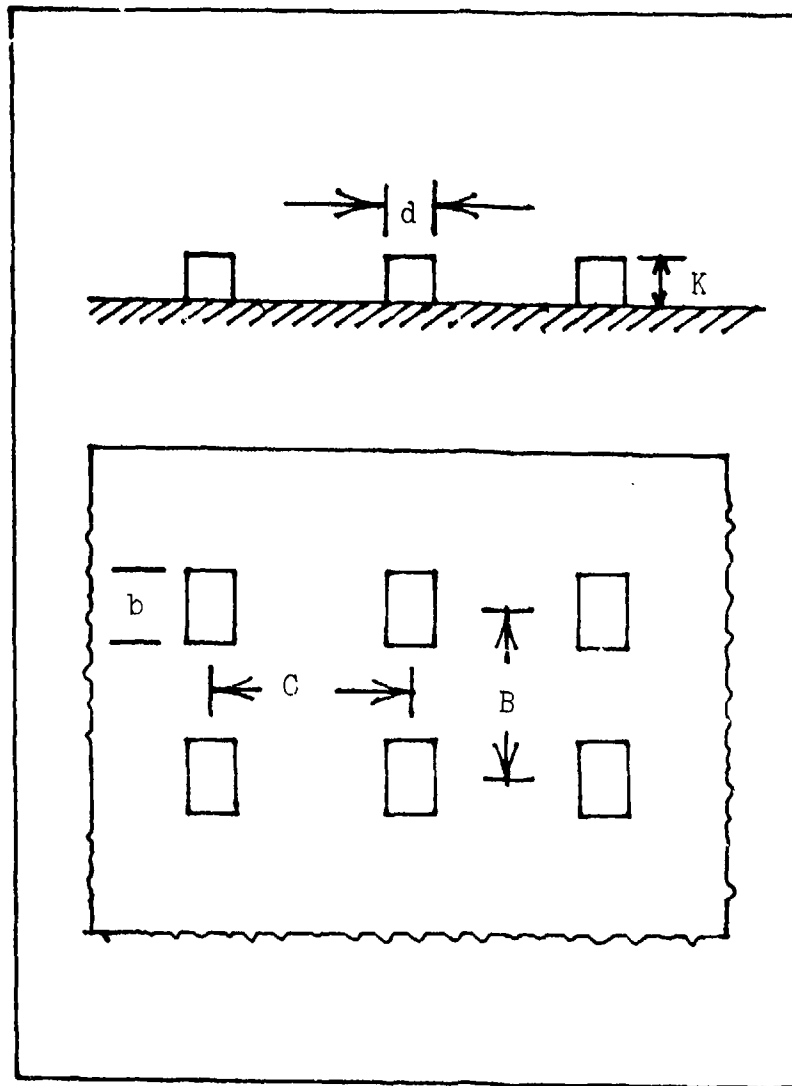


Fig. 6. Dimensions and Distribution of Roughness Elements with Rectangular Cross-section

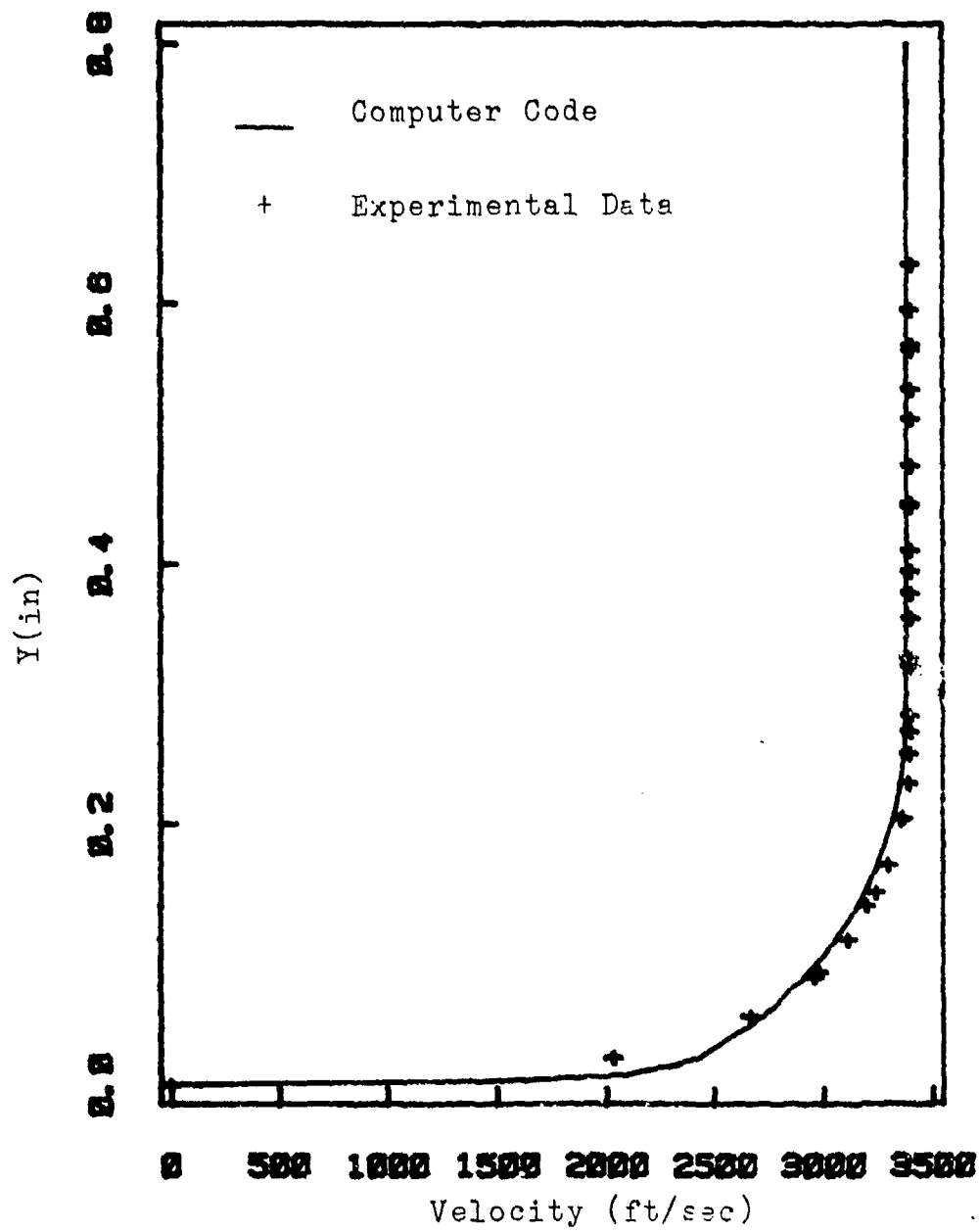


Fig. 7. Comparison of Computed Velocity Profile for Smooth Plate With Data of AFWAL (Ref 37)

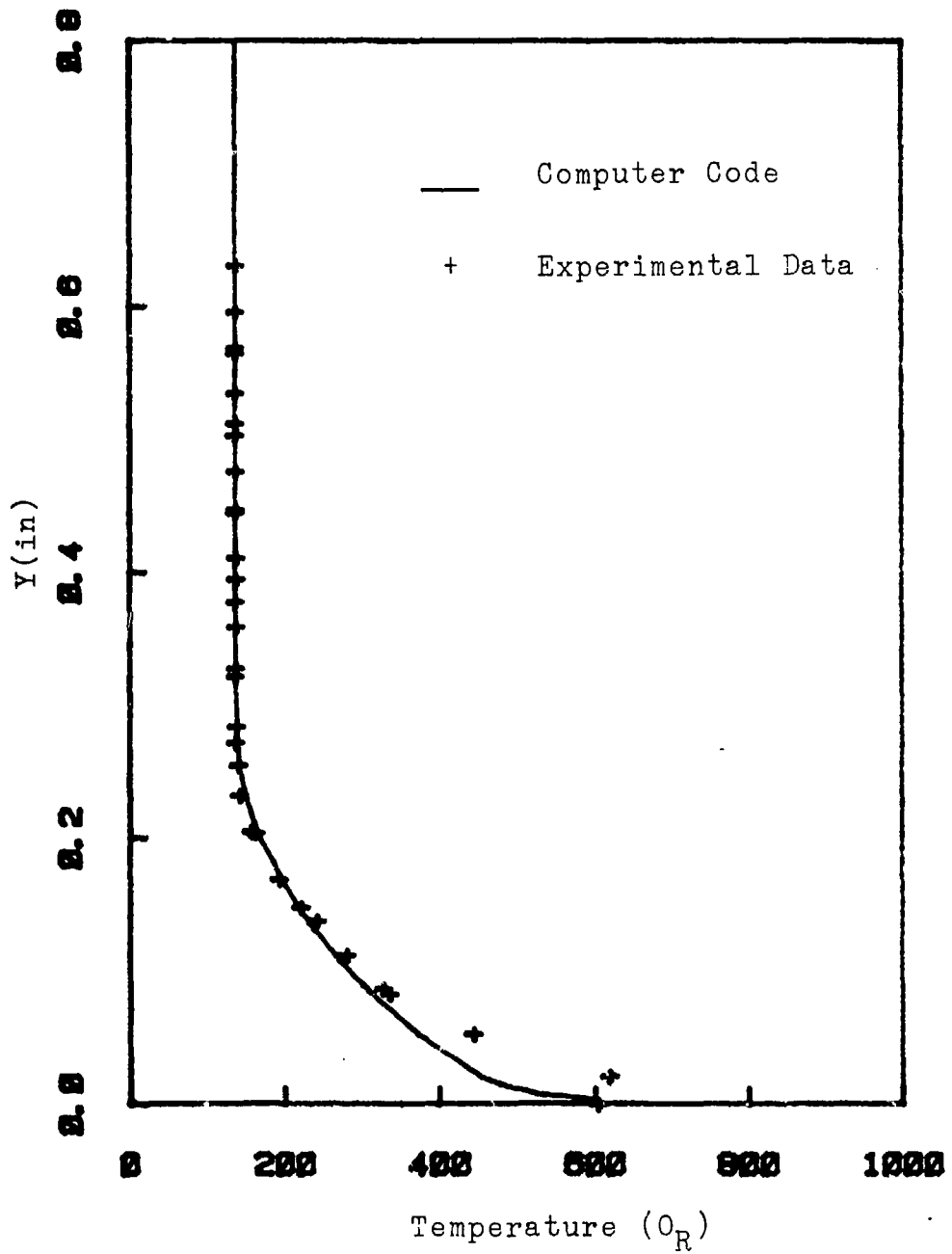


Fig. 8. Comparison of Computed Temperature Profiles for Smooth Surface With Experimental Data of AFWAL (Ref 37)

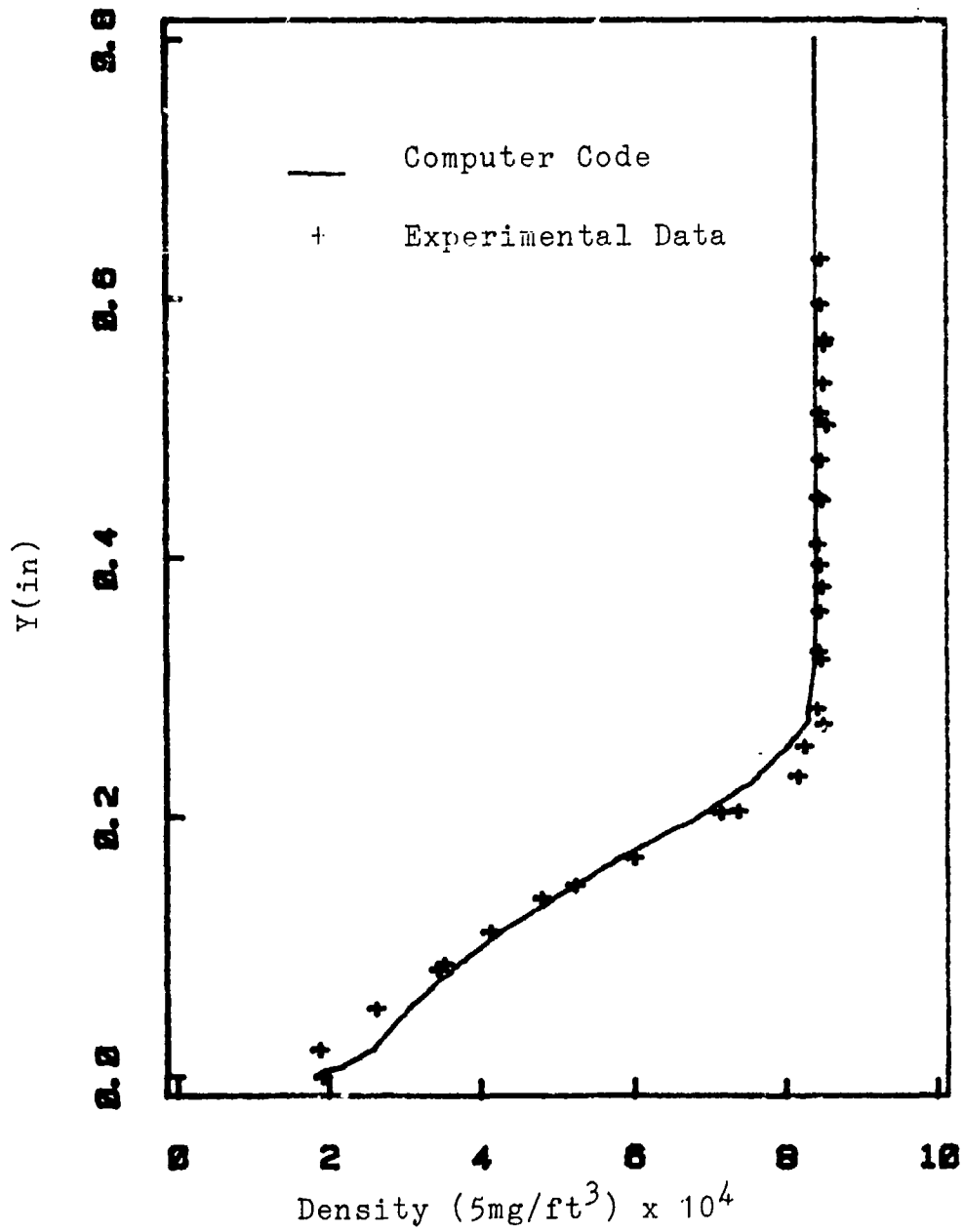


Fig. 9. Comparison of Computed Density Profile for Smooth Surface With AFWAL Data (Ref 37)

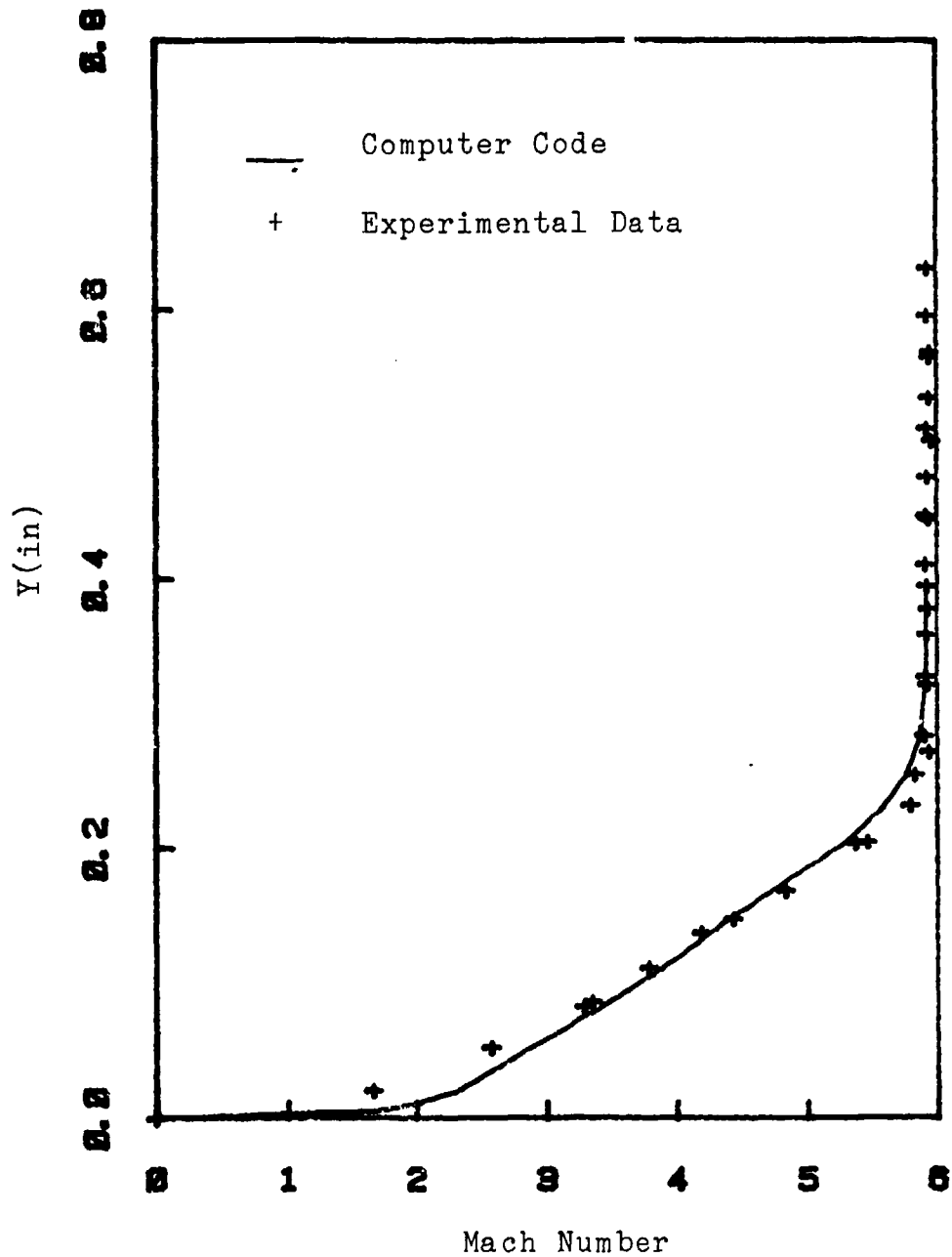


Fig. 10. Comparison of Computed Mach Number Profile for Flow Over Smooth Surface With AFWAL (Ref 37)

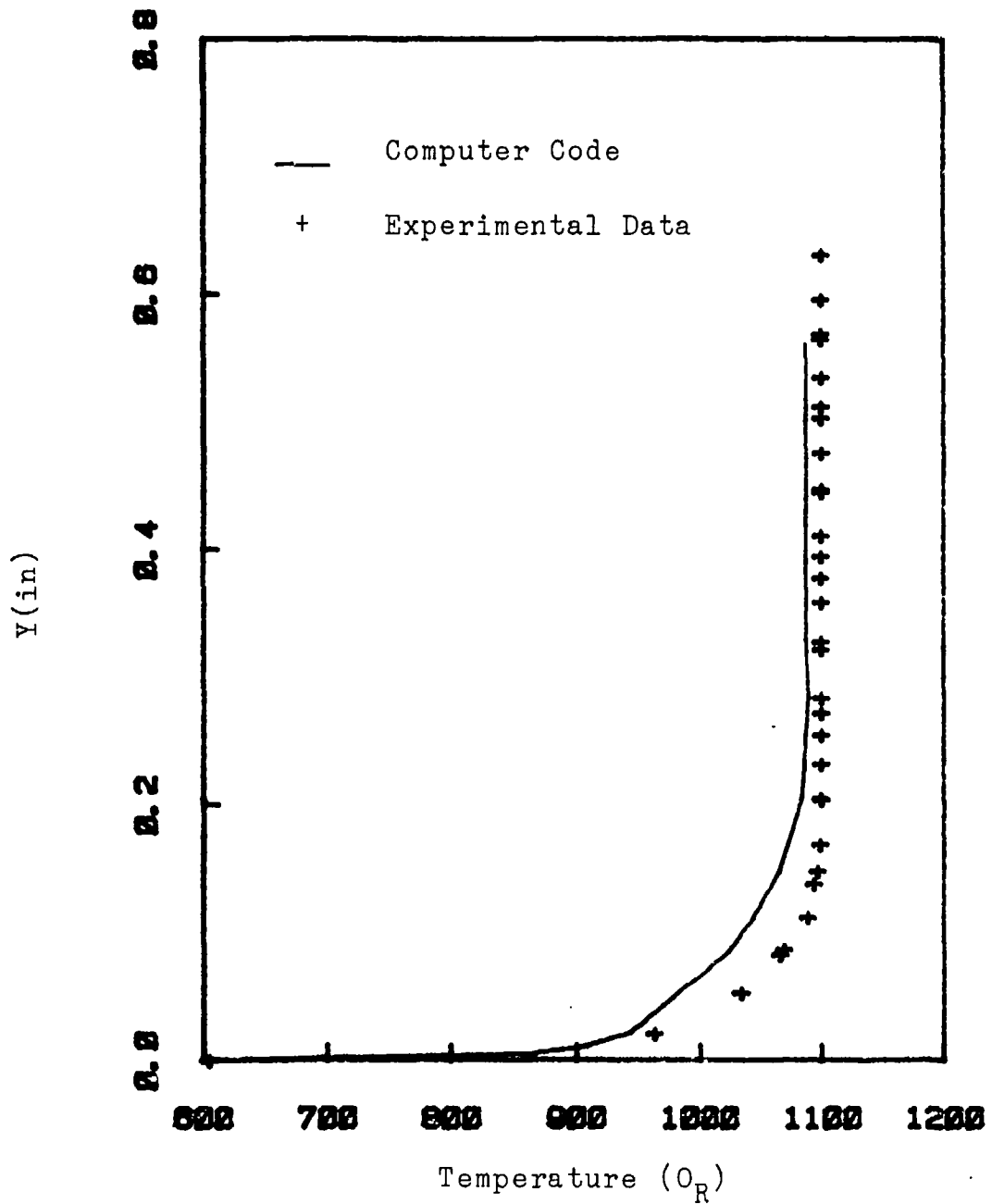


Fig. 11. Comparison of Calculated Total Temperature Profiles for Smooth Surface with AFWAL (Ref 37)

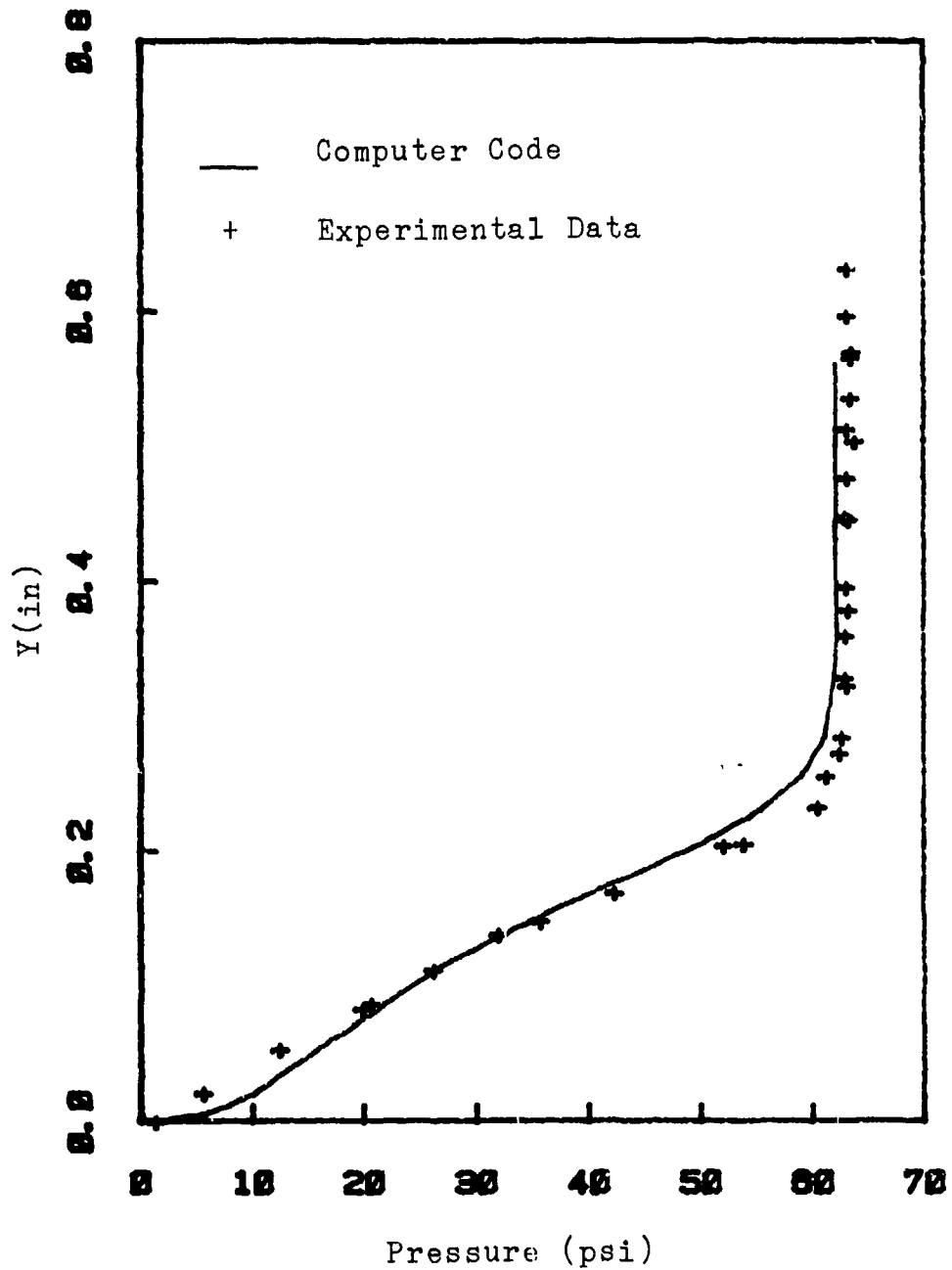


Fig. 12. Comparison of Computed Pressure Profile for Smooth Surface With AFWAL Data (Ref 37)

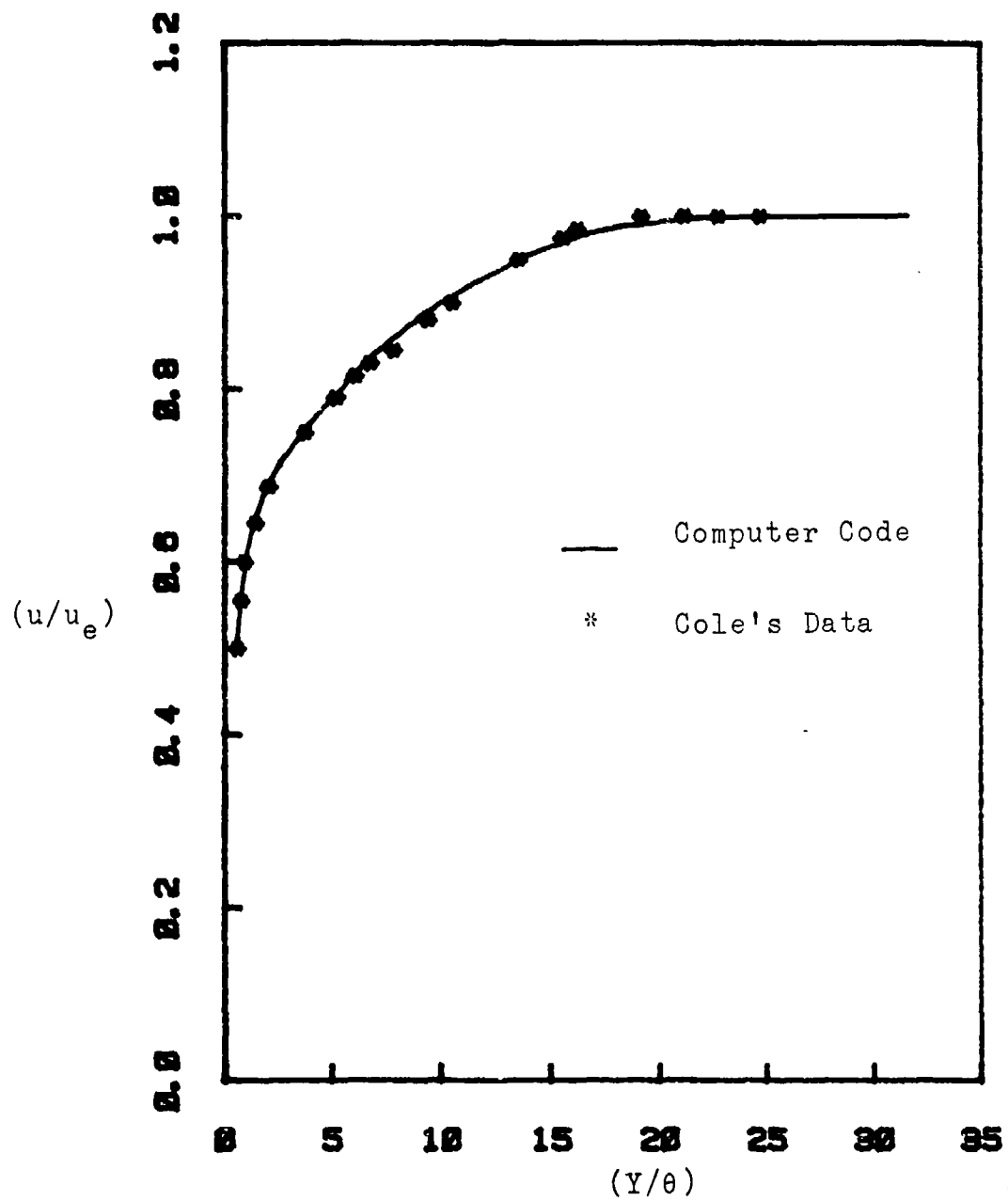


Fig. 13. Comparison of Computer Velocity Profiles for Flow Over Smooth Surfaces With Cole's Data (Ref 38)

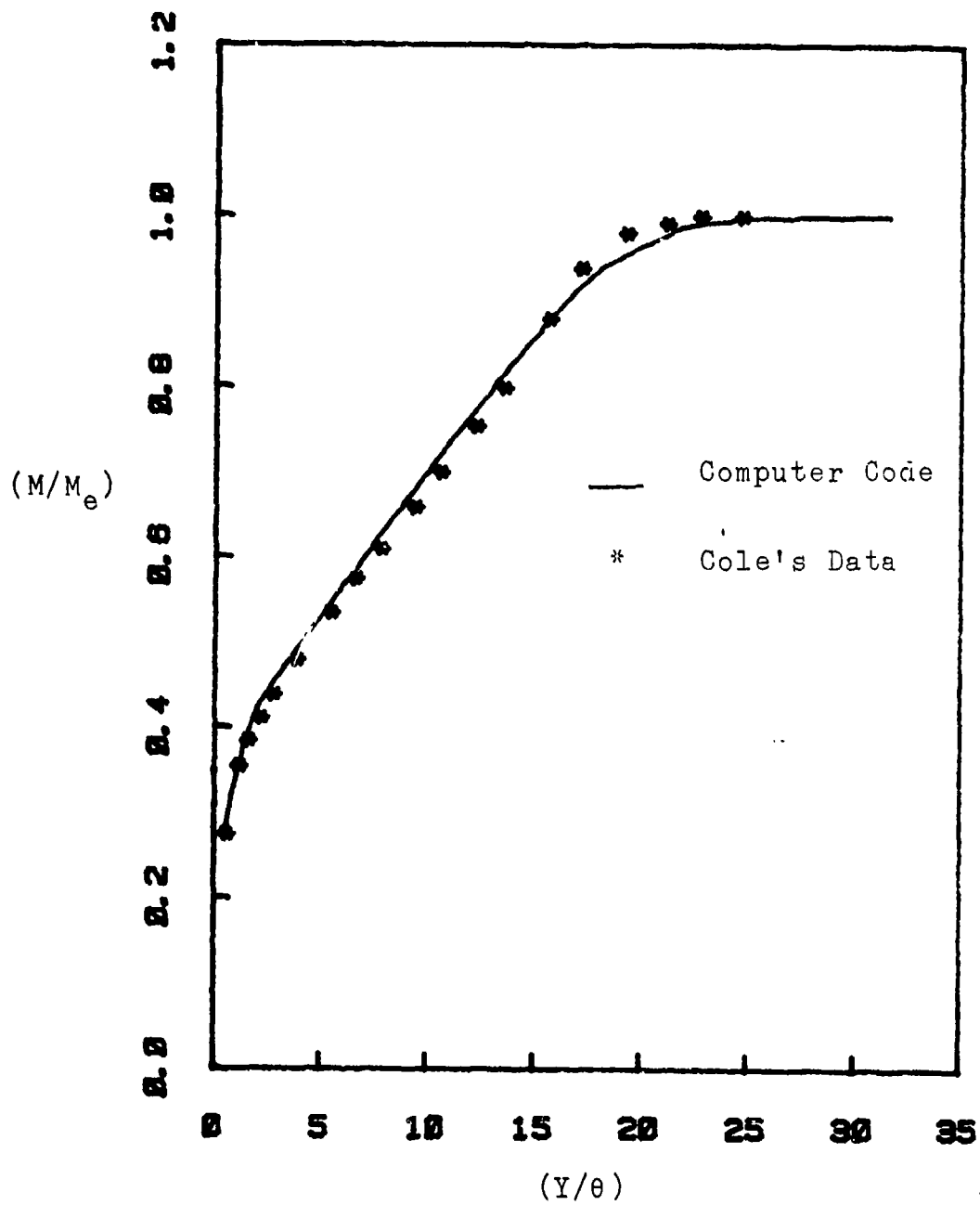


Fig. 14. Comparison of Computer Mach Number Profile With Cole's Data (Ref 38)

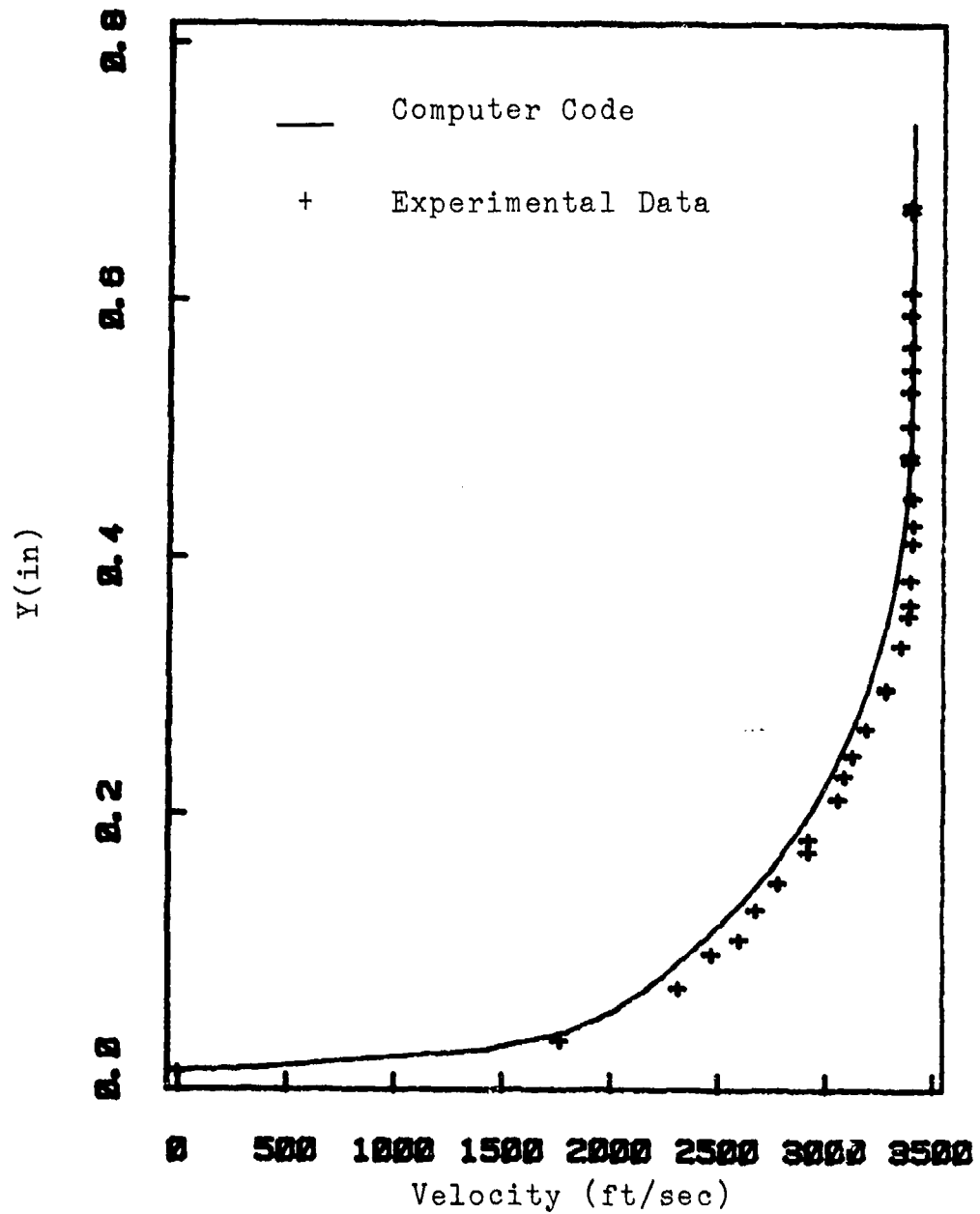


Fig. 15. Comparison of Computer Velocity Profile for Rough Surface With Experimental Data of AFWAL) (Ref 40)

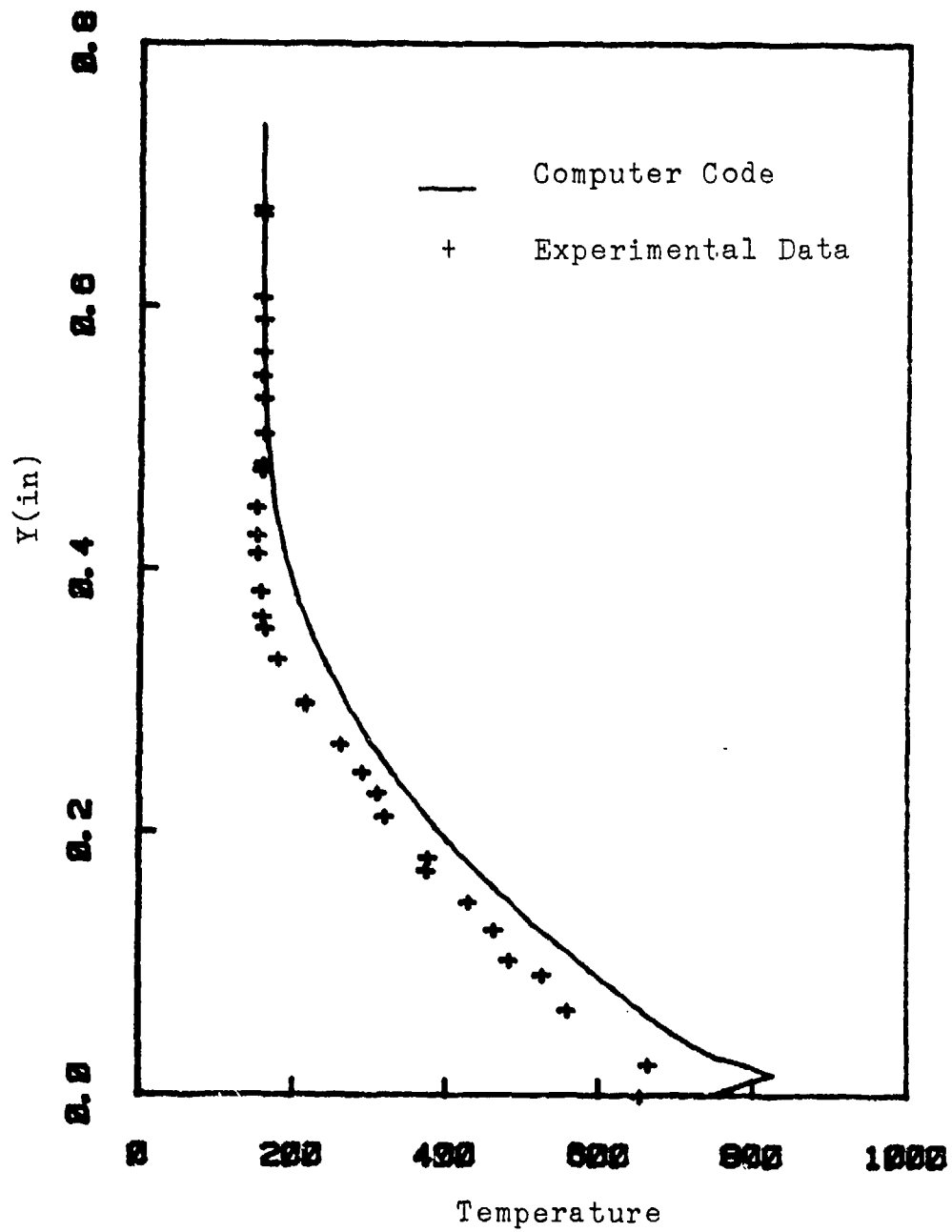


Fig. 16. Comparison of Temperature Profile for Rough Surface With Experimental Data AFWAL (Ref 40)

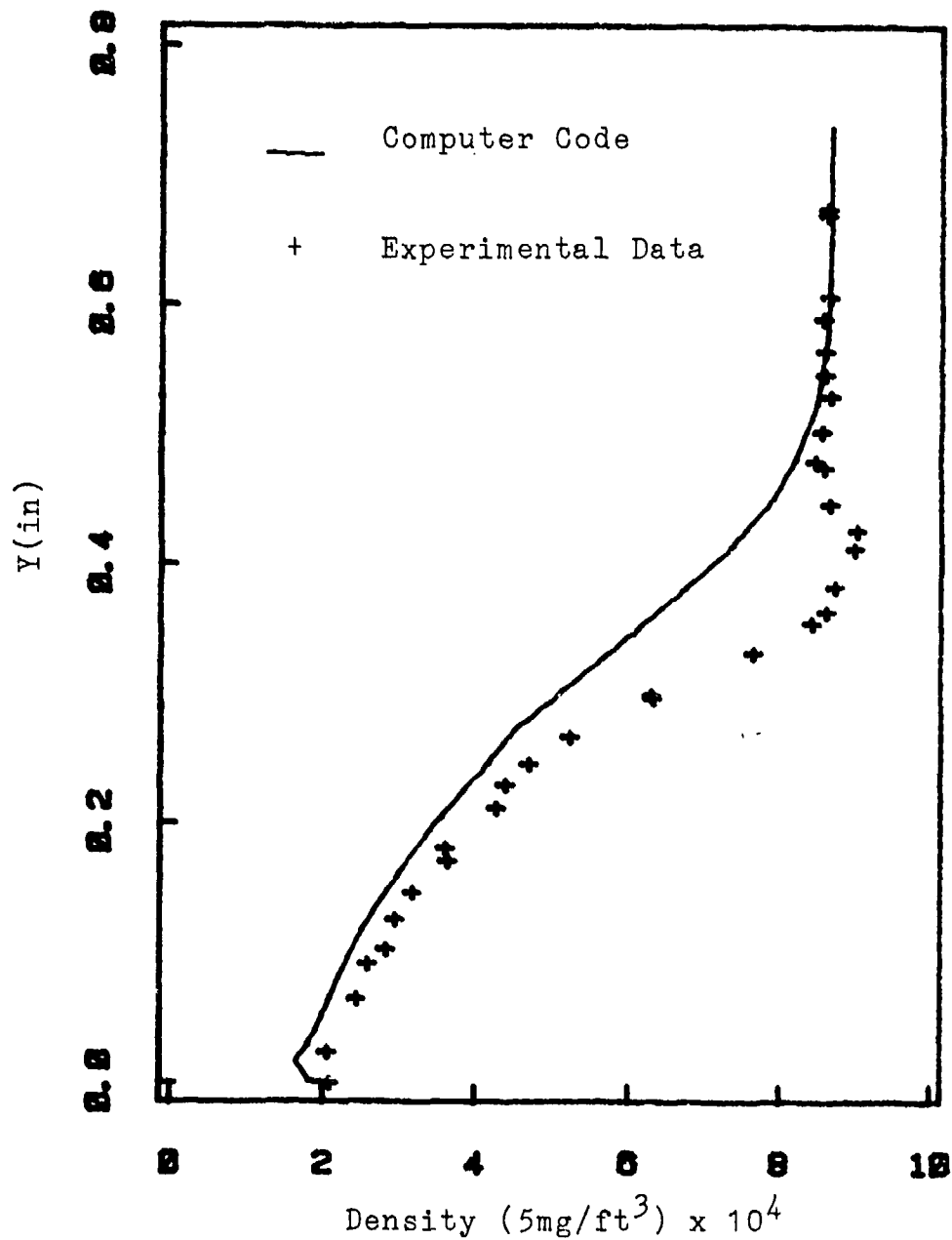


Fig. 17. Comparison of Computed Density Profile for Rough Surface With AFWAL (Ref 40)

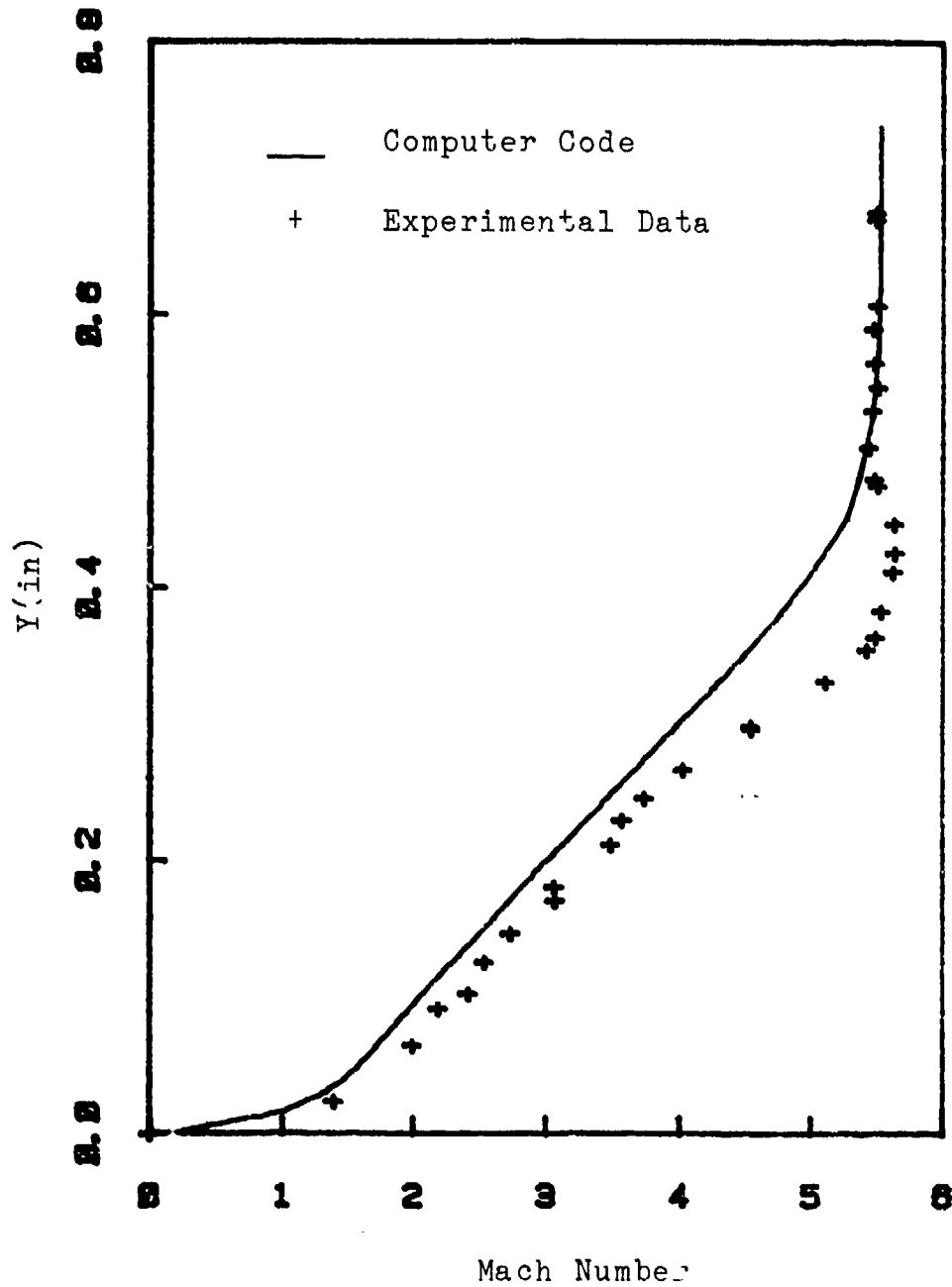


Fig. 18. Comparison of Computed Mach Number Profiles for Rough Surface With AFWAL (Ref 40)

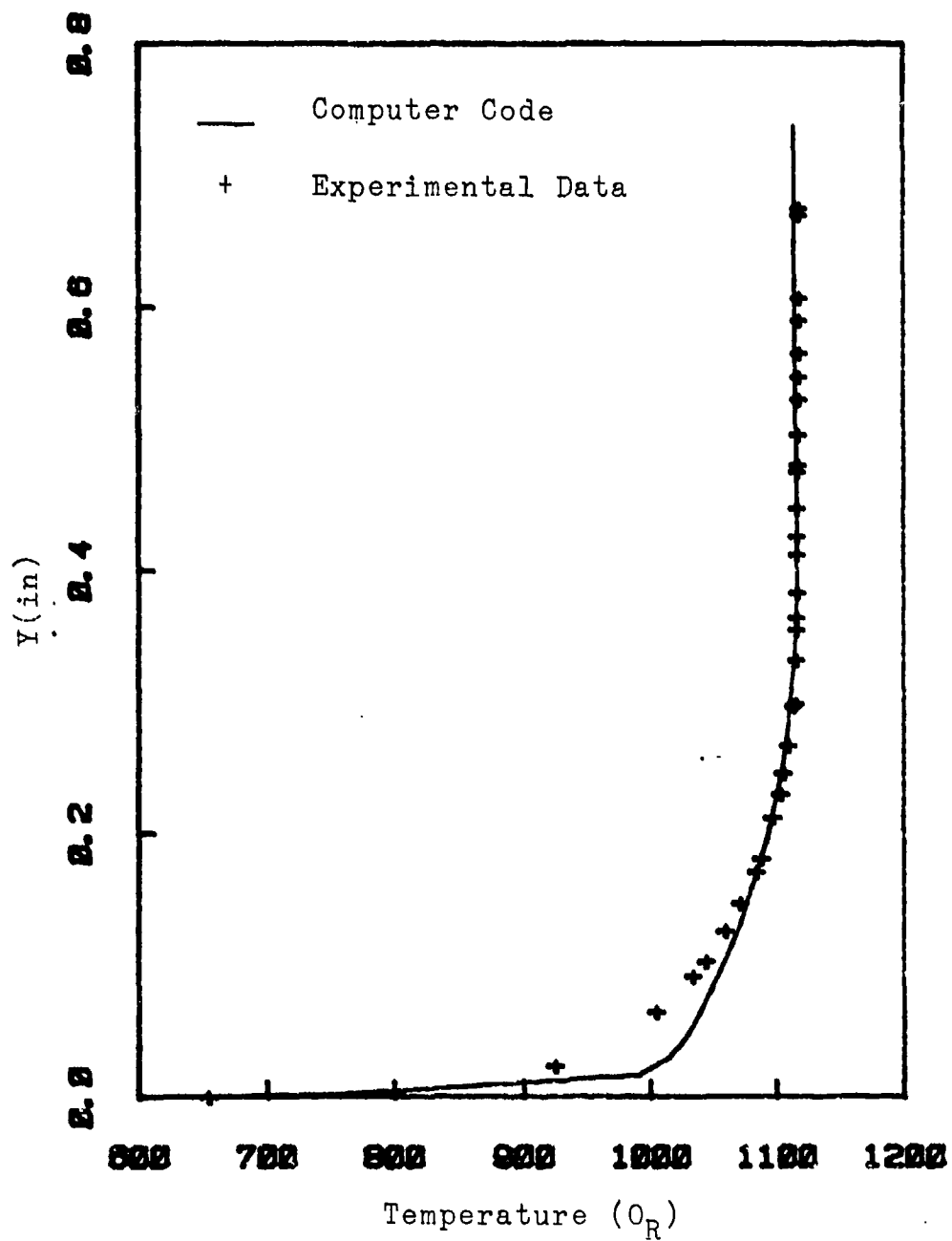


Fig. 19. Comparison of Calculated Total Temperature Profile for Rough Plate With AFWAL (Ref 40)

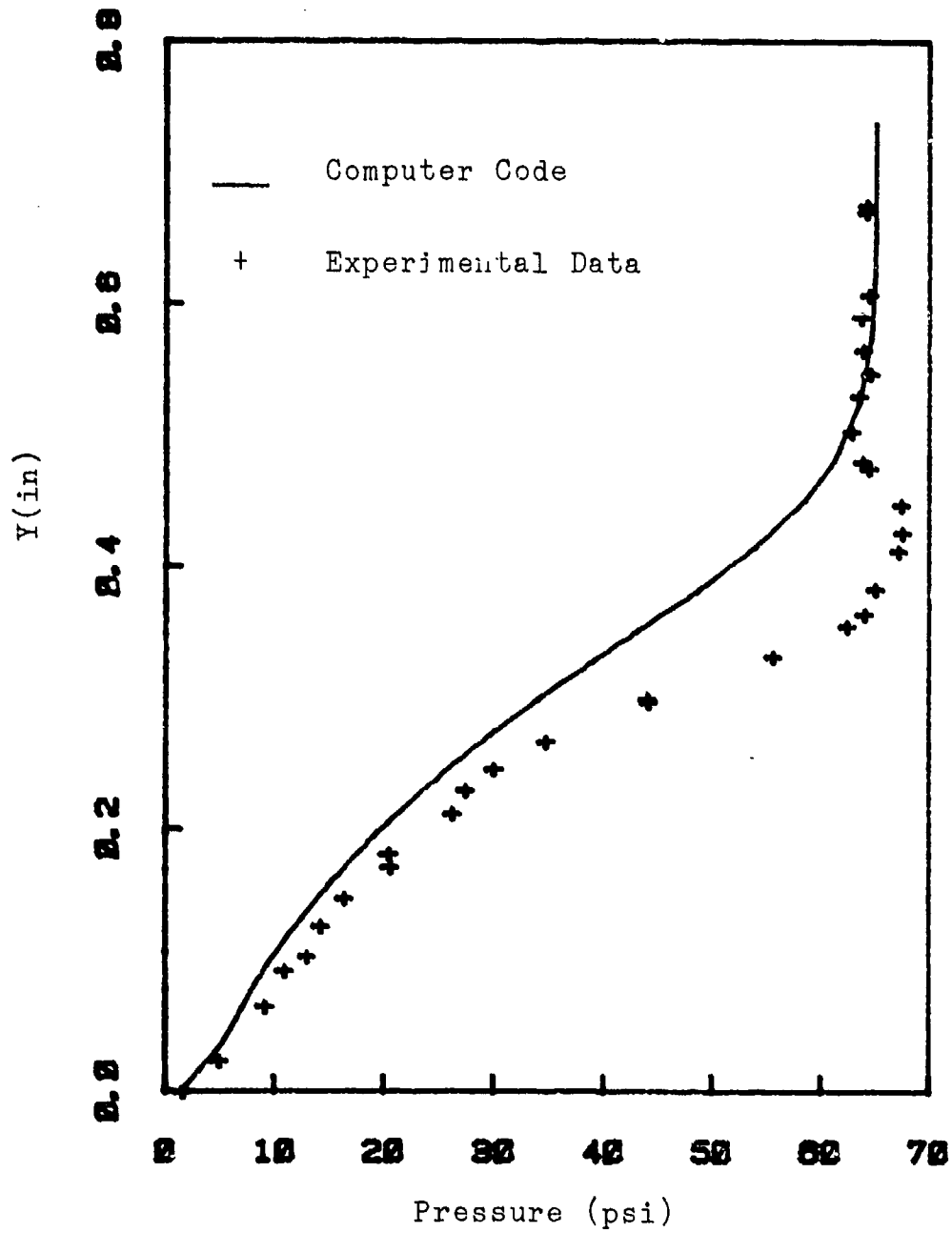


Fig. 20. Comparison of Computed Pressure Profile for Rough Surface With AFWAL Data (Ref 40)

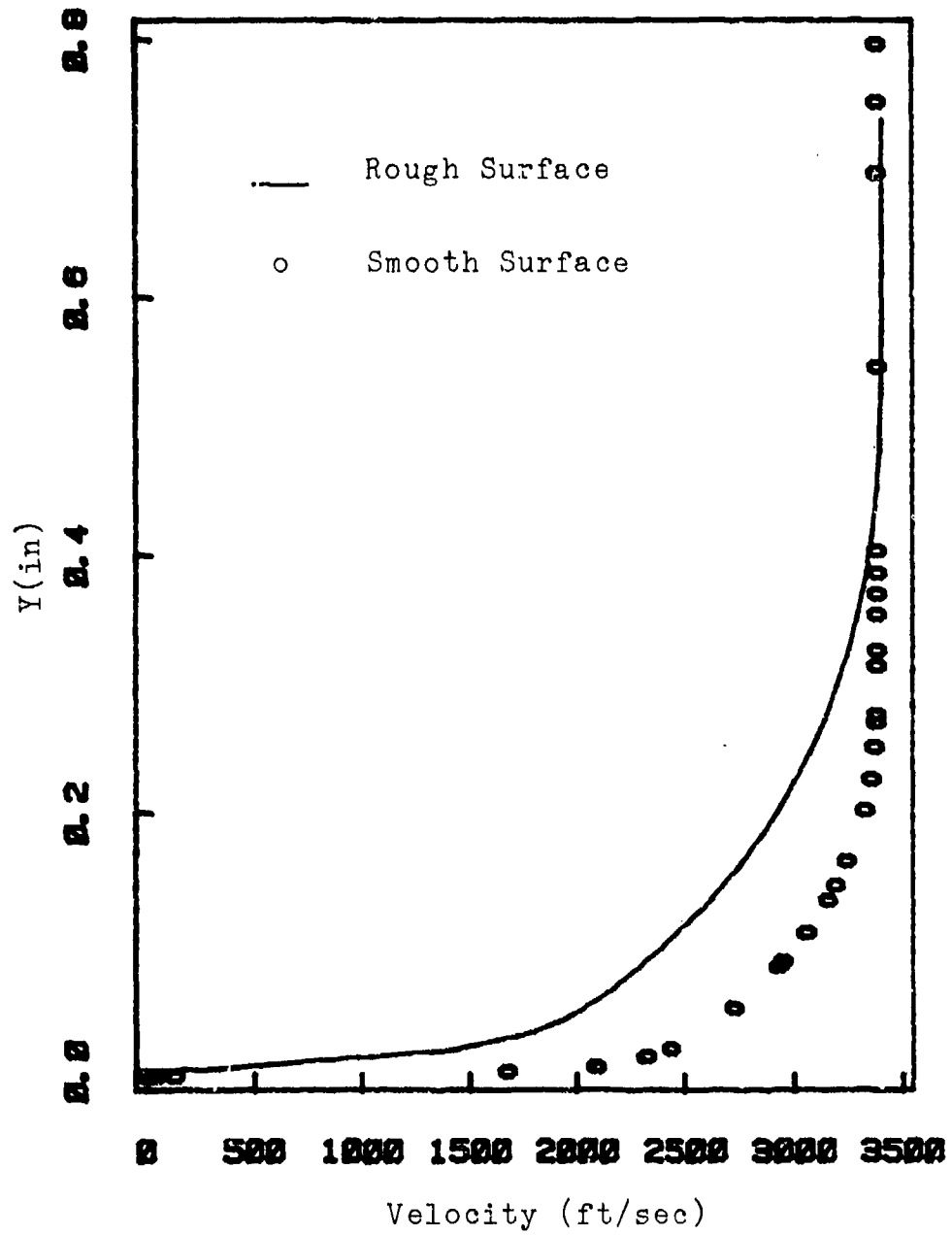


Fig. 21. Comparison of Computed Velocity Profiles for Flows Over Smooth and Rough Surfaces

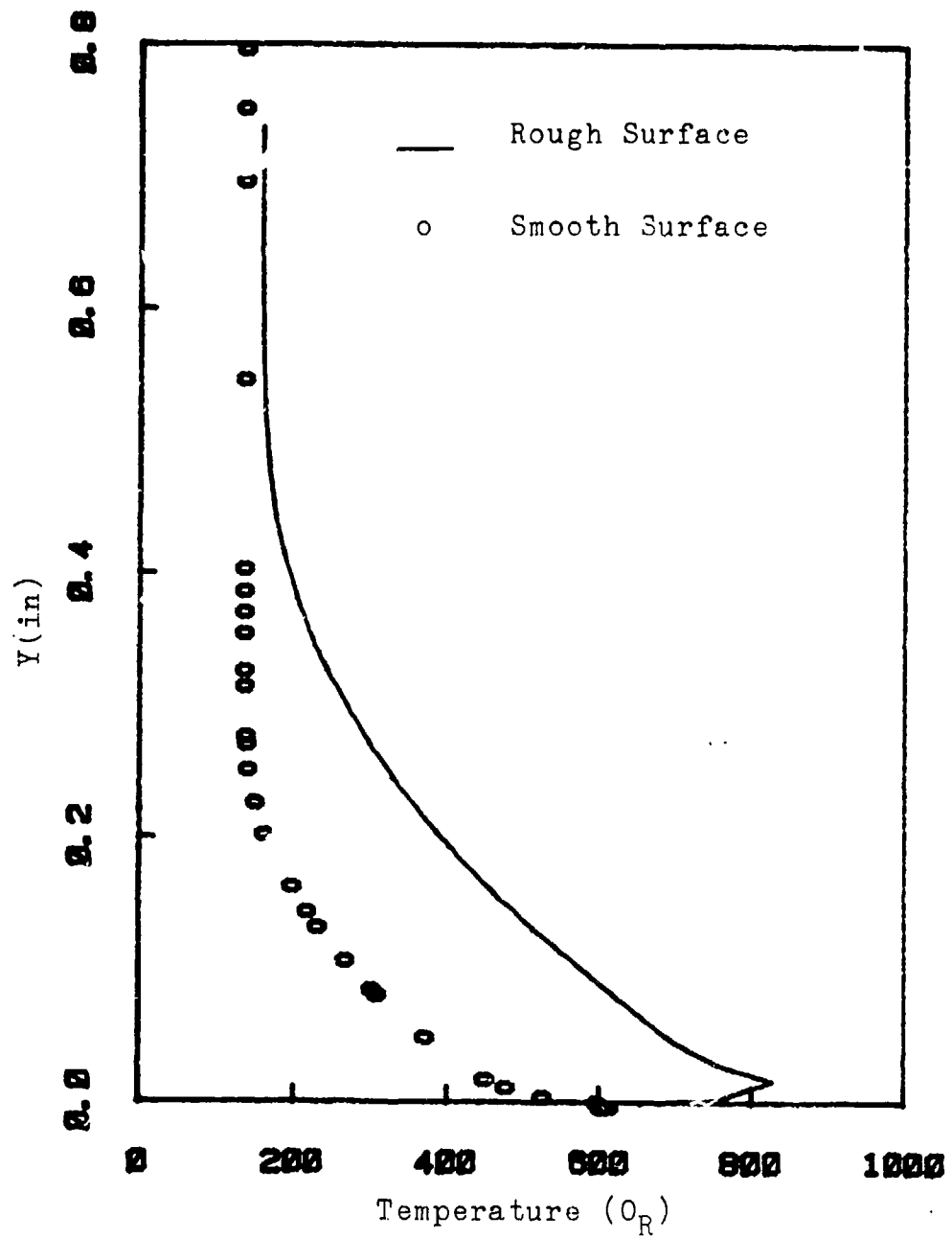


Fig. 22. Comparison of Computed Temperature Profile for Smooth and Rough Surfaces

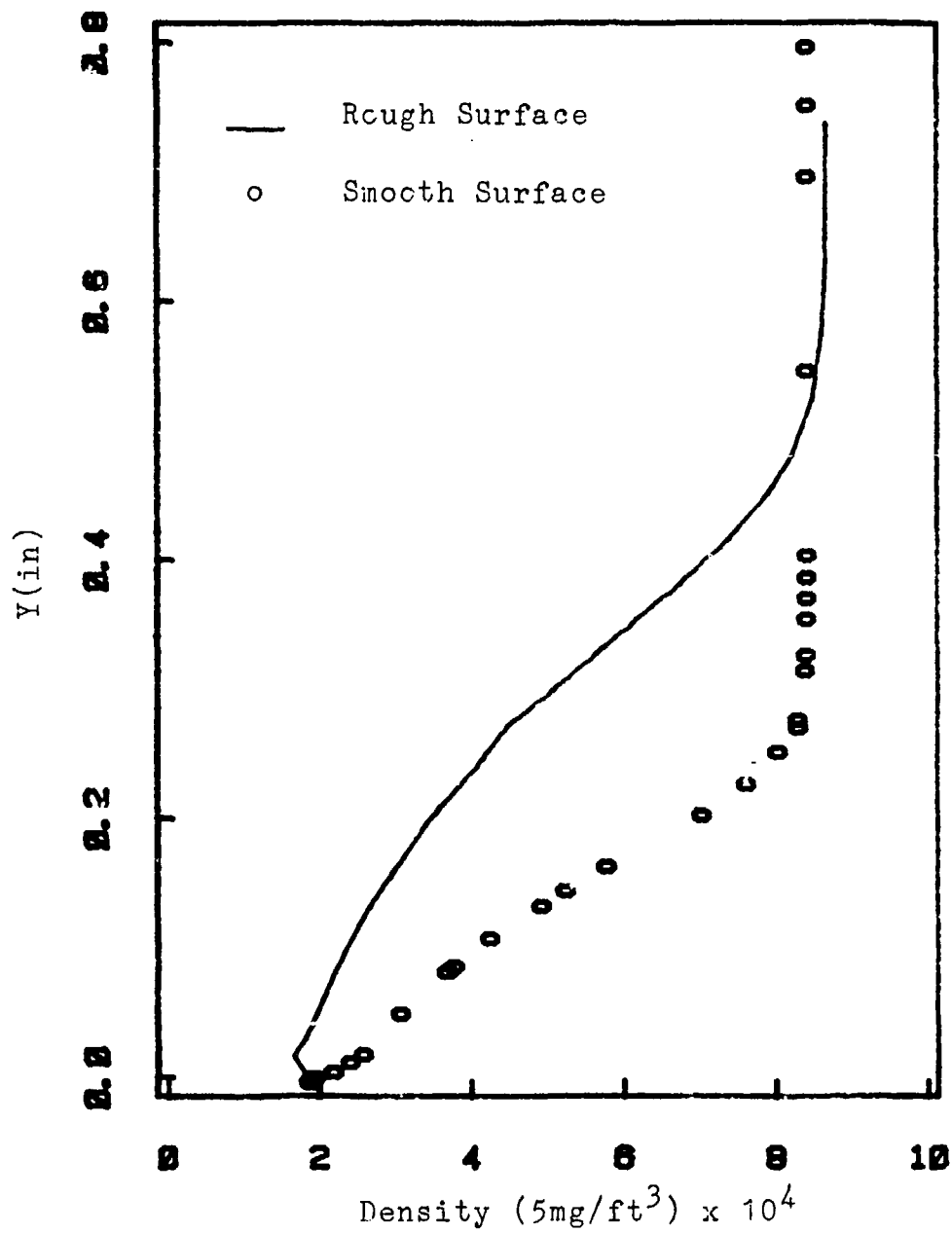


Fig. 23. Comparison of Computed Density Profiles for Smooth and Rough Surfaces

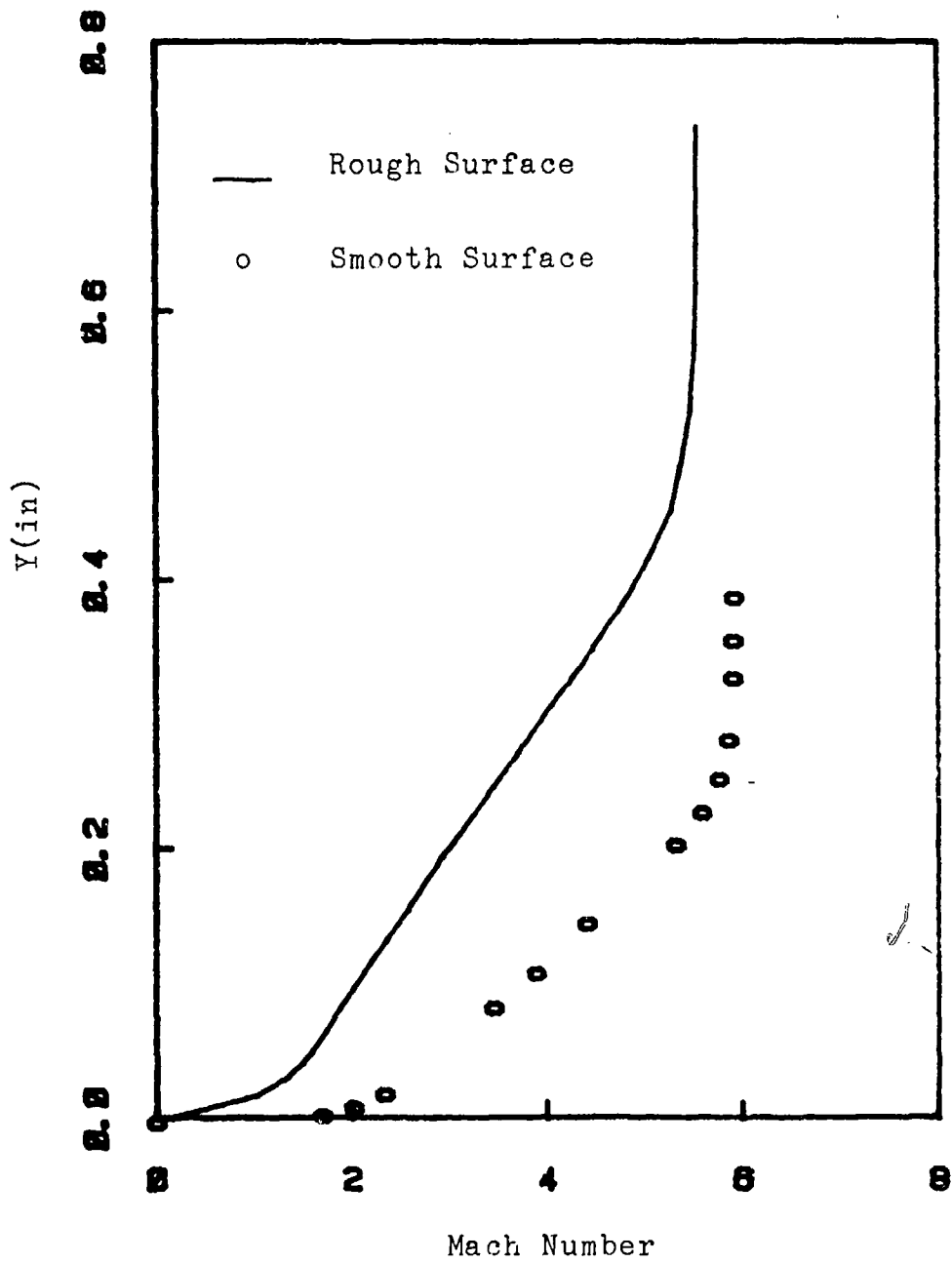


Fig. 24. Comparison of Calculated Mach Number Profiles for Smooth and Rough Surfaces

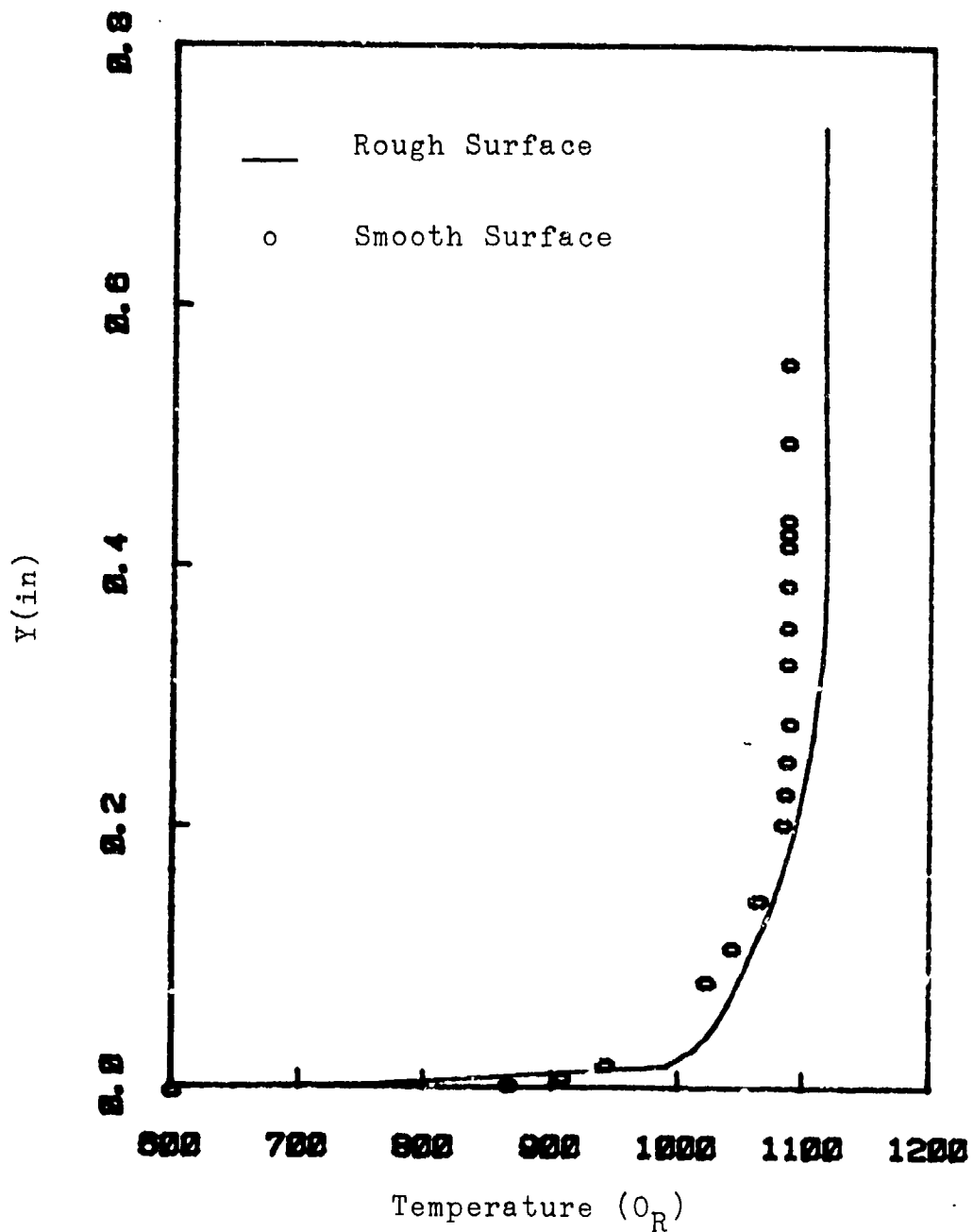


Fig. 25. Comparison of Computed Total Temperature Profiles for Smooth and Rough Flat-Plate

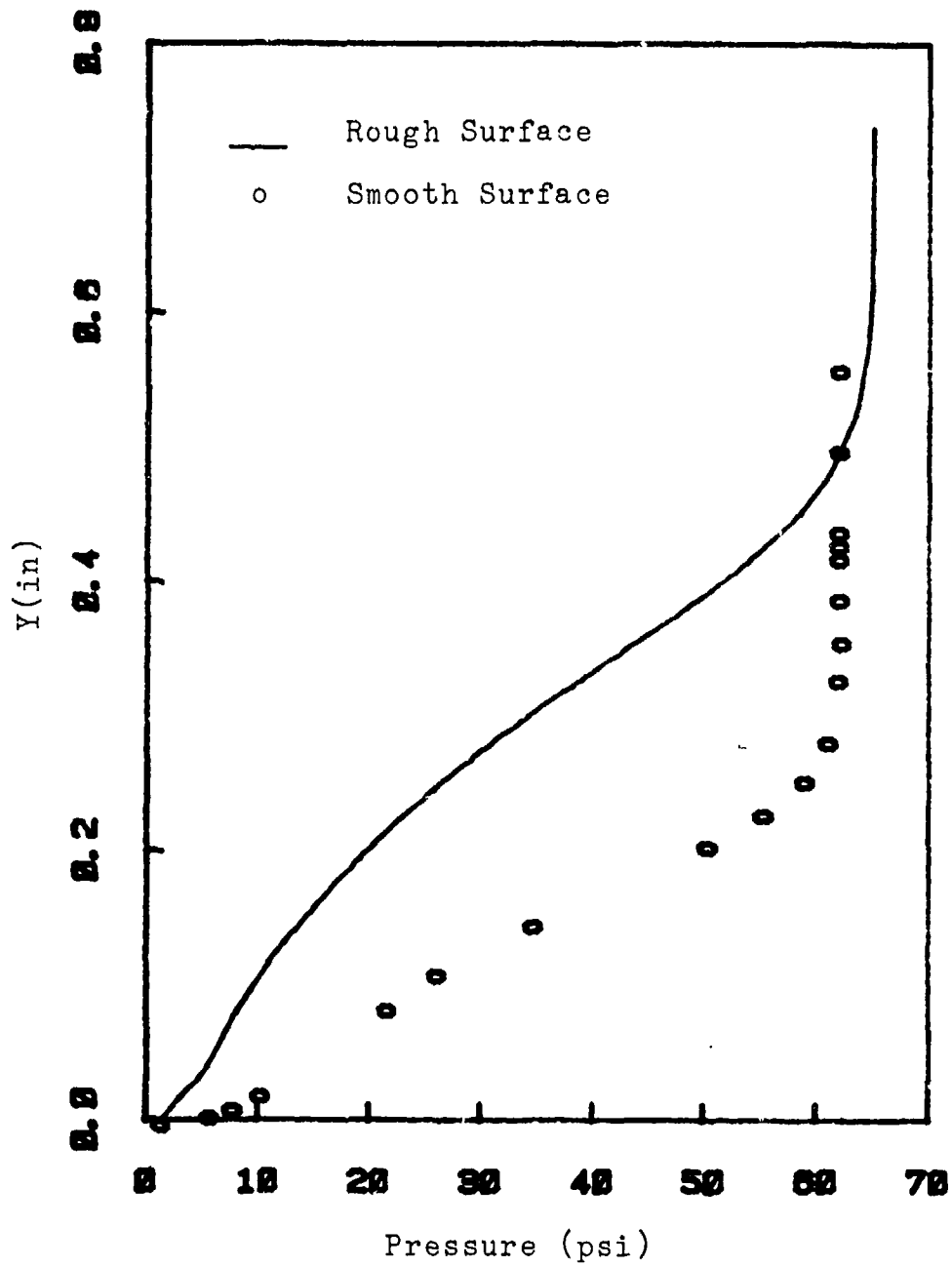


Fig. 26. Comparison of Computed Pressure Profiles for Smooth and Rough Surfaces

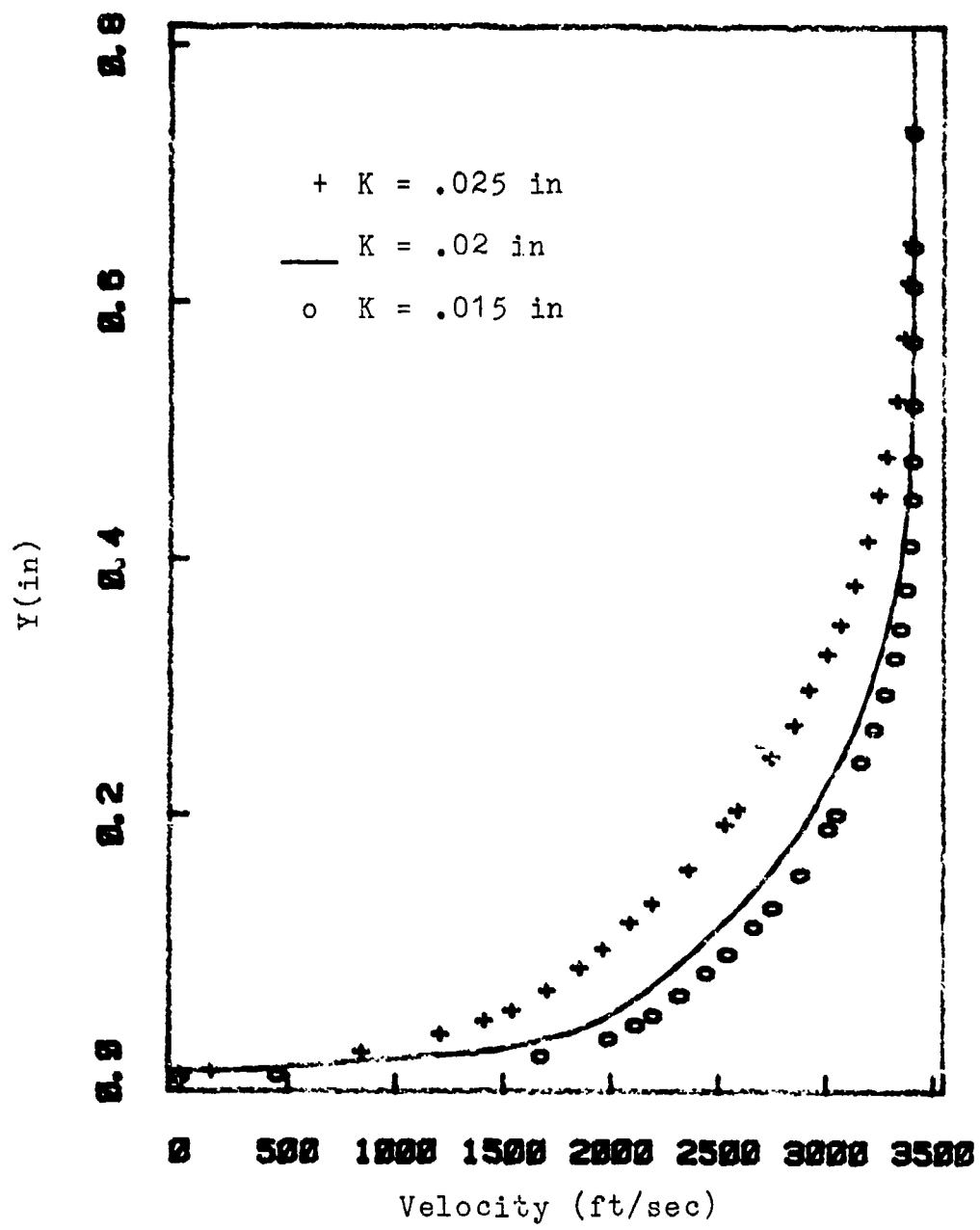


Fig. 27. Comparison of Velocity Profiles With Different Roughness Height

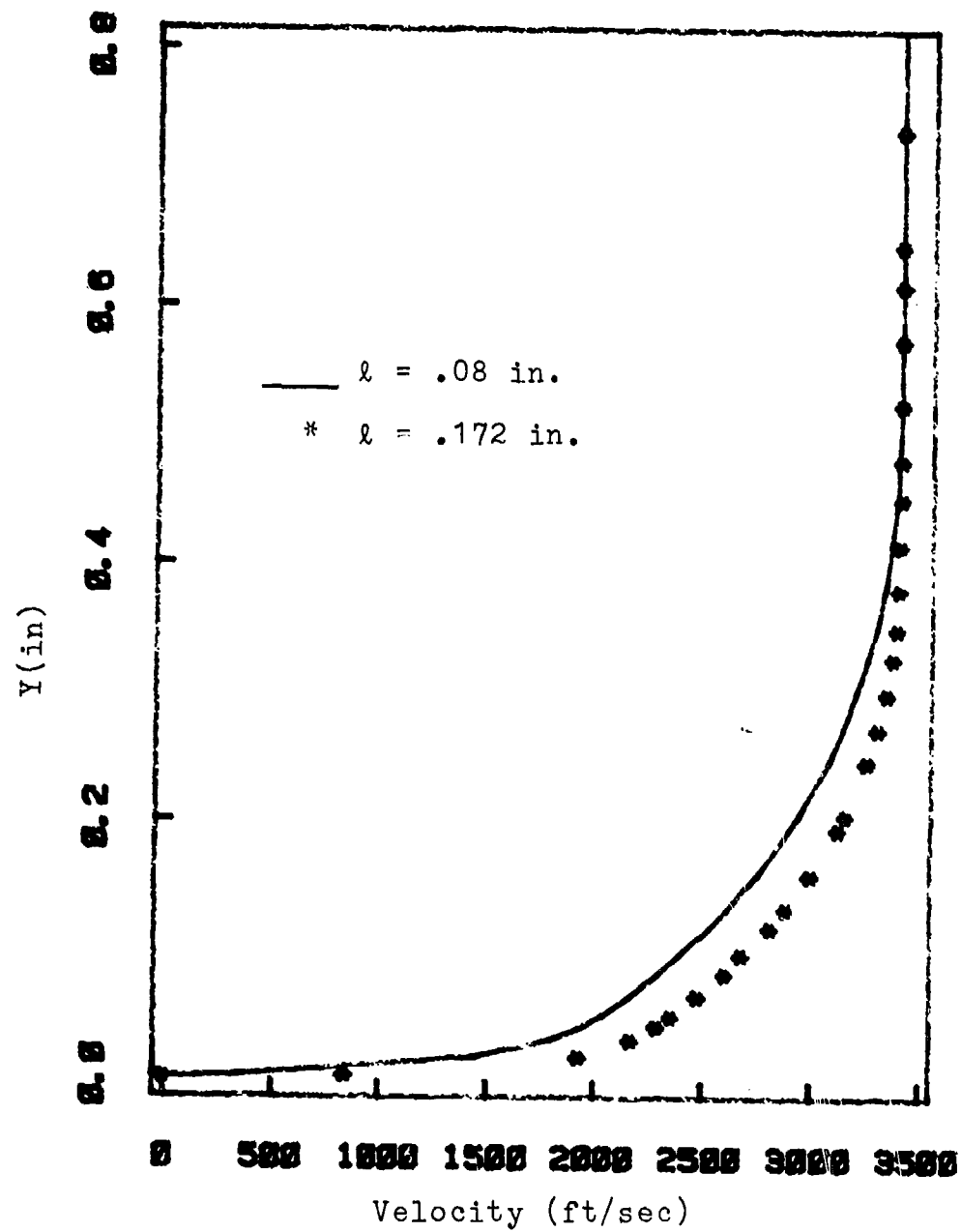


Fig. 28. Comparison of Velocity Profiles With Different Roughness Density

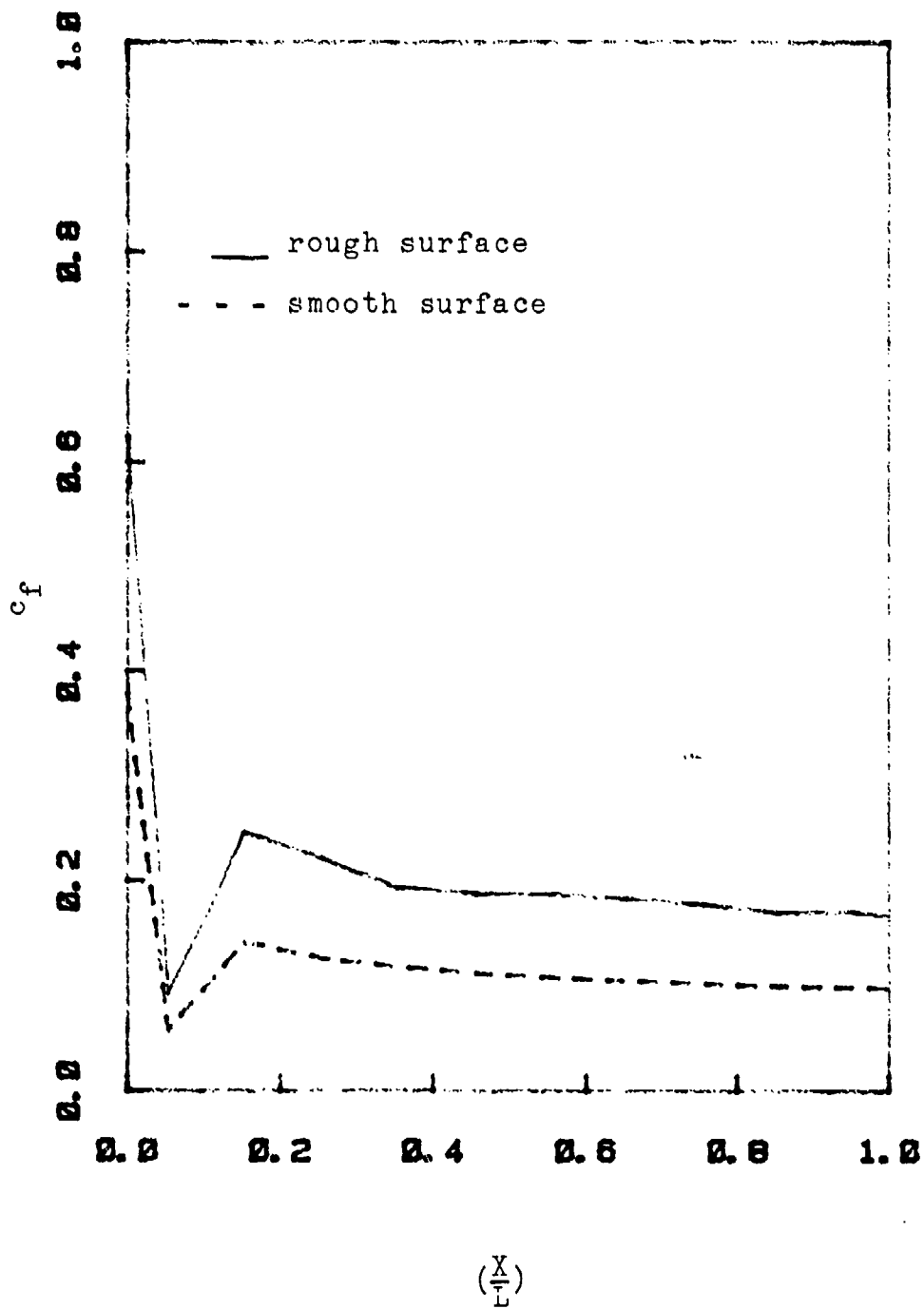


Fig. 29. Comparison of Skin Friction Coefficient With and Without Surface Roughness

Table I

Data for Smooth Flat Plate (Ref 37) Probe
Boundary Layer Profiles

Y Inch	$P_t(y)$ psia	$T_t(y) +$ O_R	$M(y)$	$T(y)$ O_R	$U(y)$ ft/sec	$f(y) \times 10^4$ #sec ² /ft ⁴
0	1.385	604.62	0	604.62	0	1.9234
.021	5.65	963.35	1.666	619.37	2032.11	1.8776
.053	12.52	1034.0	2.578	443.87	2661.67	2.6199
.083	19.98	1066.0	3.292	336.54	2959.25	3.4555
.087	20.73	1069.0	3.355	328.75	2981.07	3.5374
.112	26.25	1089.0	3.789	281.28	3113.96	4.1345
.138	32.01	1094.0	4.194	242.12	3197.95	4.8031
.148	35.75	1097.0	4.438	222.13	3240.80	5.2352
.169	42.39	1099.0	4.840	193.35	3297.33	6.0147
.204	52.14	1100.0	5.375	162.27	3355.21	7.1667
.205	53.94	1100.0	5.469	157.57	3363.61	7.3804
.232	60.53	1100.0	5.797	142.47	3390.46	8.1627
.255	61.23	1100.0	5.831	141.03	3393.00	8.2458
.272	63.50	1100.0	5.939	136.57	3400.88	8.5153
.284	62.73	1100.0	5.903	138.05	3398.27	8.4239
.322	63.18	1100.0	5.924	137.18	3399.80	8.4773
.328	63.00	1100.0	5.915	137.53	3399.19	8.4560
.359	63.10	1100.0	5.920	137.33	3399.53	8.4678
.378	63.31	1100.0	5.930	136.93	3400.24	8.4928
.395	63.09	1100.0	5.920	137.35	3399.50	8.4666
.411	62.90	1100.0	5.911	137.72	3398.85	8.4441
.445	63.37	1100.0	5.933	136.82	3400.45	8.4999
.447	62.97	1100.0	5.914	137.58	3399.09	8.4524
.476	63.18	1100.0	5.924	137.18	3399.80	8.4773
.503	63.91	1100.0	5.959	135.79	3402.25	8.5640
.512	63.18	1100.0	5.924	137.18	3399.80	8.4773
.535	63.50	1100.0	5.939	136.57	3400.88	8.5153
.565	63.58	1100.0	5.943	136.42	3401.15	8.5248
.569	63.65	1100.0	5.946	136.28	3401.39	8.5331
.596	63.17	1100.0	5.924	137.20	3399.77	8.4761
.631	63.24	1100.0	5.927	137.06	3400.01	8.4845

Table II

Data of Dr. Cole's Experiment for Turbulent
Flow Over Smooth Surface (Ref 38)

<u>y/θ</u>	<u>u/u_e</u>	<u>y/θ</u>	<u>M/M_e</u>
0.60	0.500	0.60	.275
0.80	0.555	1.19	.355
0.98	0.60	1.60	.385
1.50	0.645	2.20	.412
2.10	0.687	2.80	.439
3.80	0.750	3.70	.480
5.20	0.790	5.50	.535
6.10	0.815	6.65	.575
6.80	0.830	7.85	.610
7.85	0.845	9.45	.659
9.45	0.880	10.70	.700
10.55	0.900	12.30	.756
13.60	0.950	13.65	.799
15.60	0.975	15.70	.880
16.25	0.985	17.19	.939
19.20	1.00	19.30	.980
21.20	1.00	21.20	.992
22.80	1.00	22.80	1.00
24.75	1.00	24.75	1.00

Table III

Data for Rough Flat Plate (Ref 40) Probe
Boundary Layer Profiles

Y Inch	$P_t(y)$ psia	$T_t(y)$ O_R	+ $M(y)$	$T(y)$ O_R	$U(y)$ ft/sec	$f(y) \times 10^4$ #sec ² /ft ⁴
0	1.632	654.52	0	654.52	0	2.0936
.024	4.97	925.0	1.3992	664.72	1767.63	2.0614
.065	9.19	1000.50	1.9980	558.84	2314.34	2.4521
.092	10.93	1035.0	2.1962	526.80	2470.01	2.6012
.103	13.05	1045.0	2.4156	482.22	2599.26	2.8417
.126	14.34	1060.0	2.5398	462.86	2677.44	2.9605
.147	16.50	1072.0	2.7351	429.47	2777.34	3.1907
.171	20.61	1085.0	3.0724	375.70	2918.07	3.6473
.181	20.50	1089.0	3.0639	378.46	2920.62	3.6208
.212	26.28	1098.0	3.4845	320.27	3055.59	4.2786
.230	27.50	1104.0	3.5670	311.46	3084.56	4.3997
.246	30.05	1106.0	3.7334	292.00	3126.03	4.6928
.267	34.80	1110.0	4.0251	261.77	3191.08	5.2348
.297	44.20	1114.0	4.5476	216.89	3281.73	6.3179
.299	44.10	1115.0	4.5424	217.49	3282.47	6.3005
.332	55.70	1116.0	5.1147	179.07	3353.78	7.6522
.355	62.50	1117.0	5.4222	162.35	3385.34	8.4404
.364	64.09	1117.0	5.4917	158.85	3391.54	8.6263
.383	65.08	1117.0	5.5344	156.75	3395.26	8.7420
.412	67.25	1117.50	5.6271	152.40	3403.83	8.9917
.426	67.60	1117.50	5.6419	151.71	3405.05	9.0326
.447	67.50	1117.50	5.6377	151.90	3404.70	8.6703
.475	64.50	1117.50	5.5094	158.05	3393.85	8.6002
.480	63.90	1117.50	5.4834	159.34	3391.57	8.4819
.503	62.92	1118.0	5.4407	161.56	3388.52	8.5601
.530	63.59	1118.0	5.4699	160.08	3391.14	8.6704
.547	64.60	1119.0	5.5137	158.05	3396.51	3.5968
.565	63.97	1119.0	5.4864	159.40	3394.12	8.5968
.590	63.77	1119.0	5.4778	159.83	3393.35	8.5735
.607	64.50	1119.0	5.5094	158.26	3396.13	8.6587
.670	64.27	1119.0	5.4995	158.75	3395.26	8.6319

Table IV

Free Stream Condition for Smooth and Rough
Experimental Data (Ref. 37, 40)

	<u>Smooth Surface</u>	<u>Rough Surface</u>
M_∞	5.92	5.534
$T_o (O_R)$	1087	1122.94
P_o (psia)	1980	2003.53
T_w/T_o	.5538	.5829
L (in)	17.15	17.20

Table V

Comparison of Thickness for Smooth and Rough Cases

<u>Parameter</u>	<u>Smooth</u>	<u>Rough</u>
M_e	5.92	5.54
P_o (psia)	1995.38	2003.53
T_o (0_R)	1098.38	1122.94
T_w/T_o	.5538	.5884
Re_θ	16701.92	62954.7
δ (in)	.2069	.4735
δ^* (in)	.0992	.3792
θ (in)	.00793	.0295

V. Conclusions and Recommendations

The original computer, ITRACT, solved the compressible turbulent boundary layer over smooth surface. The purpose of this study was to extend the usefulness of the computer code by incorporating a modification for inclusion of the effect of surface roughness on compressible turbulent boundary layer. In this study, the roughness model proposed by Finson and Clark and followed by Christoph and Pletcher was employed without invoking the modification of the turbulence model. Roughness was represented by distributed sources and sinks in the appropriate governing equations. The most important term was a sink term in the mean momentum equation representing form drag due to roughness elements. The governing boundary equations were cast in a form to account for blockage effects of the roughness elements. With the computer code modified to include the effect of surface roughness, compressible turbulent boundary layer flows perturbed by the roughness elements could be solved. The roughness model employed and the modified computer code were verified through comparison of the calculated results with the experimental data of Dr. Fiore for compressible turbulent flow over rough surface.

As a result of incorporating a roughness model in the computer code to predict the effect of surface

roughness on the compressible turbulent boundary-layer, the following conclusions were reached:

1. The results presented here are quite encouraging, in that a rather basic model yields results that are in agreement with many observed trends regarding the influence of surface roughness.

2. The assumptions inherent to this model are limited to the basic nature of the flow around the roughness elements, and no approximations have been made regarding profiles of the boundary layer quantities, turbulence level, or relations between the momentum and energy fluxes.

3. The computer code is capable to handle roughness elements of any general shape. It is not restricted to roughness elements with circular cross-section only. The following areas are identified for further study and improvement to the method described and the computer code:

1. The Levy-Lees transformed coordinate system could not properly capture the turbulent boundary layer thickness, specifically, for the rough surface case. The transformed coordinate η became too large and it was necessary to monitor the numerical solutions and add points in the outer region to accommodate the boundary layer growth. A better turbulence grid generation for this type of flow can be used, such as that proposed by Carter et al.

2. The form drag coefficient and spacing between the elements be allowed to vary.

3. The effect of one element on another be included.

4. It would be useful to have better data to study on the effects of roughness density and shape for distributed roughness.

5. The combined effect of roughness and mass addition and the effect of roughness at strongly supersonic or hypersonic edge Mach numbers may be examined.

6. A model to accurately predict the heat transfer augmentation due to roughness elements be incorporated. Moreover, the calculated skin friction augmentation due to roughness elements be compared with experimental data to establish its accuracy.

Bibliography

1. Holden, M. "Studies of Aero-thermodynamics Phenomena Influencing the Performance of Hypersonic Re-entry Vehicles," SAMSO-TR-79-47, Calspan Corporation, Buffalo, N.Y., April 1979.
2. Nikuradse, J., "Stromungsgestze is rauhen Rohren," NACA TM1292, 1950.
3. Schlichting, H. Boundary Layer Theory, McGraw-Hill, New York, 1968.
4. Bellermann, D. "Contribution a l'Etude de la Connec-tion Forces Turbulent Long de Plagues Regvevses," Int. J. Heat & Mass Transfer 9, (1966).
5. Dvorak, F.A. "Calculation of Turbulent Boundary layers on Rough Surfaces in Pressure Gradient," AIAA Journal, Vol 7, No. 9, Sep 1969, pp 1752-1759.
6. Chen, K.K. "Compressible Turbulent Boundary-Layer Heat Transfer to Rough Surfaces in Pressure Gradient," AIAA Journal, Vol 10 No. 5, May 1972.
7. Owen, P.R. and Thomson, W.R. "Heat Transfer Across Rough Surfaces," J. of Fluid Mech., Vol 15, 1963.
8. Dahm, T.J. et al. "Passive Noretip Technology (Part II) Program, SAMSO-TR-77-11, Oct 1976, Acurex Corp., Mountain View, Calif.
9. Healzer, J.M., Moffat, R.J. and Keys. "The Turbulent Boundary Layer on a Rough, Porous Plate: Experimental Heat Transfer with Uniform Blowing," Report No. HMT-18, May 1974.
10. Reda, D. "Compressible Turbulent Skin Friction on Rough and Rough/Wavy Walls," AIAA Paper 74-574, Palo Alto, Calif, 1974.
11. Tuncer Cebeci and K.C. Chang. "Calculation of Incom-pressible Rough-Wall Boundary-Layer Flows", AIAA Journal Vol 16, No 7, July 1978.
12. Roha, J.C. "Turbulent Boundary Layer in Incompressible Flow," Progress in Aerospace Science, Vol 2.

13. Hodge & Adams J.C. "The Calculation of Comp. Turbulent and Relaminarization Boundary Layer Over Smooth and Rough Surfaces Using an Extended Mixing Length Hypothesis," AEDC-TR-77-96, Feb 1978.
14. Saffman, P.G. and Wilcox, D.C. "Turbulence Model Prediction for Turbulent Boundary Layers," AIAA Journal, Vol 12, No 4, April 1970.
15. Finson, M.L. and Clark, A.S., "The Effect of Surface Roughness Character on Turbulent Re-entry Heating," AIAA Paper 80-1459, 1980.
16. Christoph G.H., Pletcher R.H., "Prediction of Rough-Wall Skin Friction and Heat Transfer," AIAA Paper No. 82-0031, Jan 20, 1982.
17. Shang, J.S., Hankey, W.L., and Dwoyer, D.L. "Numerical Analysis of Eddy Viscosity Models in Supersonic Turbulent Boundary Layers," AIAA Paper No. 73-164, 1973.
18. Van Driest, E.R. "Turbulent Boundary Layer in Compressible Fluids," Journal of Aeronautical Science, Vol 18, No. 3, Mar 51.
19. Harris, J.E. "Numerical Solution of the Equations for Compressible Laminar, Transitional and Turbulent Boundary Layer and Comparison with Exp. Data." Tech Report NASA-TR-R-368, N71-32164, 1-29, 67-71. Hampton, Virginia, Langley Research Centre (Mar 1951)
20. Beauregard, A.J. "An Analytic Study of the Effect of Mass Transfer on Compressible Turbulent Boundary Layer," MS Thesis GA/MC/76D-3.
21. Coles, D. "Measurement of the Boundary-Layer on a Smooth Flat-Plate in Supersonic Flow," California Inst of Technology, Rept. ND20-71, 1953.
22. Van Driest, E.R. "On Turbulent Flow Near the Wall," J. of Aeronautical Science, Vol 23, No. 11, Nov 1956.
23. Rotta, J.C. Heat Transfer and Temperature Distribution in Turbulent Boundary Layers at Supersonic and Hypersonic Flow., AGARDO graph 97, Pt. I, May 1965.
24. Rochelle, Williams C. Prandtl Number Distribution in a Turbulent Boundary Layer with Heat Transfer at Supersonic Speeds. DRL-508(Grants DA-ORD-31-124-61-G3 and DA-ORD(D)-31-124-G132), University of Texas, Oct 1963.

25. Meier, H.U.; and Rotta J.C. "Experimental and Theoretical Investigation of Temperature Distribution in Supersonic Layers; AIAA Paper No. 70-744, Jun-Jul 1970.
26. Finson, M.L. "A Model for Rough Wall Turbulent Heating and Skin-Friction", AIAA Paper No. 82-0199, June 1982.
27. Cebeci, T., Smith, A.M.G., and Mosinskis, G. "Calculations of Compressible Adiabatic Turbulent Boundary-Layer," AIAA Paper No. 69-687, Jun 1969.
28. Klebanoff, P.S., Characteristics of Turbulence in a Boundary Layer with Zero Pressure Gradient, NACA Rep 1247, 1955.
29. Smith, A.M.O. and Cebeci, T. "Solution of the Boundary-Layer Equations for Incompressible Turbulent Flow," Proceedings of the 1968 Heat Transfer and Fluid Mechanics Institute, 1968, Stanford Univ. Press.
30. Simpson, R.L., Whitten D.G., and Moffat, R.J. "An Experimental Study of the Turbulent Prandtl Number of Air With Injection and Suction, Int J. Heat Mass Transfer, Vol 13, No. 1, Jan, 1970.
31. Probstern, R.F. and Elliott, D. "The Transverse Curvature Effect in Compressible Axially Symmetric Laminar Boundary-Layer Flow," Journal of Aeronautical Science, Vol 23, 1956.
32. Carter, J.E., Edwards, D.E., and Werle, M.J., "A New Coordinate Transformation for Turbulent Boundary Layer Flows, NASA CP-2166, Numerical Grid Generation Techniques, Oct, 1980.
33. Hinzi, J.O. Turbulence. New York: McGraw-Hill, Inc., 1975.
34. Tennekes, H. and Lumley, J.L. A First Course in Turbulence. Cambridge: The MIT Press, 1972.
35. Shapiro, A.H. The Dynamics and Thermodynamics of Compressible Fluid Flow. New York: Ronald Press Company, 1959.
36. Cebeci, T., and Smith, A.M.O. Analysis of Turbulent Boundary Layers. Academic Press, NY, San Fransisco, London, 1974.
37. Fiore, A.W. Experimental Data for Turbulent Flow Over Smooth Flat-Plate. Air Force Wright Aeronautical Laboratories, Wright-Patterson AFB, June 1983.

38. Cole, D. "Measurement in the Boundary Layer on a Smooth Flat-Plate in Supersonic Flow III Measurements in a Flat-Plate Boundary Layer at the Jet Propulsion Laboratory," California Inst of Technology, Rept KD20-71, 1953.
39. Hodge, Department of Aeronautics and Astronautics, Air Force Institute of Technology, Wright-Patterson AFB, Ohio. Personal Communications.
40. Fiore, A.W. Experimental Data for Compressible Turbulent Flow Over Rough Flat-Plate. AirForce Wright Aeronautical Laboratories, WPAFB, Ohio, Jun 1983.

Appendix 'A'

Derivation of Source Term for Energy Equation

Including a sink term $R_u = -\frac{1}{2} \rho u^2 C_D \frac{D(y)}{\ell^2}$ in the mean momentum equation (equ.) requires inclusion of an appropriate source term $R_h = \frac{1}{2} \rho u^3 C_D \frac{D(y)}{\ell^2}$ in the static enthalpy equation such that the total enthalpy is not altered.

The mean static enthalpy equation after addition of source term, R_h , may be written as

$$\begin{aligned} \bar{\rho} u \frac{\partial \bar{h}}{\partial x} + \rho \bar{u} \frac{\partial \bar{h}}{\partial y} = \bar{u} \frac{d\bar{p}}{dx} + \frac{\partial}{\partial y} \left[\frac{\bar{u}}{\text{Pr}} \frac{\partial \bar{h}}{\partial y} - \bar{\rho} h' v' \right] \\ + \left(\bar{u} \frac{\partial \bar{u}}{\partial y} - \bar{\rho} u v \right) \frac{\partial \bar{u}}{\partial y} + \frac{1}{2} C_D \frac{\bar{\rho} u^3}{\ell^2} \frac{D(y)}{\ell^2} \end{aligned} \quad (\text{A.1})$$

Rewriting the mean momentum equ

$$\begin{aligned} \frac{d\bar{p}}{dx} = \frac{\partial}{\partial y} \left[\bar{u} \frac{\partial \bar{u}}{\partial y} - \bar{\rho} u' v' \right] - \rho \bar{u} \frac{\partial u}{\partial x} + \rho \bar{v} \frac{\partial u}{\partial y} \\ - \frac{1}{2} \rho u^2 C_D \frac{D(y)}{\ell^2} \end{aligned} \quad (\text{A.2})$$

Substitute (A.2) in (A.1) to get,

$$\begin{aligned} \bar{\rho} \bar{u} \left(\frac{\partial \bar{h}}{\partial x} + \bar{u} \frac{\partial \bar{u}}{\partial x} \right) + \rho \bar{v} \left(\frac{\partial \bar{h}}{\partial y} + \bar{u} \frac{\partial \bar{u}}{\partial y} \right) = \\ \frac{\partial}{\partial y} \left[\bar{u} \bar{u} \frac{\partial \bar{u}}{\partial y} - \bar{u} \bar{\rho} u' v' + \frac{\bar{u}}{\text{Pr}} \frac{\partial \bar{h}}{\partial y} - \bar{\rho} h' v' \right] \end{aligned} \quad (\text{A.3})$$

To express $\bar{\rho} h' v'$, $\frac{\partial \bar{h}}{\partial y}$ in term of total-enthalpy, the fluctuating total enthalpy may be expressed as: (Ref 36:76-77)

$$H' = h' + \bar{u} u' \quad (\text{A.4})$$

Multiplying both sides (A.4) by $\rho v'$ and averaging,

$$\rho \overline{H'v'} = \rho \overline{h'v'} + \bar{u} \rho \overline{u'v'} \quad (\text{A.5})$$

Noting that,

$$\frac{\partial \bar{H}}{\partial x} = \frac{\partial \bar{h}}{\partial x} + \bar{u} \frac{\partial \bar{u}}{\partial x} \quad (\text{A.6})$$

and,

$$\frac{\partial \bar{H}}{\partial y} = \frac{\partial \bar{h}}{\partial y} + \bar{u} \frac{\partial \bar{u}}{\partial y} \quad (\text{A.7})$$

Substituting equations (A.5), (A.6), and (A.7) in (A.3)

$$\rho \bar{u} \frac{\partial \bar{H}}{\partial x} + \rho \bar{v} \frac{\partial \bar{H}}{\partial y} = \frac{\partial}{\partial y} \left[\bar{u} \bar{u} \frac{\partial \bar{u}}{\partial y} - \rho \overline{H'v'} + \frac{\mu}{Pr} \frac{\partial \bar{H}}{\partial y} - \frac{\mu}{Pr} \bar{u} \frac{\partial \bar{u}}{\partial y} \right] \quad (\text{A.8})$$

Heat transfer normal to the main flow, q_y , is given by (Ref 36:66)

$$-q_y = \frac{\mu}{Pr} \frac{\partial \bar{H}}{\partial y} - \frac{\mu}{Pr} \bar{u} \frac{\partial \bar{u}}{\partial y} \quad (\text{A.9})$$

Substitute (A.9) in (A.8) to get,

$$\rho \bar{u} \frac{\partial \bar{H}}{\partial x} + \rho \bar{v} \frac{\partial \bar{H}}{\partial y} = \frac{\partial}{\partial y} \left[\bar{u} \bar{u} \frac{\partial \bar{u}}{\partial y} - q_y - \rho \overline{H'v'} \right] \quad (\text{A.10})$$

It is evident from equation (A.10), which is the total-enthalpy equation, that the addition of the source term, R_h , to the static enthalpy equation, has not altered the total enthalpy equation.

Appendix 'B'

Derivation of Conservation Equations Including the Roughness Effect in Levy-Lees Variables

(B1) Roughness Effects

Equations (15), (16), (20), and (21) are repeated here for convenience:

Sink term included in the mean momentum equation:

$$R_u = -\frac{1}{2} \rho u^2 C_D \frac{D(y)}{\ell^2} \quad (\text{B.1})$$

Source term included in the mean static enthalpy equation:

$$R_h = +\frac{1}{2} \rho u^3 C_D \frac{D(y)}{\ell^2} \quad (\text{B.2})$$

Blockage terms:

$$B(y) = \left(1 - \frac{\pi D^2(y)}{4\ell^2} \right) \quad (\text{B.3})$$

$$f(y) = \left(1 - \frac{D(y)}{\ell} \right) / B(y) \quad (\text{B.4})$$

(B2) Conservation Equations in Physical Plane

(a) Continuity Equation:

Introducing the blockage effect in continuity equation as explained earlier in Chapter II, Equation (4) becomes

$$1 - \frac{D(y)}{\ell} \frac{\partial}{\partial x} (r^j \rho u) + 1 - \frac{\pi D^2(y)}{4\ell^2} \frac{\partial}{\partial y} (r^j \rho \tilde{v}) = 0 \quad (\text{B.4})$$

Dividing thru by $B(y)$, (B4) becomes:

$$f(y) \frac{\partial}{\partial x} (r^j \rho u) + \frac{\partial}{\partial y} (r^j \rho \tilde{v}) = 0 \quad (\text{B.5})$$

(b) Momentum Equation:

Introducing the blockage effect and adding the sink term, the momentum equation (equation (5)) becomes:

$$\begin{aligned} \rho u \left\{ 1 - \frac{D(y)}{l} \right\} \frac{\partial u}{\partial x} + \rho \tilde{v} \left\{ 1 - \frac{\pi D^2(y)}{4l^2} \right\} \frac{\partial u}{\partial y} = \\ - \left\{ 1 - \frac{D(y)}{l} \right\} \frac{dp}{dx} + \left\{ 1 - \frac{\pi D^2(y)}{4l^2} \right\} \frac{1}{r^j} \left[\frac{\partial}{\partial y} r^j (\mu \frac{\partial u}{\partial y} - \rho \overline{u'v'}) \right] \\ - \frac{1}{2} \rho u^2 C_D \frac{D(y)}{l^2} \end{aligned} \quad (B.6)$$

Dividing thru by $B(y)$, (B.6) becomes:

$$\begin{aligned} f(y) \rho u \frac{\partial u}{\partial x} + \rho \tilde{v} \frac{\partial u}{\partial y} = \\ -f(y) \frac{dp}{dx} + \frac{1}{r^j} \frac{1}{B(y)} \frac{\partial}{\partial y} \left[B(y) r^j (\mu \frac{\partial u}{\partial y} - \rho \overline{u'v'}) \right] \\ - \frac{1}{2} \rho u^2 \frac{C_D D(y)}{B(y) l^2} \end{aligned} \quad (B.7)$$

(c) Energy Equation:

Introducing the blockage effect and adding the source term, the energy equation (equation (6)) becomes:

$$\begin{aligned} \left\{ 1 - \frac{D(y)}{l} \right\} \rho u \frac{\partial (C_p T)}{\partial x} + B(y) \rho \tilde{v} \frac{\partial}{\partial y} (C_p T) \\ = u \left\{ 1 - \frac{D(y)}{l} \right\} \frac{du}{dx} + \frac{1}{r^j} \frac{\partial}{\partial y} \left[B(y) r^j \frac{Kl}{C_p} \frac{\partial (C_p T)}{\partial y} \right] \\ + B(y) u \left(\frac{\partial u}{\partial y} \right)^2 + \frac{1}{r^j} \frac{\partial}{\partial y} \left[B(y) r^j (-C_p \rho \overline{v'T'}) \right] \\ - B(y) \rho \overline{u'v'} \frac{\partial u}{\partial y} + \frac{1}{2} \frac{\rho u^3}{L^2} C_D \frac{D(y)}{l^2} \end{aligned} \quad (B.8)$$

Dividing thru by $B(y)$, Equation (B.6) becomes:

$$\begin{aligned}
 f(y) \rho u \frac{\partial T}{\partial x} + \rho \tilde{v} \frac{\partial T}{\partial y} &= f(y) \frac{u}{C_p} \frac{dp}{dx} \\
 + \frac{1}{B(y)} \frac{1}{r^j C_p} \frac{\partial}{\partial y} &\left[B(y) r^j \frac{K \ell}{C_p} \frac{\partial}{\partial y} (C_p T) \right] + \frac{\mu}{C_p} \left[\frac{\partial u}{\partial y} \right]^2 \\
 + \frac{1}{B(y)} r^j C_p \frac{\partial}{\partial y} &\left[B(y) r^j (-C_p \rho \overline{v' T'}) \right] - \frac{\rho \overline{u' v' T'}}{C_p} \frac{\partial u}{\partial y} \\
 &+ \frac{1}{2B(y)} \frac{\rho u^3}{C_p} \frac{C_D}{\ell^2} D(y) \quad (B.9)
 \end{aligned}$$

(B3) Transformation to Levy-Lees Variables

The transformation of Probstein-Elliott and Levy-Lees (Ref 31) is used to transform equations (B.5), (B.7), and (B.9). The Levy-Lees variables ξ, η are defined as follows:

$$\xi(x) = \int_0^x \rho_e u_e \mu_e r_o^{2j} dx \quad (B.10)$$

and

$$\eta(x, y) = \frac{\rho_e u_e r_o^j}{2\xi} \int_0^y t^j \frac{\rho}{\rho_e} dy \quad (B.11)$$

The partial-derivative operator in the new coordinate system (ξ, η) becomes

$$\left[\frac{\partial}{\partial y} \right]_{\xi} = \frac{\mu_e u_e r_o^j t^j}{2\xi} \frac{\rho}{\rho_e} \left[\frac{\partial}{\partial y} \right]_{\xi} \quad (B.12)$$

$$\left[\frac{\partial}{\partial x} \right]_{\eta} = \frac{\rho_e u_e \mu_e r_o^{2j}}{2\xi} \left[\frac{\partial}{\partial \xi} \right]_{\eta} + \frac{\partial \eta}{\partial x} \left[\frac{\partial}{\partial y} \right]_{\xi} \quad (B.13)$$

Equations (B.10) and (B.11) gives a transformation

$$\frac{\partial \xi}{\partial x} = \rho e u e \mu e r o^{2j} \quad (B.14)$$

$$\frac{\partial \eta}{\partial y} = \frac{t^j u e r o^j \rho}{2\xi} \quad (B.15)$$

The dependent variable F , θ , and V are defined as:

$$F = \frac{u}{ue}, \quad \theta = \frac{T}{Te}$$

$$V = \frac{2\xi}{\rho e u e \mu e r o^{2j}} \left[f(y) F \eta_x + \frac{r^j t^j \rho \tilde{v}}{2\xi} \right] \quad (B.16)$$

Continuity Equation

Equation (B.5) may be written as:

$$\frac{\partial}{\partial y} \{r^j \rho \tilde{v}\} = -f(y) \frac{\partial}{\partial x} (r^j \rho u)$$

Integrating both sides from wall ($y=0$) to source point y in the field:

$$r^j \rho \tilde{v} = - \int_0^y f(y) \frac{\partial}{\partial x} (r^j \rho u) dy + r o^j \rho w v w$$

Using Equation (B.13)

$$r^j \rho \tilde{v} = - \left(\xi_x \left(\frac{\partial}{\partial \xi} \right)_{\eta} + \eta_x \frac{\partial}{\partial y} \right) \int_0^y f(y) (r o^j \rho u) y_{\eta} d_{\eta} + r o^j \rho u v w$$

Expanding,

$$r^j \rho \tilde{v} = -\xi_x \frac{\partial}{\partial \xi} \left(\int_0^{\eta} f(y) (r o^j \rho u) \frac{2\xi}{t^j u e r o^j \rho} d\eta \right) - \eta_x \frac{\partial}{\partial \eta} \left(\int_0^{\eta} f(y) (r o^j \rho u) \frac{2\xi}{t^j u e r o^j \rho} d\eta \right) + r o^j \rho u v w$$

Using Equation (B.16)

$$r^j_{\rho\tilde{v}} = -\xi_x \frac{\partial}{\partial \xi} \left(\int_0^{\eta} f(y) F \sqrt{\frac{2\xi}{t^j}} d\eta \right) - \eta_x \frac{\partial}{\partial \eta} \left(\int_0^{\eta} f(y) F \sqrt{\frac{2\xi}{t^j}} d\eta \right) + r^j_{\rho\omega} v\omega$$

This equation can be re-written as:

$$r^j_{\rho\tilde{v}} = \frac{\xi_x}{2\xi t^j} \left[-\sqrt{2\xi} \frac{\partial}{\partial \xi} \left(\sqrt{2\xi} \int_0^{\eta} f(y) F d\eta \right) + \frac{r^j_{\rho\omega} v\omega}{\xi_x} \sqrt{2\xi} t^j \right] - \frac{2\xi}{\xi_x} \eta_x \int_0^{\eta} f(y) F d\eta \quad (B.17)$$

Simplifying, the first two terms on the RHS of the above equation are defined as:

$$v = \left[-\sqrt{2\xi} \frac{\partial}{\partial \xi} \left(\sqrt{2\xi} \int_0^{\eta} f(y) F d\eta \right) + \frac{r^j_{\rho\omega} v\omega}{\xi_x} \sqrt{2\xi} t^j \right] \quad (B.18)$$

Substituting (B.18) in Equation (B.17)

$$r^j_{\rho\tilde{v}} = \frac{\xi_x}{\sqrt{2\xi} t^j} v - \frac{\sqrt{2\xi}}{\xi_x} \eta_x \int_0^{\eta} f(y) F d\eta$$

$$r^j_{\rho\tilde{v}t^j} = \frac{\xi_x}{2\xi} v - 2\xi \eta_x \int_0^{\eta} f(y) F d\eta$$

\tilde{v} is given by:

$$\tilde{v} = \frac{1}{r^j_{\rho t^j}} \left[\frac{\xi_x}{2\xi} v - 2\xi \eta_x \int_0^{\eta} f(y) F d\eta \right] \quad (B.19)$$

solving for the dependent variable V,

$$V = \frac{2\xi}{\xi_x} \{ r^j \rho \tilde{v} t^j + 2\xi \eta_x f(y) F \}$$

substituting for ξ_x and re-arranging,

$$V = \frac{2\xi}{\rho e u e \mu e r o^{2j}} \left[f(y) F \eta_x + \frac{r^j t^j \rho \tilde{v}}{2\xi} \right]$$

which is the same as Equation (B.16).

To obtain the continuity equation, differentiate equation (B.17) w.r.t. η , as follows:

$$V \eta = - 2\xi \frac{\partial}{\partial \xi} \{ 2\xi f(y) F \} + 0$$

Simplifying

$$V \eta = -2\xi f(y) F \xi - f(y) F$$

Rearranging the above equation as

$$V \eta + f(y) F + 2\xi f(y) F \xi = 0 \quad (B.20)$$

The continuity equation in Levy-Lees variable including the blockage effect is obtained.

Momentum Equation

Rewriting the momentum equation (B.7) as:

$$f(y) \rho u \frac{\partial u}{\partial x} + \rho \tilde{v} \frac{\partial u}{\partial y} = -f(y) \frac{dp}{dx} + \frac{1}{r^j} \frac{1}{B(y)} \frac{\partial}{\partial y} \left[B(y) r^j \left(\mu \frac{\partial u}{\partial y} - \rho \overline{u'v'} \right) \right] - \frac{1}{2} \rho u^2 \frac{C_D D(y)}{B(y) \ell^2} \quad (B.21)$$

Equation (B.21) is divided into small terms I, II, III, and IV for convenience. Each term will be tackled individually. Considering term I,

$$\begin{aligned}
 I &= f(y) \rho u \frac{\partial u}{\partial x} + \rho \tilde{v} \frac{\partial u}{\partial y} \\
 &= f(y) \rho u e F \xi_x \frac{\partial}{\partial \xi} + \eta_x \frac{\partial}{\partial \eta} + \frac{\rho}{\rho_0^j \rho t^j} \\
 &\quad \frac{\xi_x v}{2\xi} - 2\xi \eta_x f(y) F \eta_x f(y) \frac{\partial}{\partial \eta} u e F \\
 &= f(y) \rho u e^2 F \xi_x F_\xi + f(y) \rho u e^2 F \eta_x F_\eta \\
 &\quad + f(y) \rho u e F^2 \xi_x u e_\xi + \frac{\rho}{\rho_0^j \rho t^j} \frac{t^j u e \rho_0^j \rho}{2\xi} \\
 &\quad \frac{\xi_x v}{2\xi} u e F_\eta - 2\xi \eta_x f(y) u e F F_\eta
 \end{aligned}$$

$$\begin{aligned}
 I &= f(y) \rho u e^2 F \xi_x F_\xi + f(y) \rho u e^2 / F \eta_x F_\eta \\
 &\quad + f(y) \rho u e F^2 \xi_x u e_\xi + \frac{u e^2 \rho}{2\xi} \frac{\xi_x v}{2\xi} F_\eta - f(y) \eta_x \rho u e / F F_\eta
 \end{aligned}$$

$$\begin{aligned}
 I &= f(y) \rho u e^2 F \xi_x F_\xi + f(y) \rho u e \xi_x F^2 u e_\xi \\
 &\quad + \frac{\rho u e^2 \xi_x v}{2\xi} F_\eta \quad (B.22)
 \end{aligned}$$

Considering term II,

$$II = -f(y) \frac{dp}{dx}$$

From invicid flow

$$\frac{dp_e}{d\xi} = -\rho_e u e \frac{du_e}{d\xi}$$

Substituting in II above,

$$II = +f(y) \rho e u e u_{e_x} = f(y) \rho e u e \xi_x u e_{\xi}$$

$$II = f(y) \rho e u e \xi_x u e_{\xi} \quad (B.23)$$

Considering term III now,

$$III = \frac{1}{B(y)} \frac{1}{r^j} \left(B(y) r^j \left[\mu \frac{\partial u}{\partial y} - \rho u' v' \right] \right)$$

But;

$$\epsilon \Gamma = -\rho \frac{\overline{u'v'}}{\partial u / \partial y}$$

Where Γ is the intermittency factor.

$$\begin{aligned} III &= \frac{1}{B(y)} \frac{1}{r^j} \eta_y \left[B(y) r^j (\mu + \epsilon \Gamma) \frac{\partial u}{\partial y} \right] \\ &= \frac{1}{B(y)} \frac{1}{r^j} \eta_y \left[B(y) r^j (\mu + \epsilon \Gamma) u e \bar{F}_n^{-r_y} \right] \eta \\ &= \frac{1}{B(y)} \frac{1}{r^j} \left[\frac{t^j u e r o^j \rho}{2\xi} \right] \left[\frac{B(y) r^j (\mu + \epsilon \Gamma) u e t^j u e r c^j \rho F_n}{2\xi} \right] \eta \\ III &= \frac{1}{B(y)} \frac{u e^3 r o^{2j} \rho}{2\xi} \{ t^{2j} (\mu + \epsilon \Gamma) \rho F_n \} \eta \end{aligned}$$

Finally, considering term IV,

$$\begin{aligned}
 IV &= -\frac{1}{2} C_D \frac{D(y)}{B(y)\ell^2} \rho v^2 \\
 &= -\frac{1}{2} C_D \frac{D(y)}{B(y)\ell^2} \rho ue^2 F^2 \\
 IV &= -\frac{1}{2} C_D \frac{D(y)}{B(y)\ell^2} \rho ue^2 F^2 \tag{B.25}
 \end{aligned}$$

Substitute Equation (B.22) to (B.25) in Equation (B.21)

$$\begin{aligned}
 &f(y) \rho ue^2 F \xi_x F_\xi + f(y) \rho ue \xi_x F^2 ue_\xi + \frac{\rho ve^2 \xi_x v}{2\xi} F_\eta \\
 &= f(y) \rho e ue \xi_x ue_\xi + \frac{ue^3 ro^{2j} \rho}{B(y) 2\xi} \{B(y) t^{2j} (\mu + \epsilon\Gamma) \rho F_\eta\}_\eta \\
 &\quad - \frac{1}{2} C_D \frac{D(y)}{B(y)\ell^2} \rho ue^2 F^2 \tag{B.26}
 \end{aligned}$$

Simplifying:

$$\begin{aligned}
 &\frac{ue^2}{2\xi} \rho F \xi_x \{2\xi f(y) F_\xi + f(y) \frac{2\xi}{ue} F ue_\xi\} \\
 &+ \frac{\rho ue^2 \xi_x v}{2\xi} F_\eta = f(y) \rho e ue \xi_x ue_\xi + \frac{ue^3 ro^{2j} \rho}{B(y) 2\xi} \\
 &\quad \{t^{2j} (\mu + \epsilon\Gamma) \rho F_\eta\}_\eta - \frac{1}{2} C_D \frac{D(y)}{B(y)\ell^2} \rho ue^2 F^2
 \end{aligned}$$

Dividing the above equation by $\xi_x \frac{ue^2}{2\xi} \rho$

$$\begin{aligned}
 & 2\xi f(y) F F_\xi + f(y) \frac{2\xi}{ue} F^2 ue_\xi + VF_\eta \\
 &= f(y) \frac{\rho e}{\rho} \frac{2\xi}{ue} ue_\xi + \frac{uero^{2j}}{B(y)\xi_x} \{B(y) t^{2j} (\mu + \epsilon\Gamma)\rho F_\eta\}_\eta \\
 & \qquad \qquad \qquad - \frac{1}{2} C_D \frac{D(y)}{B(y)\lambda^2} \frac{2\xi}{\xi_x} F^2 \qquad (B.27)
 \end{aligned}$$

Substituting β , as defined earlier by eqn (35):

$$\begin{aligned}
 & 2\xi f(y) F F_\xi + f(y) \beta F^2 + VF_\eta = f(y)\theta\beta \\
 & \qquad \qquad \qquad + \frac{uero^{2j}\rho}{B(y)\rho ue ue ro^{2j}} \{t^{2j} B(y)(\mu + \epsilon\Gamma)\rho F_\eta\}_\eta \\
 & \qquad \qquad \qquad - C_D \frac{D(y)}{B(y)\lambda^2} \frac{2\xi}{\rho ue ue ro^{2j}} F^2
 \end{aligned}$$

Simplifying further,

$$\begin{aligned}
 & 2\xi f(y) F F_\xi + f(y)\beta(F^2 - \theta) + VF_\eta = \\
 & \frac{1}{B(y)} \left[B(y)t^{2j}(\mu + \epsilon\Gamma) \frac{\rho}{\rho e} \frac{1}{ue} F_\eta \right]_\eta - C_D \frac{D(y)}{B(y)\lambda^2} \frac{\xi F^2}{\rho ue ue ro^{2j}} \\
 & = \frac{1}{B(y)} \{B(y)t^{2j}(1 + \frac{\epsilon\Gamma}{\mu})\lambda F_\eta\}_\eta - C_D \frac{D(y)}{B(y)\lambda^2} \frac{\xi F^2}{\rho ue ue ro^{2j}}
 \end{aligned}$$

$$= \frac{1}{B(y)} \{B(y)t^{2j} \bar{\epsilon} \& F_{\eta}\}_{\eta} - C^D \frac{D(y)}{B(y)\ell^2} \frac{\xi F^2}{\rho u \epsilon \mu \epsilon r o^{2j}}$$

Hence, the momentum equations become:

$$2\xi f(y)FF_{\xi} + F(y)\beta(F^2 - \theta) + VF_{\eta} = \frac{1}{B(y)} \{B(y)t^{2j} \bar{\epsilon} \& F_{\eta}\}_{\eta} - C_D \frac{D(y)}{B(y)\ell^2} \frac{\xi F^2}{\rho u \epsilon \mu \epsilon r o^{2j}}$$

The source-sink term is defined as follows:

$$\phi_{ss} = \frac{C_D D(y)}{B(y)\ell^2} \frac{\xi}{r o^{2j} \rho u \epsilon \mu \epsilon} \quad (B.28)$$

To obtain the final form of mean-momentum equation including the effect of surface roughness, in the Levy-Lees variables, substitute (B.28) in the momentum eqn above,

$$2\xi f(y)FF_{\xi} + f(y)\beta(F^2 - \theta) + VF_{\eta} = \frac{1}{B(y)} \{B(y)t^{2j} \bar{\epsilon} \& F_{\eta}\}_{\eta} - \phi_{ss}F^2 \quad (B.29)$$

Energy Equation:

Rewriting the Energy equation (B9) as:

$$f(y)\rho u \frac{\partial T}{\partial x} + \rho \tilde{v} \frac{\partial T}{\partial y} = f(y) \frac{u}{C_p} \frac{dp}{dx} + \frac{1}{B(y)} r^j \frac{\partial}{\partial y}$$

$$\left[B(y)r^j \frac{K\ell}{C_p} \frac{\partial}{\partial y} (C_p T) \right] + \frac{\mu}{C_p} \left(\frac{\partial u}{\partial y} \right)^2 + \frac{1}{B(y)} r^j \frac{\partial}{\partial y}$$

$$\{B(y)r^j (-C_p \rho \overline{v'T'})\} - \frac{\rho \overline{u'v'}}{C_p} \frac{\partial u}{\partial y} + \frac{1}{2B(y)} \frac{\rho u^3 C_D D(y)}{L^2 C_p} \quad (B.30)$$

Eqn (B.20) is divided into small terms I, II, III, and IV for convenience. Each term will be considered individually. First, considering term I,

$$\begin{aligned}
 I &= f(y)\rho u \frac{\partial T}{\partial x} + \rho \tilde{v} \frac{\partial T}{\partial y} \\
 &= f(y)\rho u e F \frac{\partial (Te\theta)}{\partial x} + \frac{\rho}{\rho r_o^j t^j} \left[\frac{\xi_x}{2\xi} v - \sqrt{2\xi} \eta_x f(y) F \right] \frac{\partial (Te\theta)}{\partial y} \\
 &= f(y)\rho u e F \left[\xi_x \frac{\partial}{\partial \xi} + \eta_x \frac{\partial}{\partial \eta} \right] Te\theta + \frac{T \eta_y}{\rho r_o^j t^j} \frac{\xi_x V}{\sqrt{2\xi}} - 2\xi \eta_x f(y) F \theta_\eta \\
 &= f(y)\rho u e F \xi_x Te \theta_\xi + f(y)\rho u e F \xi_x \theta Te_\xi + \frac{T \eta_y \xi_x}{\rho r_o^j t^j \sqrt{2\xi}} V \theta_\eta \\
 &\quad + f(y)\rho u e F T \eta_x \theta_\eta - \frac{T \eta_y \sqrt{2\xi} \eta_x f(y)}{\rho r_o^j t^j} F \theta_\eta
 \end{aligned}$$

$$\text{But } \eta_y = \frac{\rho r_o^j t^j}{\sqrt{2\xi}} \quad \xi_x = \rho r_o^{2j} u e u e$$

Term I becomes:

$$\begin{aligned}
 I &= f(y)\rho u e F T e \xi_x \theta_\xi + f(y)\rho u e \xi_x F \theta Te_\xi + T e \frac{\rho r_o^j t^j}{\sqrt{2\xi}} \frac{V \theta_\eta \xi_x}{\rho r_o^j t^j \sqrt{2\xi}} \\
 &\quad + f(y)\rho u e \eta_x T e F \theta_\eta - \frac{T e \sqrt{2\xi} \eta_x}{\rho r_o^j t^j} \frac{\rho r_o^j t^j}{\sqrt{2\xi}} f(y) F \theta_\eta
 \end{aligned}$$

$$\begin{aligned}
 I &= f(y)\rho u e F T e \xi_x \theta_\xi + f(y)\rho u e \xi_x F \theta Te_\xi \\
 &\quad + \frac{\rho u e}{2\xi} T e \xi_x V \theta_\eta \quad (B.31)
 \end{aligned}$$

$$II = f(y) \frac{u}{C_p} \frac{dp}{dx} + \frac{1}{B(y)r^j C_p} \frac{\partial}{\partial y} \{B(y)r^j \frac{K\ell}{C_p} \frac{\partial}{\partial y} (C_p T)\} + \frac{\mu}{C_p} \left(\frac{\partial u}{\partial y}\right)^2$$

But: $\frac{dp}{dx} = \xi_x \rho_e u_e u_{e\xi}$ and $\frac{K\ell}{C_p} = \frac{\mu}{Pr}$

Hence, term II becomes:

$$II = -f(y) \frac{u_e^F}{C_p} (\xi_x \rho_e u_e u_{e\xi}) + \frac{1}{B(y)r^j C_p} \eta_y \frac{\partial}{\partial y} \{B(y)r^j \frac{\mu}{Pr} C_p T_e \eta_y \theta_\eta\} + \left(\frac{\mu}{C_p} u_e^F \eta_y\right)^2 \quad (B.32)$$

$$III = \frac{1}{B(y)r^j C_p} \frac{\partial}{\partial y} \{B(y)r^j (-C_p \overline{\rho v' T'})\} - \frac{\overline{\rho u' v'}}{C_p} \frac{\partial u}{\partial y}$$

But: $-C_p \overline{\rho v' T'} = +K_T \frac{\partial T}{\partial y}$ and $-\overline{\rho u' v'} = \epsilon \frac{\partial u}{\partial y}$

$$III = \frac{\eta_y}{B(y)r^j C_p} \frac{\partial}{\partial y} \{B(y)r^j (K_T \frac{\partial T}{\partial y})\} + \frac{\epsilon}{C_p} \left(\frac{\partial u}{\partial y}\right)^2$$

$$= \frac{\eta_y}{B(y)r^j C_p} \frac{\partial}{\partial y} \{B(y)r^j K_T T_e \eta_y \theta_\eta\} + \frac{\epsilon}{C_p} (u_e^F \eta_y)^2 \quad (B.33)$$

$$IV = \frac{1}{2B(y)} \frac{\rho u^3}{C_p} \frac{C_D D(y)}{\ell^2} = \frac{1}{2B(y)} \frac{C_D D(y)}{\ell^2} \frac{\rho u_e^3}{C_p} F^3 \quad (B.34)$$

Substitute (B.31) to (B.34) in (B.30)

$$\begin{aligned}
 & f(y)\rho u_e F T_e \xi_x \theta_\xi + f(y)\rho u_e \xi_x F \theta T_e \xi + \frac{\rho u_e}{2\xi} T_e \xi_x V \theta_\eta \\
 & = -f(y) \frac{u_e F}{C_p} (\xi_x \rho_e u_e u_{e\xi}) + \frac{1}{B(y)r^j C_p} \eta_y \frac{\partial}{\partial \eta} \{B(y)r^j \frac{\mu}{Pr} C_p T_e \eta_y \theta_\eta\} \\
 & + \frac{\mu}{C_p} (u_e F \eta_y)^2 + \frac{\eta_y}{B(y)r^j C_p} \frac{\partial}{\partial \eta} \{B(y)r^j K_T T_e \eta_y \theta_\eta\} \\
 & + \frac{\epsilon}{C_p} (u_e F \eta_y)^2 + \frac{1}{2B(y)} \frac{C_D D(y)}{C_p l^2} \rho u_e^3 F^3
 \end{aligned}$$

Multiplying the above equn by $2\xi/\rho T_e u_e \xi_x$,

$$\begin{aligned}
 & 2\xi f(y) F \theta_\xi + 2\xi f(y) \frac{F}{T_e} \theta T_{e\xi} + V \theta_\eta = \\
 & -f(y) \frac{2\xi F}{\rho T_e C_p} (\rho_e u_e u_{e\xi}) + \frac{\eta_y}{B(y)r^j C_p} \frac{\partial}{\partial \eta} \left[B(y)r^j \frac{\mu}{Pr} \frac{C_p \eta_y (2\xi)}{\rho u_e \xi_x} \theta_\eta \right] \quad \text{I}_A \\
 & + 2\xi \frac{\mu}{C_p} \frac{u_e F \eta_y^2}{\rho T_e \xi_x} + \frac{\eta_y}{B(y)r^j C_p} \frac{\partial}{\partial \eta} \left[B(y)r^j \frac{K_T 2\xi \eta_y}{\rho u_e \xi_x} \theta_\eta \right] \quad \text{I}_B \\
 & + \frac{2\xi \epsilon}{C_p} \frac{u_e F \eta_y^2}{\rho T_e \xi_x} + \frac{1}{2B(y)} \frac{C_D D(y)}{C_p l^2} 2\xi \frac{u_e^2 F^3}{\rho T_e \xi_x} \quad \text{I}_C \quad (B.35)
 \end{aligned}$$

From invicid flow

$$T_o = T_e + \frac{1}{2} \frac{u_e^2}{C_p} \quad T_{e\xi} = -\frac{u_e}{C_p} u_{e\xi}$$

or

$$\frac{2\xi}{C_p T_e} T_{e\xi} = \frac{u_e^2}{C_p T_e} \frac{2\xi}{u_e} u_{e\xi} = -\frac{u_e^2}{C_p T_e} \beta = -\alpha\beta \quad (B.36)$$

$$2\xi f(y)F \theta_\xi + V\theta_\eta = I_A + II_A + I_B + II_B + III_A \quad (B.37)$$

$$\begin{aligned} I_A + I_B &= \frac{1}{B(y)r^j} \frac{\partial}{\partial y} \left[B(y)r^j \frac{\mu}{Pr} \frac{\eta_y^2 (2\xi)}{u_e \xi_x} + \frac{K_T}{C_p} \frac{2\xi \eta_y^2}{\rho u_e \xi_x} \theta_\eta \right] \\ &= \frac{1}{B(y)r^j} \frac{\partial}{\partial \eta} \left[B(y)r^j \frac{\mu}{Pr} + \frac{K_T}{C_p} \frac{2\xi \eta_y^2}{\rho u_e \xi_x} \theta_\eta \right] \end{aligned}$$

But $\frac{K_T}{C_p} = \frac{\epsilon}{Pr_t}$

$$\begin{aligned} &= \frac{1}{B(y)r^j} \frac{\partial}{\partial \eta} \left[B(y)r^j \left(\frac{\mu}{Pr} + \frac{\epsilon}{Pr_t} \right) \frac{2\xi r_o^{2j} t^{2j} \rho u_e^2}{2\xi \rho u_e r_o^{2j} \rho_e \mu_e u_e} \theta_\eta \right] \\ &= \frac{1}{B(y)r^j} \frac{\partial}{\partial \eta} \left[t^{2j} B(y)r^j \left(1 + \frac{\epsilon}{\mu} \right) \frac{Pr}{Pr_t} \frac{\rho \mu}{\rho_e \mu_e} \frac{1}{Pr} \theta_\eta \right] \\ &= \frac{1}{B(y)r^j} \frac{\partial}{\partial \eta} \left[t^{2j} r^j B(y) \hat{\epsilon} \frac{g}{Pr} \theta_\eta \right] \quad (B.38) \end{aligned}$$

Where

$$\hat{\epsilon} = 1 + \frac{\epsilon}{\mu} \frac{\text{Pr}}{\text{Pr}_t}$$

$$\ell = \frac{\rho \mu}{\rho_e u_e}$$

$$\begin{aligned} \text{II}_A + \text{II}_B &= 2\xi \frac{\mu}{C_p} \frac{u_e}{\rho T_e} \frac{F \eta^2 \eta_y^2}{\xi_x} + \frac{2\xi \epsilon}{C_p} u_e \frac{F \eta^2 \eta_y^2}{\rho T_e \xi_x} \\ &= 2\xi \frac{u_e}{\rho T_e} \frac{\eta_y^2}{\xi_x} \left[\frac{\mu}{C_p} + \frac{\epsilon}{C_p} \right] F \eta^2 \\ &= 2\xi \frac{u_e}{\rho C_p T_e} \frac{r_o^{2j} t^{2j} \rho^2 u_e^2}{2\xi (r_o^{2j} \rho_e u_e u_e)} \mu \left[1 + \frac{\epsilon}{\mu} \right] F \eta^2 \\ &= t^{2j} \frac{\rho \mu}{\rho_e u_e} \frac{u_e^2}{C_p T_e} \{\bar{\epsilon}\} F \eta^2 \\ &= t^{2j} \ell \alpha \bar{\epsilon} F \eta^2 \quad (\text{B.39}) \end{aligned}$$

where $\bar{\epsilon} = 1 + \frac{\epsilon}{\mu}$ and $\alpha = \frac{u_e^2}{C_p T_e}$

$$\text{III}_A = \frac{1}{2B(y)} \frac{C_D D(y)}{\ell^2} 2\xi \frac{\rho u_e^2 F^3}{C_p \rho T_e \xi_x}$$

Re-arranging

$$\text{III}_A = \frac{C_D D(y)}{B(y) \ell^2} \frac{u_e^2}{C_p T_e} \frac{\xi F^3}{r_o^{2j} \rho_e u_e u_e}$$

Using definition for α and ϕ_{ss}

$$III_A = \alpha \phi_{ss} F^3 \quad (B.40)$$

Substituting (B.38) to (B.40) in (B.37) we have:

$$2\xi f(y)F\theta_\xi + V\theta_\eta = \frac{1}{B(y)r^j} \frac{\partial}{\partial \eta} \left\{ t^{2j} r^j B(y) \hat{\epsilon} \frac{\xi}{Pr} \theta_\eta \right\}$$

$$= t^{2j} \xi \alpha \bar{\epsilon} F^2 + \alpha \phi_{ss} F^2$$

$$2\xi f(y)F\theta_\xi + V\theta_\eta - \frac{1}{B(y)r^j} \left[t^{2j} r^j B(y) \hat{\epsilon} \frac{\xi}{Pr} \theta_\eta \right]_\eta$$

$$- t^{2j} \xi \alpha \bar{\epsilon} F_n^2 - \alpha \phi_{ss} F^3 = 0 \quad (B.41)$$

Appendix C

Difference Relations

Three point central differencing relations for η and three point or two point backward differencing relations are used to reduce the transformed continuity, momentum and energy equations to finite difference form. It is assumed that all data are known at the solution station $i-2$ and $i-1$ (Fig 3), and the unknown quantities need to be determined at the grid points for "i" station. The finite difference equations were derived with the stipulation that a function could be described at any point by a Taylor series expansion about another point. For the present study the approximation was made that for any functional value F ,

$$F(i-1,j) = F(i,j) - \Delta\xi_{i-1} \frac{\partial F(i,j)}{\partial \xi} + \frac{\Delta\xi_{i-1}^2}{2} \frac{\partial^2 F(i,j)}{\partial \xi^2} \quad (C.1a)$$

and

$$F(i+1,j) = F(i,j) - (\Delta\xi_{i-2} + \Delta\xi_{i-1}) \frac{\partial F(i,j)}{\partial \xi} + \frac{(\Delta\xi_{i-1} + \Delta\xi_{i-2})^2}{2} \frac{\partial^2 F(i,j)}{\partial \xi^2} + \dots \quad (C.1b)$$

The scaling factor for ξ derivative are defined as follows:

$$Y1 = \frac{2(\Delta\xi_{i-2} + 2\Delta\xi_{i-1})}{(\Delta\xi_{i-1} + \Delta\xi_{i-2})} \quad (C.2)$$

$$Y2 = \frac{2(\Delta\xi_{i-1} + \Delta\xi_{i-2})}{(\Delta\xi_{i-2})} \quad (C.3)$$

$$Y3 = \frac{2\Delta\xi_{i-1}^2}{\Delta\xi_{i-2}(\Delta\xi_{i-1} + \Delta\xi_{i-2})} \quad (C.4)$$

$$Y4 = \frac{(\Delta\xi_{i-2} + \Delta\xi_{i-1})}{\Delta\xi_{i-2}} \quad (C.5)$$

$$Y5 = \frac{\Delta\xi_{i-1}}{\Delta\xi_{i-2}} \quad (C.6)$$

Using scaling factors defined in eqn (C.2) to (C.6), Equation (C.1a) and (C.1b) can be solved to yield

$$\left[\frac{\partial F}{\partial \xi} \right]_{i,j} = \frac{Y3 F(i-2,j) - Y2 F(i-1,j) + Y1 F(i,j)}{2\Delta\xi_{i-1}} \quad (C.7)$$

and

$$F(i,j) = Y4 F(i-1,j) - Y5 F(i-2,j) \quad (C.8)$$

Terms of the order $\Delta\xi_{i-1}$ $\Delta\xi_{i-2}$ or smaller are neglected. This procedure produces truncation errors of the order of $\Delta\xi_{i-2}$ $\Delta\xi_{i-1}$.

For obtaining expression for $\frac{\partial F}{\partial \eta}$, $\frac{\partial^2 F}{\partial \eta^2}$, etc, the Taylor series expansions are next written about the unknown grid point (i,j) in the η -direction as follows:

$$F(i,j+1) = F(i,j) + \Delta\eta_j F_\eta(i,j) + \frac{\Delta\eta_j^2}{2} F_{\eta\eta}(i,j) + \dots \quad (C.9a)$$

$$F(i,j-1) = F(i,j-1) - \Delta\eta_{j-1} F_\eta(i,j-1) + \frac{\Delta\eta_{j-1}^2}{2} F_{\eta\eta}(i,j-1) \dots \quad (C.9b)$$

Equations (A8a) and (A8b) can be solved to yield expression for $F_{\eta\eta}$ and F_η as follows:

$$F_{\eta\eta}(i,j) = \frac{Y6}{\Delta\eta_j^2} F(i,j+1) - \frac{2Y7}{\Delta\eta_j^2} F(i,j) + \frac{Y8}{\Delta\eta_j^2} F(i,j-1) \quad (C.10)$$

and

$$F_\eta(i,j) = \frac{Y9}{2\Delta\eta_j} F(i,j+1) - \frac{Y10}{\Delta\eta_j} F(i,j) - \frac{Y8}{2\Delta\eta_j} F(i,j-1) \quad (C.11)$$

where the coefficients Y6, Y7,....Y10 coefficients are defined as follows:

$$Y6 = 2 / \left[1 + \frac{\Delta\eta_{j-1}}{\Delta\eta_j} \right] \quad (C.12)$$

$$Y7 = \Delta\eta_j / \Delta\eta_{j-1} \quad (C.13)$$

$$Y8 = 2 / \left[\frac{\Delta\eta_{j-1}}{\Delta\eta_j} \left[1 + \frac{\Delta\eta_{j-1}}{\Delta\eta_i} \right] \right] \quad (C.14)$$

$$Y9 = 2 / \left[1 + \frac{\Delta\eta_j}{\Delta\eta_{j-1}} \right] \quad (C.15)$$

$$Y10 = 1 - \frac{\Delta\eta_j}{\Delta\eta_{j-1}} \quad (C.16)$$

Finite-difference representations for $\frac{\partial\theta}{\partial\eta}$, $\frac{\partial^2\theta}{\partial\eta^2}$, $\frac{\partial\theta}{\partial\xi}$, $\frac{\partial V}{\partial\eta}$ are derived simultaneously.

All of these are substituted in equations (30) to (32) to obtain the corresponding finite-difference equation. Due to their recurring appearance, the following symbols and their definitions are introduced:

$$FM1 = Y4 F(i-1, j) - Y5 F(i-2, j)$$

$$TM1 = Y4 T(i-1, j) - Y5 T(i-2, j)$$

and (C.17)

$$FM2 = Y2 F(i-1, j) - Y3 F(i-2, j)$$

$$TM2 = Y2 T(i-1, j) - Y3 T(i-2, j)$$

Non-linear terms of the form, $(G \frac{\partial H}{\partial \xi})$, where G and H represent any typical dependent variable, appearing in the governing equations need to be linearized in order to obtain a system of linear difference equations. Quantities of this type are linearized by using equation (C.7) and (C.8), i.e.,

$$(G \frac{\partial H}{\partial \xi})_{i,j} = \{Y_A G(i-1,j) - Y_5(i-2,j)\} \{Y_3 H(i-2,j) - Y_2 H(i-1,j) + Y_4 H(i,j)\} / 2\Delta\xi_{i-1} + C(\Delta\xi_{i-1} \Delta\xi_{i-2}) \quad (C.18)$$

For example,

$$(F \frac{\partial F}{\partial \xi})_{i,j} = FM1 \{Y_2 FM1 - Y_3 FM2\} \quad (C.19)$$

The procedure used to linearize these non-linearized product terms such as $(\frac{\partial G}{\partial \eta})(\frac{\partial H}{\partial \eta})$ is as follows:

$$\begin{aligned} \{(\frac{\partial G}{\partial \eta})(\frac{\partial H}{\partial \eta})\}_{i,j} &= (\frac{\partial G}{\partial \eta})_{i-1,j} (\frac{\partial H}{\partial \eta})_{i,j} - (\frac{\partial G}{\partial \eta})_{i-1,j} (\frac{\partial H}{\partial \eta})_{i-1,j} \\ &\quad + (\frac{\partial H}{\partial \eta})_{i-1,j} (\frac{\partial G}{\partial \eta})_{i,j} \end{aligned} \quad (C.20)$$

where the terms $(\frac{\partial G}{\partial \eta})_{i-1,j}$ and $(\frac{\partial H}{\partial \eta})_{i-1,j}$ are discretized

according to eqn (C.11) but evaluated at preceding station

(i-1). The linearization for quantities of the form $(\frac{\partial G}{\partial \eta})^2$ is obtained by setting H to G in eqn (C.19).

For example:

$$\left\{ \frac{\partial F(i,j)}{\partial u} \right\}^2 = 2FY \left\{ \frac{\partial F(i,j)}{\partial \eta} \right\} - FY^2 \quad (C.21)$$

$$F^2 = 2F(i,j) F(i-1,j) - F(i-1,j)^2 \quad (C.22)$$

where FY denotes $\frac{\partial F(i-1,j)}{\partial \eta}$, a known quantity whereas $\frac{\partial F(i,j)}{\partial \eta}$ and F(i,j) are unknown.

All terms had been represented in finite difference form, and the final step incorporated these linearized models into equations (30), (31), and (32) to derive the overall system of finite difference equations (Ref 19:67-71).

Appendix D

Coefficient in Difference Equation

Equation (53) to (55) are the difference equations used to represent the partial differential equation for the conservation of momentum and energy and continuity respectively. These equations are repeated here for convenience.

Momentum:

$$\begin{aligned} &A1(n,1) F_{n-1} + A1(n,2) F_n + A1(n,3) F_{n+1} \\ &+ B1(n,1) \theta_{n-1} + B1(n,2) \theta_n + B1(n,3) \theta_{n+1} \\ &+ C1(n,1) V_{n-1} + C1(n,2) V_n + C1(n,3) V_{n+1} = D1(n) \quad (D.1) \end{aligned}$$

Energy:

$$\begin{aligned} &A2(n,1) F_{n-1} + A2(n,2) F_n + A2(n,3) F_{n+1} \\ &+ B2(n,1) \theta_{n-1} + B2(n,2) \theta_n + B2(n,3) \theta_{n+1} \\ &+ C2(n,1) V_{n-1} + C2(n,2) V_n + C2(n,3) V_{n+1} = D2(n) \quad (D.2) \end{aligned}$$

Continuity:

$$\begin{aligned} &A3(n,1) F_{n-1} + A3(n,2) F_n + A3(n,3) F_{n+1} \\ &+ B3(n,1) \theta_{n-1} + B3(n,2) \theta_n + B3(n,3) \theta_{n+1} \\ &+ C3(n,1) V_{n-1} + C3(n,2) V_n + C3(n,3) V_{n+1} = D3(n) \quad (D.3) \end{aligned}$$

These equations are obtained from equations (48), (49), and (50) and the difference quotients presented in Appendix 'C'. The coefficients A1(n,1), B1(n,1) and so forth in equations (D.1), (D.2), and (D.3) are functions of known quantities evaluated at station i-1, and i-2.

The coefficients are as follows:

$$A1(N,1) = Y8 * XL * (2. * XLM1 * EM1 / DY - (XLM1 * EYM1 + EM1 * XLPM1 * TY + BYPP * EM1 * XLM1 / BYM1 - VM1)) \quad (D.4)$$

$$A1(N,2) = -(4. * XL * XLM1 * EM1 * Y7 / DY + 2. * XL * (XLM1 * EYM1 + BYPP * EM1 * XLM1 / BYM1 + EM1 * XLPM1 * TY - VM1) * Y10 - 2. * DX2 * FM1 * (XFY(N) * XBE + XSS(N)) * SEP + SEP * (2. * Y1 * FM1 - FM2) * XFY(N) * X) \quad (D.5)$$

$$A1(N,3) = XL * (2. * XLM1 * EM1 * Y6 / DY + (XLM1 * EYM1 - EM1 * XLPM1 * TY + BYPP * EM1 * XLM1 / BYM1 - VM1) * Y9) \quad (D.6)$$

$$B1(N,1) = -XL * EM1 * XLPM1 * FY * Y8 \quad (D.7)$$

$$B1(N,2) = DX2 * XBE * XFY(N) - 2. * XL * EM1 * XLPM1 * FY * Y10 \quad (D.8)$$

$$B1(N,3) = XL * EM1 * XLPM1 * FY * Y9 \quad (D.9)$$

$$C1(N,1) = C1(N,3) = 0. \quad (D.10)$$

$$C1(N,2) = DX2 * FY \quad (D.11)$$

$$A2(N,1) = -2. * XL * XAL * XLM1 * EM1 * FY * Y8 \quad (D.12)$$

$$A2(N,2) = -(4. * XL * XAL * XLM1 * EM1 * FY * Y10 + SEP * X * Y1 * TM1 - TM2) * XFY(N) - 3. * DX2 * XAL * XSS(N) * FM1 * X * SEP \quad (D.13)$$

$$A2(N,3) = 2. * XL * XAL * XLM1 * EM1 * FY * Y9 \quad (D.14)$$

$$B2(N,1) = XL * Y8 * (2. * XLM1 * ETM1 / (PR * DY) - (XLM1 * EYM1 + 2. * XLPM1 * ETM1 * TY + BYPP * XLM1 * ETM1 / BYM1 - PR * VM1) / PR) \quad (D.15)$$

$$B2(N,2) = (4. * XL * XLM1 * ETM1 * Y7 / (PR * DY) + XLM1 * EYM1 + 2. * XLPM1 * ETM1 * TY + BYPP * XLM1 * ETM1 / BYM1 - PR * VM1) * XL * Y10 * 2.0 / PR + SEP * X * Y1 * XFY(N) * FM1 \quad (D.16)$$

$$B2(N,3) = XL * (2. * XLM1 * ETM1 * Y6 / DY + (XLM1 * EYM1 + 2. * XLPM1 * ETM1 * TY + BYPP * XLM1 * ETM1 / BYM1 - PR * VM1) * Y9) / PR \quad (D.17)$$

$$C2(N,2) = -DX2 * TY \quad (D.18)$$

$$C2(N,1) = C2(N,3) = 0. \quad (D.19)$$

$$A3(N,1) = A3(N,3) = 0. \quad (D.20)$$

$$A3(N,2) = (DX2 + X * Y1) * XFY(N) \quad (D.21)$$

$$B3(N,1) = B3(N,2) = B3(N,3) = 0. \quad (D.22)$$

$$C3(N,1) = -XL * Y8 \quad (D.23)$$

$$C3(N,2) = -2. * XL * Y10 \quad (D.24)$$

$$C3(N,3) = XL * Y9 \quad (D.25)$$

$$D1(N) = DX2 * FY * (EM1 * XLPM1 * TY - VM1) - FM1 * X * SEP * (XBE * XFY(N) * DX2 + X * Y1 + DX2 * XSS(N)) * SEP \quad (D.26)$$

$$D2(N) = DX2 * (XLPM1 * ETM1 * TY / PR - VM1) * TY + DX2 * XAL * XLM1 * EM1 * FY * X * 2 - X * XFY(N) * Y1 * TM1 * FM1 * XFY(N) * SEP + DX2 * XAL * 2. * XSS(N) * FM1 * X * 3 * SEP \quad (D.27)$$

$$D3(N) = X * FM2 * XFY(N) \quad (D.28)$$

The additional quantities appearing in equations (D.4) to (D.28) are defined as follows:

$$FM1 = Y4 F(i-1,j) - Y5 F(i-2,j) \quad (D.29)$$

$$TM1 = Y4 T(i-1,j) - Y5 T(i-2,j) \quad (D.30)$$

$$VM1 = Y4 V(i-1,j) - Y5 V(i-2,j) \quad (D.31)$$

$$FM2 = Y2 F(i-1,j) - Y3 F(i-2,j) \quad (D.32)$$

$$TM2 = Y2 T(i-1,j) - Y3 T(i-2,j) \quad (D.33)$$

$XLM1 = \rho = (\rho\mu)/(\rho\mu)_e$ which may be written as

$$XLM1 = TM1 \frac{1 + \left(\frac{S}{T}\right)_e i}{TM1 + \left(\frac{S}{T}\right)_e i} \quad (\text{air only}) \quad (D.34)$$

$$XLPM1 = \rho_p = \frac{XLM1}{2TM1} \frac{\left(\frac{S}{T}\right)_e i - TM1}{\left(\frac{S}{T}\right)_e i + TM1} \quad (D.35)$$

$$EM1 = \bar{\epsilon}(i,j) = \frac{\bar{\epsilon}(i,j-1) + \bar{\epsilon}(i,j) + \bar{\epsilon}(i,j+1)}{3} \quad (D.36)$$

$$ETM1 = \hat{\epsilon}(i,j) \quad (D.37)$$

$$BYM1 = B(y)(i,j) \quad (\text{eqn 20}) \quad (D.38)$$

$$FY = \frac{Y9}{2\Delta\eta} F(i-1,j+1) - \frac{Y10}{\Delta\eta} F(i-1,j) - \frac{Y8}{2\Delta\eta} F(i-1,j-1) \quad (D.39)$$

$$TY = \frac{Y9}{2\Delta\eta} T(i-1, j+1) - \frac{Y10}{\Delta\eta} F(i-1, j) - \frac{Y8}{2\Delta\eta} F(i-1, j-1) \quad (D.40)$$

$$EYM1 = \frac{Y9}{2\Delta\eta} \bar{\epsilon}(i-1, j+1) - \frac{Y10}{\Delta\eta} \bar{\epsilon}(i-1, j) - \frac{Y8}{2\Delta\eta} \bar{\epsilon}(i-1, j-1) \quad (D.41)$$

$$ETYM1 = \frac{Y9}{2\Delta\eta} \bar{\epsilon}(i-1, j+1) - \frac{Y10}{\Delta\eta} \bar{\epsilon}(i-1, j) - \frac{Y8}{2\Delta\eta} \bar{\epsilon}(i-1, j-1) \quad (D.42)$$

$$BYPP = \frac{Y9}{2\Delta\eta} BY(i-1, j+1) - \frac{Y10}{\Delta\eta} BY(i-1, j) - \frac{Y8}{2\Delta\eta} BY(i-1, j-1) \quad (D.43)$$

$$XBE = \beta(i, j) = \left(\frac{2\xi}{u_e} \frac{du_e}{d\xi} \right)_i \quad (D.44)$$

$$XAL = \alpha(i, j) = \left(\frac{u_e^2}{T_e} \right)_i \quad (D.45)$$

$$XI = \frac{\Delta\xi}{2\Delta\eta} \quad (D.46)$$

$$XFY = f(y)(i, j) \quad (\text{eqn 21}) \quad (D.47)$$

$$XSS = \phi_{ss}(i, j) \quad (\text{eqn 37}) \quad (D.48)$$

Equations (D.1), (D.2), and (D.3) are solved simultaneously by Gaussian elimination technique.

Appendix E

PROGRAM LISTING

PROGRAM ITRACT(INPUT,OUTPUT,TAPE5=INPUT,TAPE6=OUTPUT)

```
C *****
C THIS PROGRAM SOLVES COMPRESSIBLE TURBULENT BOUNDARY-LAYER
C INCLUDING THE EFFECT OF SURFACE ROUGHNESS.THE SHAPE,HEIGHT
C AND DENCITY OF THE ROUGHNESS ELEMENTS IS SPECIFIED TO THE
C CODE IN SUBROUTINE RUFVAR.
C *****
COMMON G, PR, REY, XMINF, OMEGA, BO, TW, P10, T10, R10, VIS10, TE.
1 PE, RE, UE, VISINF, SU, EPS, DS, DYW, SI, ERROR, TC, TA, IEDGE, IEND1, INTACT,
2 PRT, XXK, BTRX, XLAM, VARPRT, XINTER, SEPO, ICHS(8), IPRN(9), EO(300),
3 EN(300), EP(300), ETO(300), ETN(300), ETP(300), FO(300), FN(300), J2DA,
4 FP(300), TN(300), TO(300), XNN(300), VN(300), VO(300), VP(300), TP(300).
5 D1(300), D2(300), D3(300)
  DIMENSION Y(300), A1(300,3), A2(300,3), A3(300,3), B1(300,3),
1 B2(300,3), B3(300,3), C1(300,3), C2(300,3), C3(300,3)
  COMMON/CPDATA/ CP(24), XP(24), DP(24), IPRES
  COMMON/BLRVAR/BYD(300), BYN(300), BYP(300), XFY(300), XSS(300).
1 XBRE, XHRE, XLS, XCD
1100 FORMAT(1H0,12X,3HS/L,15X,2HCP,15X,6HP/PINF)
1101 FORMAT(1X,3(4X,E15.9))
2008 FORMAT(1X,*PROFILE FAILED TO RELAX AT H = *,I5)
8002 FORMAT (5E10.6)
8003 FORMAT (10I5)
9002 FORMAT(1H1,47X*INTERACTING BOUNDARY LAYER SOLUTION*)
9003 FORMAT (7HOGAMMA=F6.3,4H PR=F6.3,5H MFS=F6.3,7H REYFS=E10.4,8H TFS
1(K)=F7.1,11H BO=TW/T10=F6.4,5H EPS=F8.5)
9004 FORMAT(5HOP10=,E10.4,7H RHG10=,E10.4,5H T10=,E10.4,7H VIS10=,E10.4
1,4H SI=,E10.4)
9005 FORMAT(7HOOmega=,F7.4,2X,6HPRT = ,F7.4,2X,7HBTRX = ,F7.4)
9019 FORMAT(10X,*WITH INTERMITTENCY CORRECTION*)
9020 FORMAT(10X,*WITHOUT INTERMITTENCY CORRECTION*)
9021 FORMAT(10X,*TWO-DIMENSIONAL BOUNDARY LAYER*)
9022 FORMAT(10X,*AXISYMETRICAL BOUNDARY LAYER*)
9023 FORMAT(10X,/*---- SOLUTION NEEDS MORE POINTS FOR CONVERGENC---*/)
C
C INPUT INITIAL CONDITIONS
C
  READ(5,8002) G, PR, XMINF, REY, TA
  READ(5,8002) DS, SI, OMEGA, ERROR, XXK
  READ(5,8002) BO,BTRX, PRT, XINTER, DYW
  READ(5,8003) IEDGE, INTACT, IDIFF, IEND1, MSP, J2DA , IPRES
  READ(5,8003) (ICHS(I), I = 1, 8)
```

```

READ(5,8003) (IPRN(I), I = 1. 9)
XLAM=.5*BTRX
IF(IPRES.EQ.0) GO TO 20
READ(5,8002) DPMAX
READ(5,8002) (CP(IJ), IJ=1, IPRES)
READ(5,8002) (XP(IJ), IJ=1, IPRES)
WRITE(6,1100)
XMSQ=XMINF*XMINF
DO 10 IJ=1, IPRES
PDPINF=1.0+0.5*G*XMSQ*CP(IJ)
WRITE(6,1101) XP(IJ), CP(IJ), PDPINF
10 CP(IJ)=PDPINF
CALL SMTHPR(BTRX, DPMAX, G, XMSQ)

C
C COMPUTE NONDIMENSIONALIZING QUANTITIES
C
20 Z1= 1. + (G - 1.)/2.*XMINF**2
P10 = (1./(G*XMINF**2))*(Z1**(G/(G-1.)))
T10 = (1./((G - 1.)*XMINF**2))*Z1
R10 = G*P10/(T10*(G - 1.))
TINF = T10/Z1
TW = BO*T10
IF(OMEGA .EQ. 0.) GO TO 101
VIS10 = T10**OMEGA
EPS = (((G - 1.)*XMINF**2)**(OMEGA/2.))/SQRT(REY)
VISINF = TINF**OMEGA
GO TO 102
101 TC=198.6/((G-1.)*XMINF**2*TA)
VIS10 = (T10**1.5)*(1. + TC)/(T10+TC)
EPS = (((1.+(198.6/TA))*(((G - 1.)*XMINF**2)**1.5))/((G-1.)*X
MINF**2)+(198.6/TA))/REY)**.5
VISINF = (TINF**1.5)*(1. + TC)/(TINF+TC)
102 SU=198.6

C
C OUTPUT INITIAL CONDITIONS
C
WRITE(6,9002)
WRITE(6,9003) G, PR, XMINF, REY, TA, BO, EPS
WRITE(6,9004) P10, R10, T10, VIS10, SI
WRITE(6,9005) OMEGA, PRT, BTRX
IF(XINTER.EQ.1.) WRITE(6,9019)
IF(XINTER.EQ.0.) WRITE(6,9020)
IF(J2DA.EQ.0) WRITE(6,9021)
IF(J2DA.NE.0) WRITE(6,9022)

C
C INPUT INITIAL PROFILE
C
12 MSTART=2
C INITIALIZE THE STREAMWISE LOCATION
S=SI
DS2=DS1=DS
DX2DS=DX1DS=DXDS=0.

```

```

      SEPO=1.
C     INITIALIZE THE STREAMWISE LOCATION
      Y(1)=0.0
      DO 201 LL=2,300
      DY=XXK**(LL-2)*DYW
201   Y(LL)=Y(LL-1)+DY
      DO 700 LL = 1, 300
      D1(LL)=D2(LL)=D3(LL)=XNN(LL)=0.
      VP(LL)=VN(LL)=VO(LL)=-Y(LL)
      FP(LL)=FO(LL)=FN(LL)=TP(LL)=TN(LL)=TO(LL)=EP(LL)=EO(LL)=EN(LL)=
1     ETP(LL)=ETO(LL)=ETN(LL)=BYP(LL)=BYO(LL)=BYN(LL)=1.0
700   CONTINUE
      DO 701 J = 1, 300
      DO 701 I = 1, 3
701   A1(J,I)=A2(J,I)=A3(J,I)=B1(J,I)=B2(J,I)=B3(J,I)=C1(J,I)
1     =C2(J,I)=C3(J,I)=0.
      PREF=G*XMINF**2
      TREF = (G - 1.)*XMINF**2
C
C     INITIALIZE COUNTERS
C
      ICOUN=MSTART
      IQ=IEDGE
      IG=1
      IF=1
      INJCH=0
      ITCNT1 = 1
      IIN=0
C
C     *** BEGIN FIRST-ORDER TRIDIAGONAL MATRIX SOLUTION ***
C
      DO 115 M=MSTART,IEND1
      IF(M.EQ.MSTART) MP=MSTART
      IF(M.EQ.IEND1) MP=M
      IF(M.EQ.(M/MSP)*MSP) MP=M
      S=S+DS2
      DX2DS = DX1DS
      DX1DS = DXDS
C
C     COMPUTE LOCAL PRESSURE AND PRESSURE GRADIENT
C
      CALL PRESSM(S,XMINF,G,PBG1,DPBG1,TETNF,XME)
C
C     COMPUTE LOCAL EDGE PROPERTIES
C
      PE = PBG1/PREF
      PP = DPBG1/PREF
      TE = TETNF/TREF
      UE = SQRT(2.*(T10 - TE))
      RE=G*PE/((G-1.0)*TE)
      TR=SU/(TETNF*TA)
      IF (OMEGA) 642,676,642

```

```

642 XNUE=TE**OMEGA
      GOTO689
676 XNUE=TE**1.5*(1.+198.6/(TA*TREF))/(TE+198.6/(TA*TREF))
688 CONTINUE
C
C   COMPUTE LOCAL XI AND STEP LENGTHS
C
      DXDS=RE*UE*XNUE
      IF(J2DA.NE.0) DXDS=DXDS**2
      IF(M.EQ.2) DX1DS=DX2DS=DXDS
      DX2=.5*DS2*((1.+DS2/DS1)*DX1DS+DS1*DXDS/(DS1+DS2)-DS2*DS2*DX2DS/
1 (DS1*(DS1+DS2)))
      REYNDE=RE*UE*S/XNUE
      REYEXT=REY*VISINF*REYNDE
      IF(M.EQ.2) DX1=DX2
      IF(M.EQ.2) X=DXDS*SI
      X=X+DX2
C
C   COMPUTE STEP LENGTH FUNCTIONS
C
      Y1=2.*(DX1+2.*DX2)/(DX1+DX2)
      IF(IDIFF.EQ.1) Y1 = 2.
      Y2=((DX1+DX2)/DX1)**2.0
      Y3=(DX2*DX2/(DX1*(DX1+DX2)))*2.0
      Y4=(DX1+DX2)/DX1
      Y5=DX2/DX1
      TWTE = TW/TE
C
C   COMPUTE ALPHA, BETA, AND LAMBDA
C
      DUEDX=-FP/(RE*UE*DXDS)
      XAL=UE*UE/TE
      XBE=2.0*X*DUEDX/UE
C
C   ASSIGN ROUGHNESS VARIABLES TO ELMATX
C
      CALL RUFVAR(X,XNUE)
C
6998 LENGTH=IEDGE
C
C   ASSIGN THE MATRIX ELEMENTS FOR THE FINITE DIFFERENCE EQUATIONS
      CALL ELMATX( M,DX2,X,XAL,XBE,TR,IDIFF,Y1,Y2,Y3,Y4,Y5,TWTE,ITCNT1.
1 A1,A2,A3,B1,B2,B3,C1,C2,C3)
C   ASSIGN THE MATRIX ELEMENTS FOR THE FINITE DIFFERENCE EQUATIONS
C
C
C   MATRIX INVERSION, SOLVE FOR F, THETEA AND V
C
      CALL MATEQN3(FP,TP,VP,D1,D2,D3,A1,B1,C1,A2,B2,C2,A3,B3,C3,3,LENGTH
1 ,300)
C
C   MATRIX INVERSION, SOLVE FOR F, THETEA AND V
C

```

```

ITCNT1=ITCNT1+1
N=IEDGE+1
DY=DYW*XXX**(IEDGE-2)
VK=(VP(IEDGE)/(XXX*(1.+1./XXX))-VP(IEDGE-1)*(1.-1./XXX)*XXX-
1 VP(IEDGE-2)*XXX/(1.+1./XXX))/DY
DY=DYW*XXX**(IEDGE-1)
KON=N+5
DO65IQ=N,KON
DY=DYW*XXX**(N-1)+DY
FP(IQ)=TP(IQ)=1.0
65 VP(IQ)=VP(IEDGE-1)+vK*DY
C INITIATION OF SIMILAR SOLUTIONS
IF(M.EQ.2) GO TO 8020
GO TO 8018
8020 DO 8019 I=1,KON
VO(I)=VN(I)=VP(I)
FO(I)=FN(I)=FP(I)
8019 TO(I)=TN(I)=TP(I)
C INITIATION OF SIMILAR SOLUTIONS
8018 IQ=IEDGE+1
C
C U AND THETA PROFILES ITERATIONS
TAU2=(FP(2)-FP(1))/DYW
IF(ITCNT1.EQ.2) TAU1=10.*TAU2
RT12=TAU1/TAU2-1.
TAU1=TAU2
IF(ITCNT1 .LE. 100) GO TO 7005
WRITE(6,2008) M
CALL EXIT
7005 IF(ABS(RT12).GT.ERROR) GO TO 4995
C U AND THETA PROFILES ITERATIONS
C
C
C COMPUTE BLT, BDT(DELTA STAR) AND BMT(THETA)
55 CO=TP(1)
TPI=0.
BLT=BLDT=BLMT=0.
XNN(1)=0.
DO 57 N=2,KON
DY=DYW*XXX**(N-2)
C=TP(N)
TPI=TPI+.5*DY*(CO+C)
CO=C
XNN(N)=TPI*SQRT(2.*X)/(RE*UE)
IF(J2DA.NE.0) XNN(N)=XNN(N)/S
BLDT=BLDT+(2.-FP(N)/TP(N)-FP(N-1)/TP(N-1))*(XNN(N)-XNN(N-1))/2.
BLMT=BLMT+(FP(N)*(1.-FP(N))/TP(N)+FP(N-1)*(1.-FP(N-1))/TP(N-1))
1 *(XNN(N)-XNN(N-1))/2.
IF(BLT.GT.0.) GO TO 57
IF(FP(N).GE.0.99) BLT=XNN(N)-(FP(N)-.99)*(XNN(N)-XNN(N-1))
1 /(FP(N)-FP(N-1))
57 CONTINUE

```



```

BLT=BLT*EPS
BLDT=BLDT*EPS
BLMT=BLMT*EPS
C COMPUTE BLT, BDT(DELTA STAR) AND BMT(THETA)
C
C COMPUTE THE EDDY VISCOSITY COEFFICIENT
IF(S.LE.BTRX) GO TO 58
CALL REYSTR (KON,TR,X,TREF,XNUE,XBE,S,ITCNT1)
C COMPUTE THE EDDY VISCOSITY COEFFICIENT
C
58 ITCNT1=1
C
C ASSESMENT OF GRID PONITS IN ETA
C
IF(INDCH) 71, 71, 732
71 CONTINUE
IF(M - 20) 732, 732, 72
72 IF(ABS(FP(IEDGE-15)-FP(IEDGE-16))-0.0001) 73,73,74
73 IF(ABS(TP(IEDGE-15) - TP(IEDGE-16)) - .0001) 732, 732, 74
C *****
C FOR TURBULENT FLOW SOLUTION NEEDS TO BE MONITORED CLOSE
C TO THE OUTER EDGE.WHILKE ADDING MORE POINTS THE MAXIMUM
C VALUE OF IEDGE BE RESTRICTED TO MAX. DIMENSIONS MINUS 25.
C *****
74 IF(IEDGE.GT.275) GO TO 75
IEDGE=IEDGE+1
IQ=IQ+1
WRITE(6,9023)
75 DY=DYW*XXX**(IEDGE-2)
Y(IEDGE) = Y(IEDGE-1) + DY
732 IQ = IQ - 1
C ASSESMENT OF GRID PONITS IN ETA
C
C
C COMPUTE WALL STRESS AND HEAT TRANSFER AND OUTPUT STATION
CALL CFSTND (TR,XNUE,X,S,XBE,M,BLDT,BLMT,BLT,PBG1,DPBG1,REYEXT,
1 XME,MP)
C COMPUTE WALL STRESS AND HEAT TRANSFER AND OUTPUT STATION
C
C
C SHIFT PROFILES BACK ONE XI STATION
C
NN = IQ + 5
DO 118 N=1,NN
FN(N)=FO(N)
FO(N)=FP(N)
TN(N)=TO(N)
TO(N)=TP(N)
VN(N)=VO(N)
VO(N)=VP(N)
ETN(N)=ETO(N)
ETO(N)=ETP(N)

```

```

EN(N)=EO(N)
EO(N)=EP(N)
BYN(N)=BYO(N)
BYO(N)=BYP(N)
118 CONTINUE
DX1=DX2
DS1=DS2
IF(M+1-ICHS(IG)) 114,113,114
113 DS2=2.0*DS1
IG = IG+1
INDCH = 1
IF (M.EQ.IEND1) GO TO 237
GO TO 111
114 DS2=DS1
INDCH = 0
IF (M.EQ.IEND1) GO TO 237
GO TO 111
237 IIN = 1
111 CALL PRNCHS (ICOUN,IP,IG,IQ,MSTART,IIN,M,S,Y,BLT,XME)
115 CONTINUE
STOP
END
SUBROUTINE PRESSM(S,XM,G,P,DPDX,T,YM)
COMMON/CPDATA/ CP(24),XP(24),DP(24),IPRES
100 FORMAT(5X,*WARNING...CALCULATION IS OUTSIDE OF THE PRESCRIBED PR
PRESSURE DATA, S IS LESS THAN XP(1)*)
200 FORMAT(5X,*WARNING...CALCULATION IS OUTSIDE OF THE PRESCRIBED PR
PRESSURE DATA, S IS GREATER THAN XP(END)*)
300 FORMAT(1X,5E15.9)
IR=0
IPM1=IPRES-1
IF(IPRES.EQ.0) GO TO 40
DO 20 I=1,IPRES
IF(S.LT.XP(I)) WRITE(6,100)
IF(S.GT.XP(IPRES)) WRITE(6,200)
IF(S.LE.XP(I)) IR=1
IF(IR.NE.0) GO TO 30
IF(S.GE.XP(IPM1)) IR=IPRES
IF(IR.NE.0) GO TO 30
IF((S.GE.XP(I)).AND.(S.LT.XP(I+1))) IR=I
IF(IR.EQ.0) GO TO 20
C SEEKING THE BEST FIT
RS=(S-XP(I))/(XP(I+1)-XP(I))
IF(RS.GT.0.5) IR=I+1
C SEEKING THE BEST FIT
IF(IR.NE.0) GO TO 30
20 CONTINUE
30 IF(IR.GT.IPM1) IR=IPM1
IRP=IR+1
IRM=IR-1
IF(IR.EQ.1) IRM=IR+2
C COMPUTE THE CUBIC SPLINE COEFFICENTS

```

```

X1=(XP(IRP)+XP(IRM)-2.0*XP(IR))*(XP(IRP)-XP(IRM))
X2=(XP(IRM)-XP(IR))*(XP(IRM)-XP(IR))
X3=(XP(IRP)-XP(IR))*(XP(IRP)-XP(IR))
X4=XP(IRM)-XP(IRP)
X5=XP(IRM)-XP(IR)
X6=XP(IRP)-XP(IR)
DETS=X5*X6*X4
C2=(DP(IR)*X1+DP(IRP)*X2-DP(IRM)*X3)/DETS
C3=(DP(IR)*X4-DP(IRP)*X5+DP(IRM)*X6)/DETS
C COMPUTE THE CUBIC SPLINE COEFFICIENTS
DXP=S-XP(IR)
DXP2=DXP**2
DXPF=DXP/20.
DPDX1=DP(IR)
P=CP(IR)
DO 10 I=1,20
X=I*DXPF
X2=X*X
DPDX2=DP(IR)+C2*X+C3*X2
P=P+0.5*(DPDX1+DPDX2)*DXPF
10 DPDX1=DPDX2
DPDX=DP(IR)+C2*DXP+C3*DXP2
T=P**((G-1.0)/G)
YM=SQRT(2.0*((2.0+(G-1.0)*XM*XM)/(2.0*T)-1.0)/(G-1.0))
WRITE(6,300) S,P,DPDX,T,YM
GO TO 50
40 F=1.0
DPDX=0.
T=P**((G-1.0)/G)
YM=SQRT(2.0*((2.0+(G-1.0)*XM*XM)/(2.0*T)-1.0)/(G-1.0))
50 RETURN
END
SUBROUTINE SMTHPR(BTRX,DPMAX,G,XMSQ)
COMMON/CPDATA/ CP(24),XP(24),DP(24),IPRES
100 FORMAT(1X,*FIRST CP DATA POINT YIELDS ADVERSE PRESSURE GRADIENT TO
10 STEEP FOR CALCULATION TO CONTINUE*)
200 FORMAT(1H0,11X,3HS/L,15X,2HCP,11X,6HP/PINF,14X,4HDPDX)
300 FORMAT(1X,4(4X,E15.9))
DPTOL=DPMAX*1.01
C COMPUTE THE TRAILING EDGE DPDX
IPM1=IPRES-1
IPM2=IPRES-2
DX1=XP(IPM1)-XP(IPRES)
DX2=XP(IPM2)-XP(IPRES)
DX12=DX1*DX1
DX22=DX2*DX2
DP(IPRES)=(CP(IPM2)*DX12-CP(IPM1)*DX22-CP(IPRES)*(DX12-DX22))/
1 (DX1*DX2*(DX1-DX2))
C COMPUTE THE TRAILING EDGE DPDX
10 IMAX=0
C COMPUTE THE LEADING EDGE DPDX
DX1=XP(2)-XP(1)

```

```

DX2=XP(3)-XP(1)
DX12=DX1#DX1
DX22=DX2#DX2
DP(1)=(CP(3)#DX12-CP(2)#DX22-CP(1)#(DX12-DX22))/(DX1#DX2*(DX1-
1 DX2))
IF(DP(1).GT.DPMAX) WRITE(6,100)
IF(DP(1).GT.DPMAX) CALL EXIT
C COMPUTE THE LEADING EDGE DPDX
DO 20 I=2,IPM1
IM1=I-1
IP1=I+1
DX1=XP(IM1)-XP(I)
DX2=XP(IP1)-XP(I)
DX12=DX1#DX1
DX22=DX2#DX2
DP(I)=(CP(IP1)#DX12-CP(IM1)#DX22-CP(I)#(DX12-DX22))/(DX1#DX2*
1 (DX1-DX2))
20 IF((DP(I).GT.DPTOL).AND.(XP(I).LE.BTRX)) IMAX=I
IF(IMAX.EQ.0) GO TO 50
C SMOOTHING THE CP DATA IN THE LEADING EDGE REGION
IMM1=IMAX-1
IMP1=IMAX+1
DX1=XP(IMM1)-XP(IMAX)
DX2=XP(IMP1)-XP(IMAX)
DX12=DX1#DX1
DX22=DX2#DX2
CP(IMM1)=(CP(IMP1)#DX12-CP(IMAX)#(DX12-DX22)-DX1#DX2*(DX1-DX2)
1 #DPMAX)/DX22
GO TO 10
C SMOOTHING THE CP DATA IN THE LEADING EDGE REGION
50 WRITE(6,200)
DO 30 I=1,IPRES
PC=2.0*(CP(I)-1.0)/(G*XMSQ)
30 WRITE(6,300) XP(I),PC,CP(I),DP(I)
RETURN
END

C
C *****
C
C THIS S/R HAS BEEN MODIFIED TO INCLUDE THE
C EFFECT OF SURFACE ROUGHNESS @@@@@@@@@@@@
C
C *****
C SUBROUTINE CFSTNO (TR,XNUE,X,S,XBE,M,BLDT,BLMT,BLT,PBG1,DPBG1,
1 REYEXT,XME,MP)
COMMON G,PR,REY,XMINF,OMEGA,BO,TW,P10,Y10,R10,VIS10,TE,
1 PE,RE,UE,VISINF,SU,EPS,DW,DYW,SI,ERROR,TC,TA,LEDGE,IEND1,INTACT,
2 PRT,XXK,BTRX,XLAM,VARPRT,XINTER,SEPD,ICHS(8),IPRN(9),EO(300),
3 EN(300),EP(300),ETO(300),ETN(300),ETP(300),FO(300),FN(300),J2DA,
4 FP(300),TN(300),TD(300),XNN(300),VN(300),VO(300),VP(300),TP(300),
5 D1(300),D2(300),D3(300)
COMMON/BLRVAR/BYD(300),BYN(300),BYF(300),XFY(300),XSS(300),

```

```

1 XBRE, XHRE, XLS, XCD
2000 FORMAT (1H0, 10X, 5HS/L =, E15.8)
2001 FORMAT (2), 7HXME =, E15.8, 2X, 7HPE =, E15.8, 2X, 7HDPPINF=, E15.8,
1 2Y, 7HXBF =, E15.8, 2X, 7HTW/TE =, E15.8)
2002 FORMAT (2), 7HBLT =, E15.8, 2X, 7HBLMT =, E15.8, 2X, 7HBLDT =, E15.8,
1 2X, 7HREYMT =, E15.8, 2X, 7HREYDT =, E15.8)
2003 FORMAT (2X, 7HCFND =, E15.8, 2X, 7HCFEND =, E15.8, 2X, 7HSTNO =, E15.8,
1 2X, 7HSTEND =, E15.8, 2X, 7HREYEXT=, E15.8)
TAUR=0.
FPSI=0.
FP(1)=0.
CO=FP(1)**2
DO 100 N=2, IEDGE
XYY=XNN(N)*EPS
IF(XYY-XHRE)853, 853, 854
853 DY=DYW*XXK**(N-2)
C=FP(N)**2
FPSI=FPSI+.5*DY*(CO+C)
TAUR=FPSI*.5*XCD*XBRE*UE*SQRT(2.*X)/XLS**2
CO=C
100 CONTINUE
854 TWTE=TP(1)
IF(OMEGA.EQ.0.) GO TO 855
IF(OMEGA .EQ. 1.) GO TO 8551
XLM1 = 1./(TWTE**(1. - OMEGA))
GO TO 856
855 XLM1 = (1.0+TR)*SQRT(TWTE)/(TWTE+TR)
GO TO 856
8551 XLM1 = 1.
856 CONTINUE
Y11=((2.+XXK)*(1.+XXK+XXK**2)+1.+XXK)/((1.+XXK)*(1.+XXK+XXK**2))
Y12=(1.+XXK+XXK**2)/XXK**2
Y13=(1.+XXK+XXK**2)/(XXK**3*(1.+XXK))
Y14=1./(XXK**3*(1.+XXK+XXK**2))
TAU=XLM1*RE*NXNUE*UE*UE*(-Y11*FP(1)+Y12*FP(2)-Y13*FP(3)+Y14*FP(4))
1 / (DYW*SQRT(2.*X))+TAUR
QS = XLM1*RE*NXNUE*UE*TE*(Y11*TP(1)-Y12*TP(2)+Y13*TP(3)-Y14*TP(4))
1 / (DYW*SQRT(2.*X)*PR)
IF(J2DA.NE.0) TAU=TAU*S
IF(J2DA.NE.0) QS=QS*S
STNO = 0.
IF(BO .NE. 1.) STNO = EPS*QS/((1. - BO)*(TE + .5*UE**2))
STEND = STNO/(RE*UE)
CFNO = 2.*EPS*TAU
CFENO = CFNO/(RE*UE*UE)
REYDT=REYEXT*BLDT/S
REYMT=REYEXT*BLMT/S
C SELECTION OF THE OUTPUT
IF(M.NE.MP) GO TO 1000
C SELECTION OF THE OUTPUT
C
C OUTPUT STATION DATA

```

```

C
WRITE(6,2000) S
WRITE(6,2001) XME,PBG1,DPBG1,XBE,TWTE
WRITE(6,2002) BLT,BLMT,BLDT,REYMT,REYDT
WRITE(6,2003) CFNO,CFEND,STNO,STENO,REYEXT
1000 RETURN
END
SUBROUTINE ELMATX( M,DX2,X,XAL,XBE,TR,IDIFF,Y1,Y2,Y3,Y4,Y5,TWTE,
1 ITCNT1, A1,A2,A3,B1,B2,B3,C1,C2,C3)
COMMON G, PR, REY, XMINF, OMEGA, BO, TW, P10, T10, R10, VIS10, TE,
1 PE,RE,(IE,VISINF,SU,EPS,DS,DYW,SI,ERROR,TC,TA,IEDGE,IEND1,INTACT,
2 PRT,XXK,BTRX,XLAM,VARPRT,XINTER,SEPO,ICHS(8),IPRN(9),EG(300),
3 EN(300),EP(300),ETO(300),ETN(300),ETP(300),FO(300),FN(300),J2DA,
4 FP(300),TN(300),TO(300),XNM(300),VN(300),VO(300),VP(300),TP(300),
5 D1(300),D2(300),D3(300)
COMMON/BLRVAR/BYD(300),BYN(300),BYF(300),XFY(300),XSS(300),
1 XBRE,XHRE,XLS,XCD
DIMENSION A1(300,3),A2(300,3),A3(300,3),B1(300,3),B2(300,3),
1 B3(300,3),C1(300,3),C2(300,3),C3(300,3)
C
C THE INNER EDGE BOUNDARY CONDITION
C
DO 8011 I=1,3
8011 A1(1,I)=A2(1,I)=A3(1,I)=B1(1,I)=B2(1,I)=B3(1,I)=C1(1,I)=C2(1,I)
1 =C3(1,I)=0.
A1(1,1)=1.0
B2(1,1)=1.0
D1(1)=0.
D2(1)=TWTE
IF(SEPO.EQ.0.) GO TO 8012
C3(1,1)=1.0
D3(1)=0.
GO TO 8013
8012 XL=DX2/(2.0*DYW)
A3(1,1)=DX2+X*Y1
C3(1,1)=-2.*XL*(2.+XXK)/(1.+XXK)
C3(1,2)=2.*XL*(1.+XXK)/XXK
C3(1,3)=-2.*XL/(XXK*(1.+XXK))
D3(1)=0.
C
C THE INNER EDGE BOUNDARY CONDITION
C
C THE FIELD POINTS EVALUATION
C
8013 NM1=IEDGE-1
DO 8014 N=2,NM1
DY=XXK** (N-1) *DYW
DYM1=DY/XXK
XL=DX2/(2.0*DY)
Y6=2./(1.+DYM1/DY)
Y7=DY/DYM1
Y8=2./((DYM1/DY)*(1.+DYM1/DY))

```

```

Y9=2./(1.+DY/DYM1)
Y10=1.-DY/DYM1
SEP=1.0
IF(FO(N).LE.0.) SEP=0.
IF(ITCNT1 .GT. 1) GO TO 7000
IF(IDIFF .EQ. 1) GO TO 7501
FM1=Y4*FO(N)-Y5*FN(N)
TM1=Y4*TO(N)-Y5*TN(N)
VM1=Y4*VO(N)-Y5*VN(N)
IF(SEPO.EQ.0.) VM1=VO(N)
EM1=(Y4*(EO(N-1)+EO(N)+EO(N+1))-Y5*(EN(N-1)+EN(N)+EN(N+1)))/3.
ETM1=(Y4*(ETO(N-1)+ETO(N)+ETO(N+1))-Y5*(ETN(N-1)+ETN(N)+ETN(N+1)))/3.
BYM1=(Y4*(BYO(N-1)+BYO(N)+BYO(N+1))-Y5*(BYN(N-1)+BYN(N)+BYN(N+1)))/3.
GO TO 7001
7501 FM1 = FO(N)
TM1 = TO(N)
VM1 = VO(N)
EM1=(EO(N-1)+EO(N)+EO(N+1))/3.
ETM1=(ETO(N-1)+ETO(N)+ETO(N+1))/3.
BYM1=(BYO(N-1)+BYO(N)+BYO(N+1))/3.
GO TO 7001
7000 FM1 = FP(N)
TM1 = TP(N)
VM1 = VP(N)
EM1=(EP(N-1)+EP(N)+EP(N+1))/3.
ETM1=(ETP(N-1)+ETP(N)+ETP(N+1))/3.
BYM1=(BYP(N-1)+BYP(N)+BYP(N+1))/3.
7001 IF(OMEGA .EQ. 0.) GO TO 684
IF(OMEGA .EQ. 1.) GO TO 6841
XLM1=1./(TM1*(1.-OMEGA))
XLPM1=(OMEGA-1.)*XLM1/TM1
GOTO625
6841 XLM1=1.
XLPM1=0.
GOTO625
684 XLM1=((1.+TR)*SQRT(TM1)/(TM1+TR))
XLPM1=XLM1*(TR-TM1)/(2.*TM1*(TM1+TR))
625 IF(ITCNT1.GT.1) GO TO 626
FY=(Y9*FO(N+1)/2.-Y10*FO(N)-Y8*FO(N-1)/2.)/DY
TY=(Y9*TO(N+1)/2.-Y10*TO(N)-Y8*TO(N-1)/2.)/DY
EYM1=(Y9*EO(N+1)/2.-Y10*EM1-Y8*EO(N-1)/2.)/DY
ETYM1=(Y9*ETO(N+1)/2.-Y10*ETM1-Y8*ETO(N-1)/2.)/DY
BYPP=(Y9*BYO(N+1)/2.-Y10*BYM1-Y8*BYO(N-1)/2.)/DY
GO TO 627
626 FY=(Y9*FP(N+1)/2.-Y10*FP(N)-Y8*FP(N-1)/2.)/DY
TY=(Y9*TP(N+1)/2.-Y10*TP(N)-Y8*TP(N-1)/2.)/DY
EYM1=(Y9*EP(N+1)/2.-Y10*EM1-Y8*EP(N-1)/2.)/DY
ETYM1=(Y9*ETP(N+1)/2.-Y10*ETM1-Y8*ETP(N-1)/2.)/DY
BYPP=(Y9*BYP(N+1)/2.-Y10*BYM1-Y8*BYP(N-1)/2.)/DY
627 IF(IDIFF.EQ.1) GO TO 7502

```

```

      FM2=Y2*FO(N)-Y3*FN(N)
      TM2=Y2*TO(N)-Y3*TN(N)
      GO TO 7505
7502 FM2 =2.*FO(N)
      TM2 =2.*TO(N)
7505 CONTINUE
      A1(N,1)=YB*XL*(2.*XLM1*EM1/DY-(XLM1*EYM1+EM1*XLPM1*TY+BYPP*
1 EM1*XLM1/BYM1-VM1))
      A1(N,2)=- (4.*XL*XLM1*EM1*Y7/DY+2.*XL*(XLM1*EYM1+BYPP*EM1*XLM1
1 /BYM1+EM1*XLPM1*TY-VM1)*Y10+2.*DX2*FM1*(XFY(N)*XBE+XSS(N))*SEP+
1 SEP*(2.*Y1*FM1-FM2)*XFY(N)*X)
      A1(N,3)=XL*(2.*XLM1*EM1*Y6/DY+(XLM1*EYM1+EM1*XLPM1*TY+BYPP*
1 EM1*XLM1/BYM1-VM1)*Y9)
      B1(N,1)=-XL*EM1*XLPM1*FY*Y8
      B1(N,2)=DX2*XBE*XFY(N)-2.*XL*EM1*XLPM1*FY*Y10
      B1(N,3)=XL*EM1*XLPM1*FY*Y9
      C1(N,1)=C1(N,3)=0.
      C1(N,2)=-DX2*FY
      A2(N,1)=-2.*XL*XAL*XLM1*EM1*FY*Y8
      A2(N,2)=- (4.*XL*XAL*XLM1*EM1*FY*Y10+SEP***(Y1*TM1-TM2)*
1 XFY(N)-3.*DX2*XAL*XSS(N)*FM1**2.*SEP)
      A2(N,3)=2.*XL*XAL*XLM1*EM1*FY*Y9
      B2(N,1)=XL*Y8*(2.*XLM1*ETM1/(PR*DY)-(XLM1*ETYM1+2.*XLPM1*ETM1*TY
1 +BYPP*XLM1*ETM1/BYM1-PR*VM1)/PR)
      B2(N,2)=- (4.*XL*XLM1*ETM1*Y7/(PR*DY)+(XLM1*ETYM1+2.*XLPM1*ETM1*TY
1 +BYPP*XLM1*ETM1/BYM1-PR*VM1)*XL*Y10*2.0/PR+SEP**Y1*XFY(N)*FM1)
      B2(N,3)=XL*(2.*XLM1*ETM1*Y6/DY+(XLM1*ETYM1+2.*XLPM1*ETM1*TY
1 +BYPP*XLM1*ETM1/BYM1-PR*VM1)*Y9)/PR
      C2(N,1)=C2(N,3)=0.
      A3(N,1)=A3(N,3)=0.
      A3(N,2)=(DX2+X*Y1)*XFY(N)
      B3(N,1)=B3(N,2)=B3(N,3)=0.
      C3(N,1)=-XL*Y8
      C3(N,2)=-2.*XL*Y10
      C3(N,3)=XL*Y9
      D1(N)=DX2*FY*(EM1*XLPM1*TY-VM1)-FM1**2*(XBE*XFY(N)*DX2+X*XFY(N)*Y1
1 +XSS(N)*DX2)*SEP
      D2(N)=DX2*(FM1*ETM1*TY/PR-VM1)*TY+DX2*XAL*XLM1*EM1*FY**2-X*Y1
1 *FM1*(N)*SEP+DX2*XAL*2.*XSS(N)*FM1**3*SEP
      D3(N)=X*FM2*XFY(N)
8014 CONTINUE
C
C   THE FIELD POINTS EVALUATION
C
C
C   THE OUTER EDGE BOUNDARY CONDITION
C
      DO 8015 I=1,3
8015 A1(IEDGE,I)=A2(IEDGE,I)=A3(IEDGE,I)=B1(IEDGE,I)=B2(IEDGE,I)=B3(
1 IEDGE,I)=C1(IEDGE,I)=C2(IEDGE,I)=C3(IEDGE,I)=0.
      A1(IEDGE,3)=1.0

```



```

B2(IEDGE,3)=1.0
D1(IEDGE)=1.0
D2(IEDGE)=1.0
IF(SEPO.EQ.0.) GO TO B016
XL=DX2/(2.*DYW*XXK*(IEDGE-1))
FM2=Y2*FO(IEDGE)-Y3*FN(IEDGE)
IF(IDIFF.EQ.1) FM2=2.*FO(IEDGE)
A3(IEDGE,3)=DX2+X*Y1
C3(IEDGE,1)=2.*XXK**3*XL/(1.+XXK)
C3(IEDGE,2)=-2.*XXK*(1.+XXK)*XL
C3(IEDGE,3)=2.*XXK*XL*(2.*XXK+1.)/(1.+XXK)
D3(IEDGE)=X*FM2
GO TO B017
B016 VM1=VO(IEDGE)
IF(ITCNT1.GT.1) VM1=VP(IEDGE)
C3(IEDGE,3)=1.0
D3(IEDGE)=VM1
B017 CONTINUE
C
C THE OUTER EDGE BOUNDARY CONDITION
RETURN
END
SUBROUTINE PRNCHS(ICOUN,IP,IG,IQ,MSTART,IIN,M,S,Y,BLT,XME)
COMMON G,PR,REY,XMINF,OMEGA,BO,TW,P10,T10,R10,VIS10,TE,
1 PE,RE,UE,VISINF,SU,EPS,DS,DYW,SI,ERROR,TC,TA,IEDGE,IEND1,INTACT,
2 PRT,XXK,BTRX,XLAM,VARPRT,XINTER,SEPO,ICHS(8),IPRN(9),EO(300),
3 EN(300),EP(300),ETO(300),ETN(300),ETP(300),FO(300),FN(300),J2DA,
4 FP(300),TN(300),TO(300),XNN(300),VN(300),VO(300),VP(300),TP(300),
5 D1(300),D2(300),D3(300)
DIMENSION Y(300),Z(7,16)
25 FORMAT (1H0,45X,23HPROFILE FOR STATION S =F14.8)
40 FORMAT (8HON= 15F8.4 )
41 FORMAT (8H ETA= 15F8.4 )
42 FORMAT (8H F1= 15F8.4 )
43 FORMAT (8H T1= 15F8.4 )
44 FORMAT (8H V1= 15F8.2 )
46 FORMAT (8H EO= 15F8.2)
507 FORMAT (8H Y/BLT= 15F8.4 )
509 FORMAT (8H RO/ROE=15F8.4 )
510 FORMAT (8H ML/ME= 15F8.4)
511 FORMAT (8H PT/PTE=15F8.4 )
512 FORMAT (8H PT/PE= 15F8.4 )
513 FORMAT (8H H/HE= 15F8.4 )
IF(ICOUN-IPRN(IP)) 51,38,51
C
C OUTPUT PROFILE DATA
C
38 KONT=IQ-1
J2=0
WRITE(6,25) S
DO50J1=1,KONT,15
J2=J2+1

```

```

KON=J2*15
WRITE (6,40) (XNN(N),N=J1,KON)
WRITE (6,41) (Y(N),N=J1,KON)
WRITE (6,42) (FO(N),N=J1,KON)
WRITE (6,43) (TO(N),N=J1,KON)
WRITE (6,44) (VO(N),N=J1,KON)
WRITE(6,46) (EO(N),N=J1,KON)
I=J1-1
IF(M.EQ.MSTART) GO TO 50
D0530JX=1,15
I=I+1
Z(1,JX)=EPS*XNN(I)/BLT
Z(2,JX)=FO(I)
C Z(3,JX)=TO(I)
Z(3,JX)=1./TO(I)
PTPED=(G-1.0)*TE*TO(I)
IF (PTPED) 777,777,778
777 PTPED=1.
778 Z(4,JX)=UE*Z(2,JX)/(PTPED)**.5
PTPE=Z(4,JX)*Z(4,JX)
IF(Z(4,JX)-1.0)504,504,505
504 PTPE=(1.0+(((G-1.0)/2.0)*PTPE))**(G/(G-1.0))
PTEPE=(1.0+(((G-1.0)/2.0)*XME**2))**(G/(G-1.0))
GOTO506
505 PTPE=(((G+1.0)*PTPE/2.0)**(G/(G-1.0)))*(((G+1.0)/((2.0*G*PTPE)-(G-
11.0)))**((1.0/(G-1.0))))
PTEPE=(((G+1.0)*XME**2/2.0)**(G/(G-1.0)))*(((G+1.0)/((2.0*G*XME**2)-(G-
&1.0)))**((1.0/(G-1.0))))
506 Z(5,JX)=PTPE
C Z(6,JX) = PTPE*PE/P10
Z(6,JX)=PTPE/PTEPE
Z(7,JX)=(TE*TO(I)/(UE*UE)+.5*FO(I)*FO(I))/(TE/(UE*UE)+.5)
Z(4,JX)=Z(4,JX)/XMINF
530 CONTINUE
WRITE(6,507) (Z(1,N),N=1,15)
WRITE(6,509) (Z(3,N),N=1,15)
WRITE(6,510) (Z(4,N),N=1,15)
WRITE(6,511) (Z(6,N),N=1,15)
WRITE(6,512) (Z(5,N),N=1,15)
WRITE(6,513) (Z(7,N),N=1,15)
50 CONTINUE
IF(IIN.EQ.1) RETURN
ICOUN=0
51 ICOUN=ICOUN+1
IF(M+1-ICHS(IG)) 3601,3600,3601
3600 IP=IP+1
ICOUN=IPRN(IP)
3601 CONTINUE
RETURN
END
SUBROUTINE REYSTR (KON,TR,X,TREF,XNUE,XBE,S,ITCNT1)
COMMON G, PR, REY, XMINF, OMEGA, BO, TW, P10, T10, R10, VIS10, TE,

```

```

1 PE, RE, UE, VISINF, SU, EPS, DS, DYW, SI, ERROR, TC, TA, IEDGE, IEND1, INTACT,
2 PRT, XXK, BTRX, XLAM, VARPRT, XINTER, SEPO, ICHS(B), IPRN(9), ED(300),
3 EN(300), EP(300), ETO(300), ETN(300), ETP(300), FO(300), FN(300), J2DA,
4 FP(300), TN(300), TO(300), XNN(300), VN(300), VO(300), VP(300), TP(300),
5 D1(300), D2(300), D3(300)
TTR=(TA+112.)/(TA*TREF+112.)
CO=TP(1)
DD=EP(1)=XNN(1)=TPI=BLT=0.
C SHEAR STRESS AT THE WALL AS THE SCALING FUNCTION
Y11=((2.+XXK)*(1.+XXK+XXK**2)+1.+XXK)/((1.+XXK)*(1.+XXK+XXK**2))
Y12=(1.+XXK+XXK**2)/XXK**2
Y13=(1.+XXK+XXK**2)/(XXK**3*(1.+XXK))
Y14=1./(XXK**3*(1.+XXK+XXK**2))
FETW=(-Y11*FP(1)+Y12*FP(2)-Y13*FP(3)+Y14*FP(4))/DYW
FETW=ABS(FETW)
XLM1W=(1.+TR)*SQRT(TP(1))/(TP(1)+TR)
PI2=XLM1W*FETW
C SHEAR STRESS AT THE WALL AS THE SCALING FUNCTION
DO 1 N=2,KON
DY=DYW*XXK**(N-2)
XLM1=((1.+TR)*SQRT(TP(N))/(TP(N)+TR))
C=TP(N)
TPI=TPI+.5*DY*(CO+C)
CO=C
XNN(N)=TPI*SQRT(2.*X)/(RE*UE)
IF(J2DA.NE.0) XNN(N)=XNN(N)/S
IF(BLT.EQ.0.) GO TO 2
IF(FP(N).GE.0.99) BLT=XNN(N)-(FP(N)-.99)*(XNN(N)-XNN(N-1))
1 / (FP(N)-FP(N-1))
DD=DD+((1.-FP(N))*TP(N)+(1.-FP(N-1))*TP(N-1))*DY/2.
2 PI1=SQRT(2.*X*REY/(TREF**1.5*TTR))*TPI**2/(XNUE*TP(N)**3)
IF(J2DA.NE.0) PI1= 1/S
DY=DYW*XXK**(N-1)
DYM1=DY/XXK
Y9=2./((DYM1/DY)*(1.+DYM1/DY))
Y9=2./(1.+DY/DYM1)
Y10=1.-DY/DYM1
C PI2=XLM1*EP(N)*ABS(Y9*FP(N+1)/2.-Y10*FP(N)-Y8*FP(N-1)/2.)/DY
C
C CEBICE-SMITH-MONSINKIS EDDY VISCOSITY MODEL
YPLUS=SQRT(PI1*PI2)/(26.*XLM1)
IF(YPLUS.GT.50.) YPLUS=50.
EP(N)=.16*PI1*(1.-EXP(-YPLUS))**2*ABS(Y9*
1 FP(N+1)/2.-Y10*FP(N)-Y8*FP(N-1)/2.)/(DY*XLM1)
C CEBICE-SMITH-MONSINKIS EDDY VISCOSITY MODEL
C
C TRUNCATE THE INNER REGION CALCULATION
IF(EP(N).LE.EP(N-1)) EP(N)=EP(N-1)
C TRUNCATE THE INNER REGION CALCULATION
C
1 CONTINUE
DO 3 N=1,KON

```

```

XLM1=((1.+TR)*SQRT(TP(N))/(TP(N)+TR))
DD1=.0168*SQRT(2.*X*REY/(TREF**1.5*TTR))*DD/(XNUE*XLM1*TP(N)**2)
IF(J2DA.NE.0) DD1=DD1/S
IF(DD1.LE.EP(N)) EP(N)=DD1
XXXX=.412*((S-BTRX)/XLAM)**2
IF(XXXX.GT.50.) XXXX=50.
EP(N)=EP(N)*(1.-EXP(-XXXX))
IF(XINTER.EQ.0.) EP(N)=1.+EP(N)
IF(XINTER.EQ.1.) EP(N)=1.+ (1.75/(1.+5.5*(XNN(N)/BLT)**6)+1.)*
1 EP(N) /2.75
3 ETP(N)=1.+PR*(EP(N)-1.)/PRT
C
RETURN
END
SUBROUTINE MATEQN3 (X1,X2,X3,Y1,Y2,Y3,A11,A12,A13,A21,A22,A23,
* A31,A32,A33,LC,LN,LQ)
C
C*****
C
C THIS SUBROUTINE SOLVES THE THREE SIMULTANEOUS BAND MATRIX
C EQUATIONS
C
C A11*X1 + A12*X2 + A13*X3 = Y1
C A21*X1 + A22*X2 + A23*X3 = Y2
C A31*X1 + A32*X2 + A33*X3 = Y3
C
C FOR X1, X2, AND X3
C
C A1J ARE 9 BAND MATRICES OF LENGTH LQ, WORKING LENGTH LN,
C AND WIDTH LC
C (THESE MATRICES ARE ASSUMED TO BE CORNER ADJUSTED, I.E. THE
C CORNER ELEMENTS ARE STORED IN (1,1) AND (LN,LC), ETC.)
C
C XI AND YI ARE VECTORS OF LENGTH LQ AND WORKING LENGTH LN
C
C*****
C
C DIMENSION
C * X1(LQ),X2(LQ),X3(LQ),Y1(LQ),Y2(LQ),Y3(LQ),
C * A11(LQ,LC),A12(LQ,LC),A13(LQ,LC),
C * A21(LQ,LC),A22(LQ,LC),A23(LQ,LC),
C * A31(LQ,LC),A32(LQ,LC),A33(LQ,LC)
C
C INITIALIZATION
C -----
C
C LP=LN+1
C L=(LC-1)/2
C LM=LN-L-1
C IF(LC.GE.LN) L=LN
C DO 3 I=1,LN
C X1(I)=Y1(I)

```

```

      X2(I)=Y2(I)
      X3(I)=Y3(I)
3     CONTINUE
C
C     DOWNWARD GAUSSIAN ELIMINATION WITH PIVOTING
C-----
      DO 401 K=1, LN
      IF (L.EQ.LM) L=LN
      IF (L.LT.LN) L=L+1
C
      U=ABS(A11(K,1))
      I=K
      M=1
      DO 113 J=K, L
      IF (J.EQ.K) GO TO 111
      V=ABS(A11(J,1))
      IF (V.LE.U) GO TO 111
      U=V
      M=1
      I=J
111  V=ABS(A21(J,1))
      IF (V.LE.U) GO TO 112
      U=V
      M=2
      I=J
112  V=ABS(A31(J,1))
      IF (V.LE.U) GO TO 113
      U=V
      M=3
      I=J
113  CONTINUE
      IF (I.EQ.K) GO TO 115
      IF (M.NE.1) GO TO 116
      DO 114 J=1, LC
      U=A11(K, J)
      A11(K, J)=A11(I, J)
      A11(I, J)=U
      U=A12(K, J)
      A12(K, J)=A12(I, J)
      A12(I, J)=U
      U=A13(K, J)
      A13(K, J)=A13(I, J)
      A13(I, J)=U
114  CONTINUE
      U=X1(K)
      X1(K)=X1(I)
      X1(I)=U
      GO TO 120
115  IF (M.EQ.1) GO TO 120
116  IF (M.NE.2) GO TO 118
      DO 117 J=1, LC

```

```

U=A11(K,J)
A11(K,J)=A21(I,J)
A21(I,J)=U
U=A12(K,J)
A12(K,J)=A22(I,J)
A22(I,J)=U
U=A13(K,J)
A13(K,J)=A23(I,J)
A23(I,J)=U
117 CONTINUE
U=X1(K)
X1(K)=X2(I)
X2(I)=U
GO TO 120
118 DO 119 J=1,LC
U=A11(K,J)
A11(K,J)=A31(I,J)
A31(I,J)=U
U=A12(K,J)
A12(K,J)=A32(I,J)
A32(I,J)=U
U=A13(K,J)
A13(K,J)=A33(I,J)
A33(I,J)=U
119 CONTINUE
U=X1(K)
X1(K)=X3(I)
X3(I)=U
120 CONTINUE
C
DO 128 I=K,L
IF(I.EQ.K) GO TO 123
U=A11(I,1)/A11(K,1)
DO 122 J=1,LC
IF(J.NE.1) A13(I,J-1)=A11(I,J)-A11(K,J)*U
A11(I,J)=A12(I,J)-A12(K,J)*U
A12(I,J)=A13(I,J)-A13(K,J)*U
122 CONTINUE
A13(I,LC)=0.
X1(I)=X1(I)-X1(K)*U
123 CONTINUE
U=A21(I,1)/A11(K,1)
DO 125 J=1,LC
IF(J.NE.1) A23(I,J-1)=A21(I,J)-A11(K,J)*U
A21(I,J)=A22(I,J)-A12(K,J)*U
A22(I,J)=A23(I,J)-A13(K,J)*U
125 CONTINUE
A23(I,LC)=0.
X2(I)=X2(I)-X1(K)*U
U=A31(I,1)/A11(K,1)
DO 127 J=1,LC
IF(J.NE.1) A33(I,J-1)=A31(I,J)-A11(K,J)*U

```

```

A31(I,J)=A32(I,J)-A12(K,J)*U
A32(I,J)=A33(I,J)-A13(K,J)*U
127 CONTINUE
A33(I,LC)=0.
X3(I)=X3(I)-X1(K)*U
128 CONTINUE
C
U=ABS(A21(K,1))
I=K
M=2
DO 213 J=K,L
IF(J.EQ.K) GO TO 212
V=ABS(A11(J,1))
IF(V.LE.U) GO TO 211
U=V
M=1
I=J
211 V=ABS(A21(J,1))
IF(V.LE.U) GO TO 212
U=V
M=2
I=J
212 V=ABS(A31(J,1))
IF(V.LE.U) GO TO 213
U=V
M=3
I=J
213 CONTINUE
IF(I.EQ.K) GO TO 215
IF(M.NE.2) GO TO 216
DO 214 J=1,LC
U=A21(K,J)
A21(K,J)=A21(I,J)
A21(I,J)=U
U=A22(K,J)
A22(K,J)=A22(I,J)
A22(I,J)=U
U=A23(K,J)
A23(K,J)=A23(I,J)
A23(I,J)=U
214 CONTINUE
U=X2(K)
X2(K)=X2(I)
X2(I)=U
GO TO 220
215 IF(M.NE.3) GO TO 220
216 IF(M.NE.1) GO TO 218
DO 217 J=1,LC
U=A21(K,J)
A21(K,J)=A11(I,J)
A11(I,J)=U
U=A22(K,J)

```

```

A22(K, J)=A12(I, J)
A12(I, J)=U
U=A23(K, J)
A23(K, J)=A13(I, J)
A13(I, J)=U
217 CONTINUE
U=X2(K)
X2(K)=X1(I)
X1(I)=U
GO TO 220
218 DO 219 J=1, LC
U=A21(K, J)
A21(K, J)=A31(I, J)
A31(I, J)=U
U=A22(K, J)
A22(K, J)=A32(I, J)
A32(I, J)=U
U=A23(K, J)
A23(K, J)=A33(I, J)
A33(I, J)=U
219 CONTINUE
U=X2(K)
X2(K)=X3(I)
X3(I)=U
220 CONTINUE
C
DO 228 I=K, L
IF(I.EQ.K) GO TO 223
U=A11(I, 1)/A21(K, 1)
DO 222 J=1, LC
IF(J.NE.1) A13(I, J-1)=A11(I, J)-A21(K, J)*U
A11(I, J)=A12(I, J)-A22(K, J)*U
A12(I, J)=A13(I, J)-A23(K, J)*U
222 CONTINUE
A13(I, LC)=0.
X1(I)=X1(I)-X2(K)*U
U=A21(I, 1)/A21(K, 1)
DO 225 J=1, LC
IF(J.NE.1) A23(I, J-1)=A21(I, J)-A21(K, J)*U
A21(I, J)=A22(I, J)-A22(K, J)*U
A22(I, J)=A23(I, J)-A23(K, J)*U
225 CONTINUE
A23(I, LC)=0.
X2(I)=X2(I)-X2(K)*U
223 CONTINUE
U=A31(I, 1)/A21(K, 1)
DO 227 J=1, LC
IF(J.NE.1) A33(I, J-1)=A31(I, J)-A21(K, J)*U
A31(I, J)=A32(I, J)-A22(K, J)*U
A32(I, J)=A33(I, J)-A23(K, J)*U
227 CONTINUE
A33(I, LC)=0.

```



```

X3(I)=X3(I)-X2(K)*U
228 CONTINUE
C
  IF(K.EQ.LN) GO TO 401
  U=ABS(A31(K,1))
  I=K
  M=3
  JL=K+1
  DO 313 J=JL,L
  V=ABS(A11(J,1))
  IF(V.LE.U) GO TO 311
  U=V
  M=1
  I=J
311 V=ABS(A21(J,1))
  IF(V.LE.U) GO TO 312
  U=V
  M=2
  I=J
312 V=ABS(A31(J,1))
  IF(V.LE.U) GO TO 313
  U=V
  M=3
  I=J
313 CONTINUE
  IF(I.EQ.K) GO TO 320
  IF(M.NE.3) GO TO 316
  DO 314 J=1,LC
  U=A31(K,J)
  A31(K,J)=A31(I,J)
  A31(I,J)=U
  U=A32(K,J)
  A32(K,J)=A32(I,J)
  A32(I,J)=U
  U=A33(K,J)
  A33(K,J)=A33(I,J)
  A33(I,J)=U
314 CONTINUE
  U=X3(K)
  X3(K)=X3(I)
  X3(I)=U
  GO TO 320
316 IF(M.NE.1) GO TO 318
  DO 317 J=1,LC
  U=A31(K,J)
  A31(K,J)=A11(I,J)
  A11(I,J)=U
  U=A32(K,J)
  A32(K,J)=A12(I,J)
  A12(I,J)=U
  U=A33(K,J)
  A33(K,J)=A13(I,J)

```

```

    A13(I,J)=U
317 CONTINUE
    U=X3(K)
    X3(K)=X1(I)
    X1(I)=U
    GO TO 320
318 DO 319 J=1,LC
    U=A31(K,J)
    A31(K,J)=A21(I,J)
    A21(I,J)=U
    U=A32(K,J)
    A32(K,J)=A22(I,J)
    A22(I,J)=U
    U=A33(K,J)
    A33(K,J)=A23(I,J)
    A23(I,J)=U
319 CONTINUE
    U=X3(K)
    X3(K)=X2(I)
    X2(I)=U
320 CONTINUE
C
    IL=K+1
    DO 328 I=IL,L
    U=A11(I,1)/A31(K,1)
    DO 322 J=1,LC
    IF(J.NE.1) A13(I,J-1)=A11(I,J)-A31(K,J)*U
    A11(I,J)=A12(I,J)-A32(K,J)*U
    A12(I,J)=A13(I,J)-A33(K,J)*U
322 CONTINUE
    A13(I,LC)=0.
    X1(I)=X1(I)-X3(K)*U
    U=A21(I,1)/A31(K,1)
    DO 325 J=1,LC
    IF(J.NE.1) A23(I,J-1)=A21(I,J)-A31(K,J)*U
    A21(I,J)=A22(I,J)-A32(K,J)*U
    A22(I,J)=A23(I,J)-A33(K,J)*U
325 CONTINUE
    A23(I,LC)=0.
    X2(I)=X2(I)-X3(K)*U
    U=A31(I,1)/A31(K,1)
    DO 327 J=1,LC
    IF(J.NE.1) A33(I,J-1)=A31(I,J)-A31(K,J)*U
    A31(I,J)=A32(I,J)-A32(K,J)*U
    A32(I,J)=A33(I,J)-A33(K,J)*U
327 CONTINUE
    A33(I,LC)=0.
    X3(I)=X3(I)-X3(K)*U
328 CONTINUE
C
401 CONTINUE
C

```

```

C      UPWARD GAUSSIAN ELIMINATION
C      -----
C
C      L=1
C      DO 507 K=1, LN
C      I=LP-K
C
C      U=X3(I)
C      IF(I.EQ.LN) GO TO 502
C      DO 501 J=2, L
C      IJ=I+J
501  U=U-A32(I, J-1)*X1(IJ-1)-A33(I, J-1)*X2(IJ-1)-A31(I, J)*X3(IJ-1)
C      IF(L.GE.LC) U=U-A32(I, LC)*X1(I+LC)-A33(I, LC)*X2(I+LC)
502  X3(I)=U/A31(I, 1)
C
C      U=X2(I)-A22(I, 1)*X3(I)
C      IF(I.EQ.LN) GO TO 504
C      DO 503 J=2, L
C      IJ=I+J
503  U=U-A23(I, J-1)*X1(IJ-1)-A21(I, J)*X2(IJ-1)-A22(I, J)*X3(IJ-1)
C      IF(L.GE.LC) U=U-A23(I, LC)*X1(I+LC)
504  X2(I)=U/A21(I, 1)
C
C      U=X1(I)-A12(I, 1)*X2(I)-A13(I, 1)*X3(I)
C      IF(I.EQ.LN) GO TO 506
C      DO 505 J=2, L
C      IJ=I+J
505  U=U-A11(I, J)*X1(IJ-1)-A12(I, J)*X2(IJ-1)-A13(I, J)*X3(IJ-1)
506  X1(I)=U/A11(I, 1)
C      IF(L.LT.LC) L=L+1
C
C      507 CONTINUE
C
C      RETURN
C      END
C      SUBROUTINE RUFVAR(X, XNUE)
C      COMMON G, PR, REY, XMINF, OMEGA, BD, TW, P10, T10, R10, VIS10, TE,
C      1 PE, RE, UE, VISINF, SU, EPS, DS, DYW, SI, ERROR, TC, TA, IEDGE, IEND1, INTACT,
C      2 PRT, XXK, BTRX, XLAM, VARPRT, XINTER, SEPO, ICHS(8), IPRN(9), ED(300),
C      3 EN(300), EP(300), ETO(300), ETN(300), ETP(300), FO(300), FN(300), J2DA,
C      4 FP(300), TN(300), TO(300), XNN(300), VN(300), VO(300), VP(300), TP(300),
C      5 D1(300), D2(300), D3(300)
C      COMMON/BLRVAR/BYD(300), BYN(300), BYP(300), XFY(300), XSS(300),
C      1 XBRE, XHRE, XLS, XCD
C      DIMENSION XD(300)
C      DATA PI/3.1415926535/
C
C      *****
C      INPUT DATA DIMENSIONALIZED BY L, THE
C      LENGTH OF THE MODEL.....
C      *****
C      XSR=0.

```

```

XLS=.0046
XLDS=.0046
XBRE=.0023
XDRE=.0023
XHRE=.00115
XCD=0.6
XDO=0.00023

C
  NM1=IEDGE-1
  DO 99 N=1,NM1
  XBREE=XBRE
C *****
C   XBREE IS A DUMMY VARIABLE
C *****
  XYY=XNN(N)*EPS
  IF(XSR.EQ.1) GO TO 95
  IF(XYY.LE.XHRE) GO TO 94
  XBREE=0.0
94  BYP(N)=1.0-(XBREE*XDRE)/(XLS*XLDS)
     XFY(N)=(1.0-XBREE/XLS)/BYP(N)
     XD(N)=XBREE
     GO TO 96
95  DFUNCT=SQRT((XDO**2)/4.-XYY**2)
     XD(N)=DFUNCT
     BYP(N)=1.0-(PI*XD(N)**2)/(4.*XLS**2)
     XFY(N)=(1.0-XD(N)/XLS)/BYP(N)
96  IF(J2DA.EQ.1) GO TO 97
     XSS(N)=(XCD*XD(N)*X)/(BYP(N)*XLS**2*RE*UE*XNUE)
     GO TO 99

97  XGS(N)=(XCD*XD(N)*X)/(S*BYP(N)*XLS**2*RE*UE*XNUE)
99  CONTINUE
     RETURN
     END

```

Appendix F

Four Key Subsystems Within Computer Code

Nondimensionalizing the Variables and Initializing the Grid

Prior to entering the computational loop the working variables were nondimensionalized or normalized. These variables were listed below along with a definition of each. The format selected was to present the coded variable on the left side of the equal sign and the real or physical definition on the right side of the equal sign. No explanation was included as to choice of normalizing factors.

$$Z1 = \frac{a_o^2}{a_\infty^2} = \frac{T_o}{T_\infty} = 1 + \frac{\gamma-1}{2} M_\infty^2$$

$$P10 = \frac{1}{\gamma M_\infty^2} \left[\frac{T_o}{T_\infty} \right]^{\frac{\gamma}{\gamma-1}} = \frac{1}{\gamma M_\infty^2} \frac{P_o}{P_\infty}$$

$$T10 = \frac{1}{(\gamma-1)M_\infty^2} \left[\frac{T_o}{T_\infty} \right] = \frac{T_o}{T_\infty (\gamma-1)M_\infty^2} \quad (F.1)$$

$$R10 = \frac{\gamma \left[\frac{1}{\gamma M_\infty^2} \frac{P_o}{P_\infty} \right]}{(\gamma-1) \frac{T_o}{T_\infty (\gamma-1)M_\infty^2}} = \frac{\rho_o}{\rho_\infty}$$

$$T_{INF} = \frac{T_o / (T_\infty (\gamma - 1) M_\infty^2)}{(T_o / T_\infty)} = \frac{1}{(\gamma - 1) M_\infty^2}$$

$$\frac{T_w}{T_\infty (\gamma - 1) M_\infty^2}$$

With Eq (F.1) defined for all cases, some others depended on the value of ω . If ω were not equal to zero, then

$$VISIO = \frac{T_o}{T_\infty (\gamma - 1) M_\infty^2} = \frac{u_o}{u_\infty} \left[\frac{1}{(\gamma - 1) M_\infty^2} \right]^\omega$$

$$EPS = \left[\frac{(\gamma - 1) M_\infty^2}{(Re_\infty)^{1/2}} \right]^{\omega/2} \quad (F.2)$$

$$VISINF = \left[\frac{1}{(\gamma - 1) M_\infty^2} \right]^\omega = \left[\frac{T_\infty}{T_{ref}} \right]^\omega$$

where the reference temperature was taken as $T_\infty (\gamma - 1) M_\infty^2$.

However, for the case where ω was equal to zero, the quantities of Eq (55) plus one were defined as follows:

$$TC = \frac{S}{T_\infty (\gamma - 1) M_\infty^2} = \frac{198.6}{T_{ref}}$$

$$VISIO = \left[\frac{T_o}{T_\infty (\gamma - 1) M_\infty^2} \right] \left[\frac{1 + \frac{S}{T_\infty (\gamma - 1) M_\infty^2}}{\frac{T_o}{T_\infty (\gamma - 1) M_\infty^2} + \frac{S}{T_\infty (\gamma - 1) M_\infty^2}} \right]$$

$$= \left[\frac{T_o}{T_{ref}} \right]^{1.5} \left[\frac{T_{ref} + 198.6}{T_o + 198.6} \right] = \frac{\mu_o}{\mu_{ref}}$$

$$EPS = \left[\frac{(T_\infty + 198.6) (\gamma - 1) M_\infty^2}{(T_\infty (\gamma - 1) M_\infty^2 + 198.6)} \frac{1.5}{Re_\infty} \right]^{1/2} \quad (F.3)$$

$$= \left[\frac{\left[\frac{T_{ref}}{T_\infty} \right]^{1.5} \left[\frac{T_\infty + 198.6}{T_{ref} + 198.6} \right]}{Re_\infty} \right]^{1/2} = \left[\frac{\mu_{ref}/\mu_\infty}{Re_\infty} \right]^{1/2} \quad (F.4)$$

$$VISINF = \left[\frac{T_\infty}{T_{ref}} \right]^{1.5} \left[\frac{T_{ref} + 198.6}{T_\infty + 198.6} \right]$$

These quantities were frequently used in the grid computation and provided a summary of the nondimensionalizing techniques used throughout the code. Before beginning this computation within the grid, however, there had to be an initialization of the profile.

Initialization began by defining Y in the code as the distance measured along the η axis. Any $\Delta\eta_j$ was defined as $\left(\frac{\Delta\eta_{K+1}}{\Delta\eta_K} \right)^{j-1} \Delta\eta_j$ which yielded a fine mesh of nodal points near the surface and an adequate spacing toward the edge. Y values were assigned by successively adding all $\Delta\eta$ values from the surface, to the point in question. Then, three hypothetical successive columns of nodes were created by the following statements:

$D1 = D2 = D3 = 0.$, from the surface to the edge of the boundary layer. Incorporating the notation of fig 1,

$V_{i,j} = V_{i-1,j} = V_{i-2,j} = -Y_j$, for all j from the surface to the edge of the boundary layer.

In a similar manner, three successive stations of F , θ , $\bar{\epsilon}$, and $\hat{\epsilon}$ were assigned values of 1.0. Finally, all coefficients of the system of finite difference equations were set equal to 0.

This initialization provided the primer to begin the backward differencing along the ξ direction and the central differencing along the η direction. The finite differencing system was unconditionally stable for increments of $\Delta\eta$ and $\Delta\xi$, and the iterative stepping procedure along ξ damped the error due to the grid initialization within a few steps.

Subroutine Reystr

This routine was called from the main program at each station, s_i , at and beyond the point of transition to turbulence. The purpose of this subroutine was to calculate an eddy viscosity for the inner and outer regions of the two-layer turbulent boundary layer model.

Computation within Reystr began with Taylor series expansions of F to the third order partial term about the first station at the wall. With values for $F_{j=1}$, $F_{j=2}$, $F_{j=3}$, and $F_{j=4}$, a four-point finite difference expression

was formed for $\frac{\partial F}{\partial \eta} \Big|_w$, and the coefficients of the F terms at each node, one through four, were represented by Y11, Y12, Y13, Y14 in the code. Next, a nondimensional molecular viscosity-density term was calculated for the wall with a shear stress term that followed:

$$XLM1W = \left[\frac{T_w}{T_e} \right]^{1/2} \left[\frac{T_e + 198.6}{T_w + 198.6} \right] = \frac{(\rho\mu)_w}{(\rho\mu)_e} \quad (F.5)$$

$$PI2 = \frac{(\rho\mu)_w}{(\rho\mu)_e} \frac{\partial F}{\partial \eta} \Big|_w \quad (F.6)$$

An iterative loop was begun to generate the nondimensionalized inner eddy viscosity model, $\frac{\epsilon_{inner}}{\mu}$, of Cebeci-Smith-Mosinskis for each node in the η direction for the current s_i . In the actual code and the following the calculation of a number of interim quantities that did not necessarily represent any real boundary layer characteristic, three important computations were made. First, δ/L was calculated. Next, an intermediate quantity, DD, to be used later in the outer eddy model, was calculated. Finally, PI1, another intermediate quantity used in the inner model, was computed:

$$\delta/L = XNN_j = \frac{\left[\begin{array}{c} u_j - .995 \\ u_e \end{array} \right] \left[\Delta XNN_{j-(j-1)} \right]}{\Delta \left[\begin{array}{c} u \\ u_e \end{array} \right]_{j-(j-1)}}$$

$$BD = \sum_{j=2}^{\text{edge of the boundary layer}} \left[\left(1 - \frac{u_j}{u_e} \right) \left(\frac{T_j}{T_e} \right) + \left(1 - \frac{u_{j-1}}{u_e} \right) \left(\frac{T_{j-1}}{T_e} \right) \right] \frac{\Delta \eta_{j-1}}{2} \quad (F.7)$$

$$PI1 = \left[\frac{2XRe_{\infty}}{\{(\gamma-1)M_{\infty}^2\}^{1.5} \left[\frac{T_{\infty} + 198.6}{T_{\infty}(\gamma-1)M_{\infty}^2 + 198.6} \right]} \frac{\sum_{j=2}^{\text{edge}} \frac{\Delta \eta_{j-1}}{2} \left[\frac{T_w}{T_e} + \frac{T_j}{T_e} \right]}{\frac{\mu_e}{\mu_{ref}} \left[\frac{T_j}{T_e} \right]^3 s} \right]$$

where the s was included for the case of conical flow only. Again, a $\frac{\partial F}{\partial \eta}$ term was generated, but using only a three-point central differencing scheme on this occasion. The final step of the loop was the actual computation of $\frac{\epsilon_{inner}}{\mu}$ at the current node j :

$$\frac{\epsilon_{inner}}{\mu} \Big|_j = .16(PI1)(1 - \exp(-\{(PI1)(PI2)\}^{1/2} / (26 \frac{(\rho u)_j}{(\rho u)_e})))^2 \quad (F.8)$$

$$\frac{\left[\frac{Y9}{2} F(i,j+1) - Y10 F(i,j) - \frac{Y9}{2} F(i,j-1) \right]}{\Delta \eta_j \left[\frac{(\rho u)_j}{(\rho \xi)_e} \right]}$$

where $Y8$, $Y9$, and $Y10$ were coefficients obtained through Taylor series expansions of $F(i,j-1)$ and $F(i,j+1)$ about a point $F(i,j)$. As the calculation of $\frac{\epsilon_{inner}}{\mu}$ progressed from the wall out into the field of flow, $\frac{\epsilon_{inner}}{\mu} \Big|_{j+1}$ retained its own computed value or that of $\frac{\epsilon_{inner}}{\mu} \Big|_j$, whichever was greater.

The outer law, $\frac{\epsilon_{outer}}{\mu}$, was computed through an iterative

loop similar to that of the inner model. It culminated with the expression

$$\frac{\epsilon_{\text{outer}}}{\mu} = .0168 \left[\frac{2XRe_{\infty}}{\{(\gamma-1)M_{\infty}^2\}^{1.5} \left[\frac{T_{\infty} + 198.6}{T_{\infty}(\gamma-1)M_{\infty}^2 + 198.6} \right]} \right]^{1/2} \left[\frac{DD}{\left[\frac{u_e}{u_{\text{ref}}} \right] \left(\frac{\rho\mu \right)_j \left[\frac{T_j}{T_e} \right]^2} \right]^2 s$$

where the s was included only for the case of conical flow. In order that a compatible combination of computer viscosities were retained, the values of eddy viscosity from the outer law replaced those of the inner law from the point of intersection of the graphs to the edge of the boundary layer. Graphically, this was depicted in Fig 3.

Having calculated the initial eddy values for the inner and outer viscous regions of the boundary layer, it was appropriate to subject this model to two more factors. Both were factors of degradation and were included to better describe the character of turbulent activity within the boundary layer.

Objections have been raised to the use of an eddy viscosity term, ϵ , in place of, or in addition to the molecular viscosity, μ , of a fluid, μ is a real property of a fluid, ϵ is only an effective description when a fluid is in motion, and it is clearly not a property of the fluid. But, with reservation, it has been used to express the behavior of turbulent stresses in terms of mean velocity gradients of a flowing fluid. It has been possible to obtain a satisfactory description of mean properties within turbulent

flows by assuming this flow to behave as a Newtonian fluid, incorporating an eddy viscosity model along with μ , and including two factors of intermittency when appropriate (Ref. 38:25-26). A laminar and irrotational flow became turbulent as it passed through a region of transition in which only a fraction of the time was spent in a turbulent state. During that time in laminar motion, the Reynolds stress, hence ϵ , would have been zero. Then, to adequately describe the effects of ϵ at any point by the relative fraction of time that that point would be engulfed in turbulent flow (Ref 34:117). Therefore, the first multiplicative factor, called an intermittency factor, was applied to ϵ to more accurately describe the ϵ within the transition region. The intermittency or probability factor of Dhawan and Narasimha was used for this program. The factor was computed as follows (Ref. 13:28-29):

$$\Gamma(s) = \left[1 - \exp \left[-0.412 \left[\frac{s_{\text{current}} - s_{\text{transition point}}}{(.5)^{s_{\text{transition point}}}} \right]^2 \right] \right] \quad (\text{F.10})$$

Then, the computed $\frac{\epsilon}{\mu}|_{\text{original}}$ was replaced by

$$\frac{\epsilon}{\mu}|_{\text{modified}} = (\Gamma(s)) \frac{\epsilon}{\mu}|_{\text{original}} \quad (\text{F.11})$$

The second factor was then considered. It was observed by Klebanoff that in a turbulent boundary layer with a free boundary, as the free stream was approached the turbulence became intermittent. This intermittent nature was observed

first at y/δ greater than .4 with less turbulent intensity as y/δ grew larger. It was thought that a good prediction of turbulent intensity probably depended on a correct weighting of the probability density for the turbulence of the free stream with that within the boundary. It was found that a good description of γ' was a Gaussian integral curve given by

$$\gamma' = \frac{1}{2} (1 - \text{erf}(\xi')) \quad (\text{F.12})$$

where

$$\xi' = \left(\sqrt{2} \frac{\sigma}{\delta} \right)^{-1} \left(\frac{y}{\delta} - .78 \right) = 5 \left(\frac{y}{\delta} - .78 \right) \quad (\text{F.13})$$

These expressions indicated that the edge of the boundary layer had a random character with a mean position at y/δ equal to .78. The edge vacillated from y/δ equal to .4 to y/δ equal to 1.2. Finally, if it were assumed that the free stream contributed little to the measured turbulent quantities of the boundary layer, an allowance could be made for the effect of intermittency by dividing by the factor γ' (Ref. 28:15-19).

Cebeci used the approximate expression for Eq (F.12) to give a multiplicative version:

$$\gamma' = 1 + 5.5 \frac{y}{\delta} 6^{-1} \quad (\text{Ref. 20:96}) \quad (\text{F.14})$$

which led to the coding for this second factor. If γ' were not included, then a newly defined viscosity was

$$\bar{\varepsilon} = 1 + \frac{\varepsilon}{u} \Gamma(s) \quad (\text{F.15})$$

Including γ' , Shang formed the following model:

$$\bar{\varepsilon} = 1 + \left[\frac{1.75}{\left[1 + 5.5 \left[\frac{y}{L} / \frac{\delta}{L} \right]^6 \right]} + 1 \right] \left[\frac{\varepsilon}{2.75 u} \right] \quad (\text{F.16})$$

For purposes of this study Eq (F.15) became eddy model zero, and Eq (F.16) became eddy model one. Then, whether or not γ' was included, the quantity $\hat{\varepsilon}$ was defined by

$$\hat{\varepsilon} = 1 + \frac{\text{Pr}}{\text{Pr}_t} (\bar{\varepsilon} - 1) \quad (\text{F.17})$$

In a final note, the decision of whether to use eddy model zero or eddy model one depended on the original assumption that either the free stream turbulence had an effect on the ε of the boundary layer, or it did not. This factor, γ' , was to have a definite effect on the analytical results, and this entire subroutine was included with program listing of Appendix E.

Subroutine Cfstr

Like Reustr this routine was called from the main program. But unlike Reustr, Cfstrno performed its computation throughout the laminar, transition, and turbulent regions of flow. The purpose of this routine was to calculate a Stanton number, a measure of heat transfer; the local coefficient of friction, indicative of shear stress at the surface; and Reynolds numbers based on displacement thick-

ness and momentum thickness.

Computation began with $\frac{(\rho\mu)_w}{(\rho\mu)_e}$, coded XLM1 in the program. The formula by which XLM1 was computed depended on the value of the exponent in the viscosity law of Sutherland, the value of this exponent being specified by the programmer. If the exponent were zero, then

$$XLM1 = \left[\frac{T_w}{T_e} \right]^{1/2} \left[\frac{T_o + 198.6}{T_w + 198.6} \right] \quad (F.18)$$

If this exponent were one, then XLM1 was one. Otherwise,

$$XLM1 = \frac{T_w}{T_e}^{\omega - 1} \quad (F.19)$$

Next to be calculated were transformed quantities similar to q or heat flux and τ or shear stress. First, the same four-point finite difference scheme used in Reyrstr for $\frac{\partial F}{\partial \eta}|_w$ was repeated at this point to calculate $\frac{\partial F}{\partial \eta}|_w$ and $\frac{\partial \theta}{\partial \eta}|_w$. Then the transformed τ , coded TAU, was computed:

$$TAU = \frac{(\rho\mu)_w}{(\rho\mu)_e} \frac{\rho_e}{\rho_\infty} \frac{\mu_e}{\mu_{ref}} \left[\frac{u_e}{u_\infty} \right]^2 \frac{\partial F}{\partial \eta}|_w \frac{1}{(2X)^{1/2}} + TAUR \quad (F.20)$$

where

$$TAUR = .5 \left(\frac{L}{\ell} \right)^2 \left(\frac{u_e}{u_\infty} \right) \left(\frac{\mu_{ref}}{\mu_\infty} \right)^{1/2} \left(\frac{\rho_\infty u_\infty L}{\mu_\infty} \right)^{1/2} (2X)^{-1/2} \int_0^{\eta_K} F d\eta \quad (F.21)$$

η_K is the value of η at $y = h$ (height of the roughness element).

The skin-friction coefficient is increased by the addition of the roughness element and it may be defined as:

$$c_{fw} = \frac{\tau_{sw} + D/BC}{\frac{1}{2} \rho_{\infty} U_{\infty}^2} \quad (F.22)$$

where $D = \int_0^b \int_0^h \frac{1}{2} u^2 C_D dy dz$. τ_{sw} and D/BC may be written in dimensional variables as follows:

$$\tau_w + \frac{D}{BC} = \mu_w \left. \frac{\partial u}{\partial y} \right|_w + \frac{1}{2} \frac{C_D b}{BC} \int_0^k u^2 dy$$

The dimension of the element is constant along y for the case of rectangular roughness elements. Non-dimensionalizing the variables and stretching the y coordinate,

$$\tau_w + \frac{D}{BC} = \frac{\mu_w}{\mu_{ref}} \mu_{ref} \frac{U_{\infty}}{L\epsilon} \left. \frac{\partial (u/u_{\infty})}{\partial (y/L\epsilon)} \right|_w +$$

$$\frac{C_D}{2} \frac{L}{B} \frac{L}{C} \frac{b}{L} \frac{1}{L} \int_0^k \frac{\rho}{\rho_{\infty}} \rho_{\infty} \frac{u}{u_{\infty}}^2 u_{\infty}^2 \frac{y}{L\epsilon} L\epsilon$$

Converting to transformed coordinate η ,

$$\tau_w + \frac{D}{BC} = \frac{(\mu\rho)_w}{\mu_{ref} \rho_{\infty}} \frac{U_e}{U_{\infty}}^2 \frac{\mu_{ref} U}{L\epsilon} \frac{1}{2X} \left. \frac{\partial F}{\partial \eta} \right|_w +$$

$$\frac{C_D}{2} \frac{L}{B} \frac{L}{C} \frac{b}{L} \frac{u_e}{u_{\infty}} c_{\infty} U_{\infty}^2 \epsilon \frac{1}{2X} \int_0^{\eta_k} F^2 d\eta \quad (F.23)$$

Consider: $\frac{\mu_{ref}}{L\epsilon} u_{\infty} = \frac{\mu_{ref}}{L\epsilon} u_{\infty} \frac{\rho_{\infty} u_{\infty}}{\rho_{\infty} u_{\infty}}$

$$= \epsilon \rho_{\infty} U_{\infty}^2$$

Therefore,

$$\begin{aligned} \tau_w + \frac{D}{BC} &= \epsilon (\rho_\infty U_\infty^2) \frac{(\rho\mu)_w}{(\rho_\infty \mu_{ref})} \left(\frac{u_e}{u_\infty} \right)^2 \sqrt{\frac{1}{2X}} \frac{\partial F}{\partial \eta} \Big|_w \\ &+ \epsilon (\rho_\infty U_\infty^2) \frac{C_D}{2} \frac{L}{B} \frac{L}{C} \frac{b}{L} \frac{U_e}{U_\infty} \sqrt{2X} \int_0^{\eta_k} F^2 d\eta \end{aligned} \quad (F.24)$$

Finally,

$$\begin{aligned} C_f &= \frac{\tau_w + \frac{D}{BC}}{\frac{1}{2} \rho_\infty U_\infty^2} = 2\epsilon \frac{(\rho\mu)_w}{(\rho_\infty \mu_{ref})} \left(\frac{U_e}{U_\infty} \right)^2 (2X)^{\frac{1}{2}} \frac{\theta F}{\theta r} \Big|_w \\ &+ \epsilon C_D \frac{L}{B} \frac{L}{C} \frac{b}{L} \frac{U_e}{U_\infty} \sqrt{2X} \int_0^{\eta_k} F^2 d\eta \end{aligned} \quad (F.25)$$

In the program, the increased τ due to roughness elements is defined as TAUR, by equation (F.21).

Following τ , the transformed q , coded QS, was replaced by the following expression:

$$QS = \frac{1}{(2X)^{1/2} Pr} \frac{(\rho\mu)_w}{(\rho\mu)_e} \frac{\rho_e}{\rho_\infty} \frac{u_e}{\mu_{ref}} \frac{u_e}{u_\infty} \frac{T_e}{1_\infty (\gamma-1) M_\infty^2} \frac{\partial \theta}{\partial \eta} \Big|_w \quad (F.26)$$

or,

$$QS + \frac{(\rho\mu)_w}{\rho_\infty \mu_{ref}} \frac{u_e}{u_\infty} \frac{T_e}{T_\infty (\gamma-1) M_\infty^2} Pr^{-1} (2X)^{-1/2} \frac{\partial \theta}{\partial \eta} \Big|_w$$

For the case of the axisymmetric flow, both TAU and QS were derived by the non-dimensional station, s_i . With this, preliminary calculations were completed.

A Stanton number and coefficient of friction followed next in the computation. If T_w equaled T_o , there was no heat transfer and ST, coded STMO, was zero. Otherwise,

$$\frac{\left[\frac{\mu_{ref}}{\mu_\infty} \right]^{\frac{1}{2}} \left[\frac{\rho_\infty u_\infty L}{\mu_\infty} \right]^{-\frac{1}{2}} \frac{(\rho u)_w}{\rho_\infty \mu_{ref}} \frac{u_e}{u_\infty} \frac{T_e}{T_\infty (\gamma-1) M_\infty^2} Pr^{-1} (2X)^{-\frac{1}{2}} \frac{\partial \theta}{\partial \eta} \Big|_w}{\left[1 - \frac{T_w}{T_o} \right] \left[\frac{T_e}{T_\infty (\gamma-1) M_\infty^2} + \frac{1}{2} \left(\frac{u_e}{u_\infty} \right)^2 \right]} \quad (F.27)$$

The model from which this expression came was

$$St_e = \frac{q}{\rho_e u_e (\bar{h}_e - h_w)} \quad (F.28)$$

For the calculation of c_f | local station, coded CFNO,

$$CFNO = 2 \frac{\mu_{ref}}{\mu_\infty} \left[\frac{\rho_\infty u_\infty L}{\mu_\infty} \right]^{-\frac{1}{2}} \frac{(\rho u)_w}{\rho_\infty \mu_{ref}} \left(\frac{u_e}{u_\infty} \right)^2 (2X)^{-\frac{1}{2}} \frac{\partial F}{\partial \eta} \Big|_w$$

$$+ \left(\frac{\mu_{ref}}{\mu_\infty} \right)^{\frac{1}{2}} \left(\frac{\rho_\infty u_\infty L}{\mu_\infty} \right)^{-\frac{1}{2}} \frac{C_D (XBRE) UE}{(XLS)(XLDS)} (2X)^{\frac{1}{2}} \int_0^{\eta_k} F^2 d\eta \quad (F.29)$$

With St and $c_{f_{local}}$ computed, only the transformed expressions for Re_{δ^*} and Re_θ remained. Coded as REYDT and REYMT, these quantities were computed from the following statements:

$$\text{REYDT} = \frac{\rho_e u_e x_{\text{real}}}{\mu_e} \frac{\delta^*}{L}$$

(F.30)

$$\text{REYMT} = \frac{\rho_e u_e x_{\text{real}}}{\mu_e} \frac{\theta}{L}$$

Subroutine RUFVAR

The effect of surface roughness on compressible turbulent boundary-layer is modelled by distributed sources and sinks and blockage-terms in the appropriate governing equations. This subroutine was called from the main program at each station, s_i , throughout the laminar, transition and fully turbulent regions of the flow. The purpose of this subroutine was to calculate the source/sink term (ϕ_{ss}) and the blockage terms ($f(y)$ and $B(y)$).

To initiate this subroutine, the following quantities were specified as input.

- XSR - a flagged quantity to specify whether the roughness elements are of spherical or rectangular shape
- XBRE - the breadth of the rectangular element
- XDRE - the depth of the rectangular element in the direction of flow
- XHRE - height of the roughness element
- XLS - centre to centre spacing between adjacent elements facing the flow
- XLDS - centre to centre spacing between adjacent elements in the direction of the flow

XCD - coefficient of drag
 XDO - the diameter of the roughness element with circular cross section at $y = 0$
 DFUNCT - the shape of the spherical element

The detailed dimensions of the roughness elements for rectangular cross-section are given in Fig 5. The input data is non-dimensionalized by the length of the model.

After the size, shape, and the spacing of the roughness elements are specified, the subroutine calculates the blockage terms $f(y)$ and $B(y)$ along η as follows:

(a) For Elements with Rectangular Cross-Sections

$$BYP(N) = 1.0 - \frac{XBRE * XDRE}{XLS * XLDS}$$

and

$$XFY(N) = 1.0 - \frac{(XBRE)/(XLS)}{BYP(N)}$$

(b) For Elements With Circular Cross-Sections

$$BYP(N) = 1.0 - \pi \frac{XD(N)^2}{4XLS^2}$$

and

$$XFY(N) = 1.0 - \frac{XD(N)/XLS}{BYP(N)}$$

After calculating the blockage terms, the subroutine further computes the source/sink term as follows:

$$XSS(N) = \frac{X * XCD * XD(N)}{BYP * \rho_e * u_e * \mu_e * XLS^2}$$

For elements with rectangular cross-section, $D(y)$ was set equal to $XBFE$.

This completed calculations within this routine, and further, completed the formal description of four important subsystems within ITRACT. Again, this subroutine was included with the program listing of Appendix E. In this appendix consideration was given to the important concepts of the nondimensionalization of working quantities, and initialization of the grid. Also included was a brief description of the three subroutines used in the computation of eddy viscosity, heat transfer, and skin friction and roughness variables. The theory presented in this appendix should provide a better understanding of the code in general, and the modification for surface roughness specifically.

VITA

Zakir Hussain Khan was born on 1 Jan 1953 in Nowshera, Pakistan. He did his matriculation and F.sc. with distinction from P.A.F College Sargodha in 1969 and 1971 respectively. In 1976, he graduated from College of Aeronautical Engineering, Karachi with a bachelor of aerospace engineering degree. He was commissioned in the Pakistan Air Force as a flying officer upon graduation. As an engineering officer, he was assigned to various duties in P.A.F. and did several professional courses. He was detailed for a master's course in Aeronautical Engineering at the Air Force Institute of Technology, WPAFB, Ohio in June 1982. He is a member of Institute of Engineers, Pakistan.

Permanent Address: Village Badrashi
Tehsil Nowshera
District Peshawar
(N.W.F.P.), Pakistan

REPORT DOCUMENTATION PAGE

1a. REPORT SECURITY CLASSIFICATION Unclassified		1b. RESTRICTIVE MARKINGS	
1a. SECURITY CLASSIFICATION AUTHORITY		3. DISTRIBUTION/AVAILABILITY OF REPORT Approved for public release; distribution unlimited.	
2b. DECLASSIFICATION/DOWNGRADING SCHEDULE		4. PERFORMING ORGANIZATION REPORT NUMBER(S) AFIT/GAE/AA/83D-9	
4. PERFORMING ORGANIZATION REPORT NUMBER(S) AFIT/GAE/AA/83D-9		5. MONITORING ORGANIZATION REPORT NUMBER(S)	
6a. NAME OF PERFORMING ORGANIZATION School of Engineering	6b. OFFICE SYMBOL (If applicable) AFIT/ENY	7a. NAME OF MONITORING ORGANIZATION	
6c. ADDRESS (City, State and ZIP Code) Air Force Institute of Technology Wright-Patterson AFB OH 45433		7b. ADDRESS (City, State and ZIP Code)	
8a. NAME OF FUNDING/SPONSORING ORGANIZATION Air Force Wright Aeronautical Laboratories	8b. OFFICE SYMBOL (If applicable) AFWAL/FJNM	9. PROCUREMENT INSTRUMENT IDENTIFICATION NUMBER	
8c. ADDRESS (City, State and ZIP Code) Wright-Patterson Air Force Base, Ohio 45433		10. SOURCE OF FUNDING NOS.	
11. TITLE (Include Security Classification) See Box 19		PROGRAM ELEMENT NO.	TASK NO.
13. PERSONAL AUTHOR(S) Zakir H. Khan, Sqn. Ldr. PAF		PROJECT NO.	WORK UNIT NO.
12a. TYPE OF REPORT MS Thesis	13b. TIME COVERED FROM _____ TO _____	14. DATE OF REPORT (Yr., Mo., Day) 1983 December	15. PAGE COUNT 155
16. SUPPLEMENTARY NOTATION 3 JAN 1984 Lynn E. Wclaver Dean for Research and Development Air Force Institute of Technology Wright-Patterson AFB, OH			
17. COSATI CODES		18. SUBJECT TERMS (Continue on reverse if necessary and identify by block number)	
FIELD	GROUP	SUB. GR.	
20	04	Fluid Dynamics, surface roughness, turbulent boundary layer	
19. ABSTRACT (Continue on reverse if necessary and identify by block number)			
Title: AN ANALYTIC STUDY OF THE EFFECTS OF A SURFACE ROUGHNESS ON COMPRESSIBLE TURBULENT BOUNDARY LAYER			
Thesis Chairman: Dr. Urmilla Ghia			
20. DISTRIBUTION/AVAILABILITY OF ABSTRACT UNCLASSIFIED/UNLIMITED <input type="checkbox"/> SAME AS RPT. <input type="checkbox"/> DTIC USERS <input type="checkbox"/>		21. ABSTRACT SECURITY CLASSIFICATION	
22a. NAME OF RESPONSIBLE INDIVIDUAL James K. Hodge, Capt, USAF		22b. TELEPHONE NUMBER (Include Area Code) (513)255-3517	22c. OFFICE SYMBOL AFIT/ENY

This study followed the work of Dr. Anthony Fiore, of Air Force Wright Aeronautical Laboratories, Wright-Patterson Air Force Base, Ohio. Dr. Fiore had carried out an experimental study of the effect of surface roughness on the turbulent boundary layer. Given a Fortran code, ITRACT, written primarily by Dr. Shang, that solved for the characteristics of a laminar, transitional and turbulent boundary layer on smooth surfaces. The purpose of the present study was to investigate the influence of surface roughness on a compressible turbulent boundary layer and then to extend the usefulness of the existing computer code, ITRACT, by including in it the optional capability of rough-surface boundary layer calculations.

To achieve this objective, the surface roughness was represented by distributed sources and sinks in the appropriate governing equations. The most important term is a sink term in the mean momentum equation, representing the form drag due to the roughness element. The governing boundary-layer equations for continuity, momentum, and energy were derived in a form to account for the blockage effect due to the roughness elements. The modified governing equations were then transformed using the transformation of Probstein-Elliott and Levy-Lees. The resulting equations, with appropriate boundary conditions, were solved by finite-difference techniques to determine the non-dimensional velocity components and temperature at a finite number of nodes in the boundary-layer field of the flow.

To establish the authenticity of the original code, ITRACT, some smooth surface results were first computed and compared with the experimental data of Dr. Fiore and Dr. Cole for turbulent flows over smooth surfaces. After the accuracy of the code was established for smooth-surface calculations, the code was modified in order to render it capable of predicting the influence of surface roughness on compressible turbulent flow. The modified code was then used to obtain results for rough-surface boundary layers and the computed results were compared with the experimental data of Dr. Fiore for the case of supersonic flow over a rough flat plate. The agreement between the computed and the measured velocity profiles was quite satisfactory. The corresponding temperature profiles agreed well everywhere except very near the wall; a possible reason for this discrepancy is offered in this study. Unlike the previous studies of rough-surface boundary layers, the present study makes no modification to the turbulence model employed.